



DELIVERABLE REPORT

Deliverable:	D4.2. Release estimations during ENMs and nano-enabled products value chain
Work Package:	WP4: Identification and quantification of ENM releases from nano-enabled products
Lead Beneficiary:	LEITAT
Nature of Deliverable:	Report
Dissemination Level:	Public (PU)
Delivery Date:	28/02/2019
Submitted By:	Vicenç Pomar-Portillo (LEITAT)
Revised By:	Alison Crossley (Oxford University) Richard J. Williams (NERC)
Approved By	Barry Park (GBP Consulting)



This project receives funding from the European Union's Horizon 2020 research and innovation programme under grant agreement number 642007.

This report was prepared under contract from the European Commission

Contract n° 646002, Horizon 2020

The content of this document does not necessarily reflect the official opinions of the European Commission or other institutions of the European Union.

Project acronym: NanoFASE

Project full title: Nanomaterial Fate and Speciation in the Environment

Research ID E-2356-2016

Start of the project: 1 Sept 2015

Duration: 4 years

Project coordinator: Dr. Claus Svendsen, CEH, NERC (National Environmental Research Council), Wallingford, UK.

Project website www.NanoFASE.eu

Deliverable title: Report on feedback on case study development

Deliverable n°: D4.2

Nature of the deliverable: Report

Dissemination level: Public

Lead beneficiary: LEITAT

Lead author: Vicenç Pomar

Contributing authors: Socorro Vázquez-Campos

Reviewers: Alison Crossley, Richard J. Williams, Barry Park

Citation: D4.2. Release estimations during ENMs and nano-enabled products value chain, NANOFASE (G.A. 646002)

Due date of deliverable: Month n° 42

Submitted to coordinator: Month n° 42

ABSTRACT

During nano-enabled products life cycle (i.e. production, manufacturing, use, recycling and end-of-life) nanomaterials release to the environment could occur, what needs to be studied to avoid potential environmental concerns. Hot spots, understood as those scenarios with a higher potential nanomaterial release, were determined for the different NANOFASE case studies in D1.2 – Report in the pathway analysis. In the work presented in this deliverable the hot spots were simulated in controlled laboratory conditions to determine if release occurred, and in case it did, the amount (release rate) and form (fate) were determined. The different experimental methodologies, most of them based on standardized protocols, are described together with the techniques used to characterize the nano-enabled products before and after the experimental simulation. The results and conclusions obtained were summarized in a format that can be used as input for the NANOFASE model, which includes the release rates, the release forms, the scenario from where release occurs and the environmental compartment where released nanomaterials are more likely to go.

ABSTRACT.....	5
Index of tables.....	9
Index of figures	9
1. GLOSSARY	13
1.1. Glossary of terms	13
1.2. Glossary of project partners.....	14
2. DELIVERABLE INTRODUCTION AND MAIN OBJECTIVE	15
3. HEMPEL: antifouling paints for marine applications.....	16
3.1. Introduction.....	16
3.2. Materials and methods	16
3.2.1. Tests in marine facilities	18
3.3. Results	19
3.3.1. Unexpected accident with the paint.....	19
3.3.2. ENMs characterization.....	20
3.3.3. Paints characterization	26
3.3.4. Released materials.....	30
3.3.5. Tests in marine facilities	38
3.4. Conclusions.....	41
4. INOTEX: curtains with photocatalytic activity	42
4.1. Introduction.....	42
4.2. Materials and methods	42
4.3. Results	44
4.3.1. ENMs.....	44
4.3.2. Unwashed textiles characterization	46
4.3.3. Washed textiles characterization	48
4.3.4. Washing waters characterization	52
4.4. Conclusions.....	54
5. INOTEX: camping tents with antibacterial activity.....	56
5.1. Introduction.....	56
5.2. Materials and methods	56
5.3. Results	59

5.3.1.	Starting materials.....	59
5.3.2.	Aged materials and leaching waters.....	61
5.4.	Conclusion	64
6.	INOTEX: cotton textiles with antibacterial activity	65
6.1.	Introduction.....	65
6.2.	Materials and methods	65
6.3.	Results	68
6.3.1.	ENMs characterization.....	68
6.3.2.	Textiles characterization	71
6.3.3.	Released materials characterization.....	76
6.3.4.	Dissolution experiment.....	80
6.4.	Conclusion	81
7.	FCCCO: photocatalytic coating for roads.....	82
7.1.	Introduction.....	82
7.2.	Materials and methods	82
7.2.1.	Coating application	83
7.2.2.	TiO ₂ release monitoring due to weathering and wheel abrasion	83
7.3.	Results	86
7.3.1.	ENMs characterization.....	86
7.3.2.	Coating application	87
7.3.3.	TiO ₂ release due to weathering and wheel abrasion	88
7.4.	Conclusion	90
8.	AMEPOX: conductive inks for printed circuits.....	91
8.1.	Introduction.....	91
8.2.	Materials and methods	91
8.3.	Results	92
8.4.	Conclusion	94
9.	Sunscreens (SC).....	95
9.1.	Introduction.....	95
9.2.	Materials and methods	95
9.2.1.	Sunscreens	95

9.2.2.	ICP-MS of sunscreens for total Ti content, Ti content of extracted materials and Ti content of NMs released in ultrapure water	96
9.2.3.	XRD analysis on sunscreens for crystalline phase determination	96
9.2.4.	TGA of sunscreens.....	96
9.2.5.	NM extraction from Sunscreens	96
9.2.6.	SEM-EDX of extracted materials and of NMs released in ultrapure water	97
9.2.7.	Release experiment: sunscreens released from the finger to ultrapure water	97
9.3.	Results	98
9.3.1.	ICP-MS of sunscreens for total Ti content, Ti content of extracted materials and Ti content of NMs released in ultrapure water	98
9.3.2.	XRD analysis on sunscreens for crystalline phase determination	100
9.3.3.	TGA of sunscreens.....	103
9.3.4.	FE-SEM-EDX of extracted materials and of NMs released in ultrapure water	104
9.3.5.	Release experiment: sunscreens released from the finger to ultrapure water	106
9.4.	Conclusions.....	107
10.	Polymers – Release after recycling processes	109
10.1.	Introduction	109
10.2.	Materials and methods	109
10.3.	Results.....	110
10.4.	Conclusions.....	115
11.	FIELD CAMPAIGNS	116
11.1.	Introduction.....	116
11.2.	Materials and methods	116
11.3.	Results.....	117
11.3.1.	French TiO ₂ producer	117
11.3.2.	Danish paint manufacturing site	119
11.4.	Conclusions.....	125
11.4.1.	French TiO ₂ producer	125
11.4.2.	Danish paint manufacturing site	125
12.	DISCUSSION AND FINAL CONCLUSIONS	126
13.	BIBLIOGRAPHY	129

Index of tables

Table 1 – Theoretical composition of the paints.	16
Table 2 – Results of EDX measurement on micro- Cu ₂ O sample	20
Table 3 – Results of EDX measurements on micro-Cu ₂ O particles.....	21
Table 4 - Results of EDX measurements on nano-Cu ₂ O particles.....	22
Table 5 - Results of EDX measurements on micro-Cu ₂ O particles.....	23
Table 6 – BET measurements results.....	26
Table 7 – ICPMS paints measurements results.....	26
Table 8 - Ti concentration determined by ICP-MS in the samples provided by INOTEX. .	46
Table 9 - Ag concentration in the original textiles and Ag-PEI dispersion determined by ICPMS.	61
Table 10 – Camping tent case study release rates	63
Table 11 – Ag concentration in the Ag dispersions determined by ICPMS.	70
Table 12 – ICPMS results of Ti and TiO ₂ concentration in coated papers.	87
Table 13 - Accelerated aging parameters used to simulate weathering conditions on the sample.....	109

Index of figures

Figure 1 – Painted panels for release experiments.	17
Figure 2 – Paint accident evidences. A) B) Paint aspect; C) Paint container damage.	19
Figure 3 – A) SEM and B) TEM image of micro-Cu ₂ O particles.	20
Figure 4 – micro-Cu ₂ O A) TEM image; B) TEM image treated with FIJI software; C) TEM image with higher magnification; D) diffraction patten of the particle shown in “C”; E) TEM image indicating the areas from where EDX measurements were obtained.....	21
Figure 5 – nano-Cu ₂ O A) Diffraction pattern; B) TEM image; C) TEM image magnification from image B, indicating the areas from where EDX measurements were obtained	22
Figure 6 – nano-Cu ⁰ A) B) C) TEM image; D) diffraction pattern; E) TEM image indicating the areas from where EDX measurements were obtained.	23
Figure 7 – XRD results of micro-Cu ₂ O sample	24
Figure 8 – XRD results of micro-Cu ₂ O sample.....	25
Figure 9 – XRD results of nano-Cu ₂ O sample	25
Figure 10 – XRD results of nano-Cu ⁰ sample	26
Figure 11 – SEM image and corresponding EDX spectrum of the paint containing micro-Cu ₂ O particles. A) Back-scattered electrons mode image; B) Secondary electrons mode image.	27

Figure 12 – SEM image of the paint containing micro-Cu ⁰ particles. A) Back-scattered electrons mode image; B) Secondary electrons mode image.	28
Figure 13 – SEM image and corresponding EDX spectrum of the paint containing nano-Cu ₂ O particles. A), B) Back-scattered electrons mode image.	28
Figure 14 – Cu-Pyrithione SEM image.	29
Figure 15 – SEM images of the paint containing nano-Cu ⁰ particles. A), B) Secondary electrons mode image.	29
Figure 16 – pH value of the release experiment along time in marine water.	30
Figure 17 – Copper and Zinc concentration in water released from the paints along the experiment.	31
Figure 18 - Aspect of the release waters and paints in the experiment showing the formation of the salts aggregates.	32
Figure 19 – FT-IR spectra of the aggregates formed during the paints release experiment in marine water.	33
Figure 20 - pH value of the release experiment along time in ultrapure water.	33
Figure 21 – TEM images of TiO ₂ nanoparticles before being impregnated in the textile.	45
Figure 22 – Tiodisper NA-AS sample diffraction pattern.	46
Figure 23 – SEM images and corresponding EDX spectrums of Curb sample.	47
Figure 24 – SEM images and corresponding EDX spectrums of Curb_TiO ₂ sample.	48
Figure 25 – SEM images and corresponding EDX spectrums of Curb_W5 (washed 5 times) sample.	49
Figure 26 – SEM images and corresponding EDX spectrums of Curb_TiO ₂ _W5 (washed 5 times) sample.	50
Figure 27 – Curb_TiO ₂ and Curb samples Ti concentration in textiles along washings. ..	51
Figure 28 – ICPMS plasma ionization test.	52
Figure 29 – Ti concentration in washing waters of Curb and Curb_TiO ₂ samples.	53
Figure 30 – TiO ₂ NPs released from Curb_TiO ₂ sample.	54
Figure 31 – Case study composition, textile for camping tent applications. A: Fluorocarbon based thin water repellent layer; B: Cotton fabric; C: Mixed dispersion of synthetic copolymers (acrylics and polyurethanes) impermeable layer; D: Ag nanoparticles coated with Polyethylenimine (PEI); E: Samples code.	57
Figure 32 – Visual aspect of the 4 samples. A: Tent exterior side; B: Tent interior side (showing the polyacrylic coatings).	57
Figure 33 – A) Original picture; B) Image conversion to greyscale; C) Textile recognition and area measurement by the software.	58
Figure 34 – A) Textile fragments. B) Fragments in contact with water being shacked. ...	58
Figure 35 – HR-TEM images of Ag-PEI dispersion where the two size populations can be observed.	59
Figure 36 – Ag-PEI dispersion size distribution.	60

Figure 37 – SEM images of the camping tent samples before the leaching experiment. A) Tent exterior side; B) tent interior side with one coating; C) tent interior side with two coatings.....	60
Figure 38 – SEM images of the camping tent samples after the leaching experiment. A) Tent exterior side; B) tent interior side with one coating; C) tent interior side with two coatings.....	61
Figure 39 – SEM images of the residues from freeze-dried leaching waters of samples A) TENT1_NoAg; B) TENT1_Ag; C)TENT2_NoAg; D)TENT2_Ag.	62
Figure 40 – Ag concentration in camping tents leaching waters.	63
Figure 41 – A) STEM image; B) NW length using predetermined FIJI software; C) NW recognition and length measurement using FIJI plugin.....	65
Figure 42 – Ag NMs electron microscopy images: A), B) Ag NPs; C) AgNWs_s; D) AgNWs_L	68
Figure 43 – Size distribution of Ag NMs.....	70
Figure 44 – SEM images and corresponding EDX analysis of unwashed textile containing Ag NPs.	71
Figure 45 - SEM images and corresponding EDX analysis of unwashed textile containing the shorter Ag nanowires.	72
Figure 46 - SEM images and corresponding EDX analysis of unwashed textile containing the longer Ag nanowires.	73
Figure 47 - SEM images and corresponding EDX analysis of unwashed control textile...	74
Figure 48 – ICPMS results of Ag concentration in textiles along washings. A) Total concentration; B) Comparison (%).	75
Figure 49 – Ag release to washing waters along washing cycles for the three different samples.	79
Figure 50 – Close view of the uncoated AC16 Surf S asphalt sample. A) top view, B) lateral view.	83
Figure 51 – TiO ₂ coating application on asphalt samples	83
Figure 52 – Asphalt samples distribution inside the climatic chamber	84
Figure 53 – Standardized equipment used to perform the wheel abrasion simulation. .	85
Figure 54 – Water collection and abrasion cycles planned for the climatic chamber simulation.....	85
Figure 55 – HR-TEM images of TiO ₂ dispersion used in FCCCO’s case study.....	86
Figure 56 – XRD measurement of FCCCO TiO ₂ dispersion	87
Figure 57 – TiO ₂ release along time due to weathering and wheel abrasion.	89
Figure 58 – Asphalt samples with and without coating, before and after aging.	89
Figure 59 – Field emission SEM image with EDX analysis of the release waters from AC16_TiO ₂	90
Figure 60 – Electric circuits printed with Ag Ink provided by AMEPOX.....	91
Figure 61 - A) Specimen before milling. B) Pellets of PP+MWCNT obtained after milling.	110

Figure 62 – Specimen recycled and aged during 1000h.	111
Figure 63 - FT-IR of the freeze-dried material released during aging of PP+MWCNT before and after its recycling, and the plain PP (without MWCNT).	111
Figure 64 – Weight (mg) released per nanocomposites area (m ²) due to weathering for the three polymers tested. Both fractions containing and non-containing nanomaterials (NM) are represented.	112
Figure 65 – DSC analysis of PP+MWCNT composites in the different stages.	112
Figure 66 – TGA graph of the MWCNT, PP specimen (without MWCNT) and recycled PP+MWCNT residue obtained from freeze-drying the runoff waters from the climatic chamber.	113
Figure 67 - SEM images showing the surface of PP+MWCNT specimen tests in different stages of their life cycle: PP+MWCNT (A-B), PP+MWCNT aged (C-D), PP+MWCNT recycled (E-F) and PP+MWCNT recycled aged (G-H).	114

1. GLOSSARY

1.1. Glossary of terms

ANOVA	Analysis of variance
BSE	Backscattered electrons
CPS	Counts per second
DFT	Dry Film Thickness
EDX	Energy-dispersive X-Ray Spectroscopy
ENM	Engineered nanomaterials
FE-SEM	Field Emission Scanning Electron Microscopy
FIB-SEM	Focused Ion Beam Scanning Electron Microscopy
HR-TEM	High Resolution Transmission Electron Microscopy
ICDD	International Centre for Diffraction Data
ICP-OES	Inductively coupled plasma optical emission spectroscopy
ICP-MS	Inductively coupled plasma mass spectroscopy
LCS	Life Cycle Stage
M-O	Metal Organic
MWCNT	Multiwall carbon nanotubes
NEP	Nano-enabled product
NC	Nanocomposite
NP	Nanoparticle
NW	Nanowire
PEI	Polyethylenimine
PES	Polyester
PET	Polyethylene Terephthalate
PP	Polypropylene
RSD	Relative Standard Deviation
SE	Secondary electrons
SEM	Scanning Electron Microscopy
SME	Small-to-Medium Enterprise
SS	Stainless Steel

St Dev	Standard Deviation
STEM	Scanning Transmission Electron Microscopy
TBD	To be determined
TSP	Total Suspended Particles
TEM	Transmission Electron Microscopy
VOC	Volatile Organic Compound
XRD	X-Ray Diffraction

1.2. Glossary of project partners

NERC	Natural Environment Research Council	UK
UoB	University of Birmingham	UK
LEITAT	Acondicionamiento Tarrasense	ES
EAWAG	Eidgenössische Anstalt für Wasserversorgung, Abwasserreinigung und Gewässerschutz	CH
UOXF.DJ	Oxford University	UK
HEMPEL	HEMPEL	ES
PP	Promethean Particles	UK
TUL	Technical University of Liberec	CZ
FCCCO	FCC Construcción S.A.	ES
AXME	AMEPOX	PL
ITEX	Inotex	CZ
AppNano	Applied Nanoparticles	ES
EMPA	Eidgenössische Materialprüfungs- und Forschungsanstalt	CH
INERIS	Institut National de l'Environnement Industriel et des Risques	F
ETSS	Environmental, technical and scientific services	CH
TNO	TNO Netherlands Organisation for Applied Scientific Research	NL
GBP	GBP consulting	UK

2. DELIVERABLE INTRODUCTION AND MAIN OBJECTIVE

The present document pretends to describe the different methods used to evaluate the engineered nanomaterials (ENMs) release from different nano-enabled products (NEPs) as well as the results obtained from such experiments, which can be used as input for the NANOFASE model.

The report has been structured per case study, each of them containing an introduction presenting the material, a materials and methods section, a results section and a conclusion. A final discussion and conclusion is also included at the end of the document summarizing the release rates and forms, which are the main input for nano-specific risk assessment models and tools developed in the framework of the NANOFASE project. For further information on the industrial partners and/or the case studies please refer to Deliverable 1.2 (D1.2) – Report on the pathway analysis; and deliverable 1.5 (D1.5) – Report on feedback on case study development.

3. HEMPEL: antifouling paints for marine applications

3.1. Introduction

Anti-fouling paints are a category of underwater paints employed to slow and/or facilitate detachment of subaquatic organism on the boats hull which can affect the vessel performance (saving huge amounts of fuel) and durability. Biocides, in this case based on Cu_2O and Cu^0 particles, are held in the pores and slowly ionized and released from the paint to the water to prevent an accumulation of biofilms and plankton on the boat hull. ZnO which acts as soluble filler is also present in the formulation, influencing the release mechanism. Due to the potential toxic effect on marine life, Cu and Zn release from antifouling paints when immersed in water should be investigated.

3.2. Materials and methods

The company providing the case study is HEMPEL, a world-leading coatings supplier for the decorative, protective, marine, container and yacht markets. Currently, in their commercialized antifouling paints, Cu_2O microparticles are used as biocide ingredient. Now, the company is considering using Cu_2O nanoparticles instead, since they could provide the same effect with lower amounts due to their beneficial surface to volume ratio. Since the Cu^{2+} cations are responsible for the biocide effect, in NanoFase it has been suggested to also test Cu^0 micro and nanoparticles, which could also be ionized producing the biocidal effect. Thus, from the experiments, it will be possible to study not only the composition but also the size effect on the paints release behaviour. On top of that, two types of Cu^0 nanoparticles are intended to be tested, one from a big producer and the other one from a nanoparticles provider synthesizing the materials in a smaller scale but with a higher synthesis control. All the particles were purchased in powder form except Promethean Particles' (PP) Cu^0 nanoparticles, which were provided in ethylene glycol dispersion (50 wt% of Cu).

Different characterization techniques were used on the different particles. A transmission electron microscope (JEOL JEM-2100) coupled with an energy dispersive X-Ray detector (OI Aztec 80mm² X-max), a scanning electron microscope (JEOL 6500F FEG-SEM) and a X-Ray diffraction (XRD) equipment (D5000, Bruker) were used to characterize the dried powders.

The industrial partner (HEMPEL) prepared five different paints, formulated to have the same composition except for the biocide ingredient: 1) Cu_2O microparticles from Nordox AS; 2) Cu_2O nanoparticles; 3) Cu^0 microparticles; 4) Cu^0 nanoparticles from Hongwu International Group LTD; 5) Cu^0 nanoparticles from Promethean Particles (PP). In Table 1 the theoretical composition of all the paints is shown.

Table 1 – Theoretical composition of the paints.

COMPOUNDS (wt%)	micro- Cu_2O	micro- Cu^0	nano- Cu_2O	nano- Cu^0	PP nano- Cu^0
Cu_2O (micro)	≥35 - <50	0	0	0	0
Cu^0 (micro)	0	≥35 - <50	0	0	0

Cu₂O (nano)	0	0	≥35 - <50	0	0
Cu⁰ (nano)	0	0	0	≥35 - <50	0
PP Cu⁰ (nano)	0	0	0	0	≥35 - <50
ZnO (micro)	≥5 - <20	≥5 - <20	≥5 - <20	≥5 - <20	≥5 - <20
Xylene	≥5 - <10	≥5 - <10	≥5 - <10	≥5 - <10	≥5 - <10
4-methylpentan-2-one	≥3 - <5	≥3 - <5	≥3 - <5	≥3 - <5	≥3 - <5
Ethylbenzene	≥1 - <3	≥1 - <3	≥1 - <3	≥1 - <3	≥1 - <3
Cu (metallic)	≥0,1 - <1	≥0,1 - <1	≥0,1 - <1	≥0,1 - <1	≥0,1 - <1
White spirit	≥2,5 - <10	≥2,5 - <10	≥2,5 - <10	≥2,5 - <10	≥2,5 - <10
Copper pyrithione	≥1 - <3	≥1 - <3	≥1 - <3	≥1 - <3	≥1 - <3
O-xylene	≥1 - <5	≥1 - <5	≥1 - <5	≥1 - <5	≥1 - <5

In order to characterize the different formulations, the paints were applied on polyester films from which, after dried, the paints could be easily removed. The dried paint was analysed by FIB-SEM (FEI Helios nanolab 660 Dual Beam SEM and Focused Ion Beam (FIB)) with EDX (Oxford Instruments X-Max 80 mm² SDD-EDS detector) in order to determine the particles distribution. Dried paints were also digested with an acid solution in an analytical microwave digestion system (MARS, CEM, 1600W) and later analysed by inductively coupled mass spectroscopy (ICPMS) (Agilent 7500, Agilent Technologies) in order to determine the Cu and Zn content.

For the release experiments the different paints were applied on one side of acrylic panels of 10 x 5.7 x 0.3 cm, which contained a sealing agent (Hempatex 46330) applied by air spraying on top. Once the panels were dried (24 hours), the antifouling paints were applied by air spraying and allowed to dry for 24 hours. Subsequently, an inert band (non-polishing paint) was applied as reference. The reason behind the application of the inert strip is to help monitor by microscopy both the leached layer and the polishing speed and to determine if the working mechanism of the paint is affected by the change in the size and type of copper used. In Figure 1 the different paints applied on the acrylic panels used to perform the release experiments are shown.



The release experiments were designed following an adaptation of a standard protocol: ISO 15181 – Paints and Varnishes – Determination of release rate of biocides from antifouling paints [1], which were conducted in 2 different water media: 1) ultrapure water and 2) artificial seawater, Figure 1 – Painted panels for release experiments.

D4.2 – Release estimations during ENMs and NEPs value chain

which was prepared according to the standard protocol ASTM D1141 – 98 (2003) – Standard practice for the preparation of substitute ocean water [2]. Two painted panels (total area of 114 cm²) were immersed in 600 ml of water medium at 40 ± 2 °C and stirred at 200 rpm for 45 days. Water samples were collected along time (according to the ISO protocol [1]) and further analysed by ICPMS (Agilent 7500, Agilent Technologies) to determine the Cu and Zn content. The pH of the samples collected was also measured with a pH meter (Sension+ MM374, Hach). Three replicates (a total of 6 panels) were evaluated for each sample.

3.2.1. Tests in marine facilities

In order to assess differences in antifouling performance between the selected copper based materials (Cu⁰ (nano/micro), Cu₂O (nano/micro)), the antifouling paints containing the micro and nano copper were immersed in seawater with salinity in the range of 37-38 parts per thousand at an average temperature in the range of 17-18 °C. The facilities to run the test were located in the Mediterranean Sea, in Vilanova i la Geltrú, Barcelona, Spain.

Acrylic test panels (15 x 20 cm²), sandblasted on one side to facilitate adhesion of the coating, was coated with 80 µm (Dry film thickness, DFT) of a commercial chlorinated rubber (Hempatex 46330) applied by air spraying. After a minimum drying time of 24 hours in the laboratory at room temperature the paint was applied with a Doctor Blade type applicator, with four gap sizes with a film width of 80 mm. One layer of paint around 90-100 µm (DFT) was applied. After at least 72 hours drying, the test panels were fixed on a rack and immersed in sea water. The immersed painted panels assessment was made based on the presence/absence of the following:

1. Slime - this group is composed of the micro-organisms (singularly cannot be seen with the naked eye but collectively produce a glossy appearance or brown-greenish shine on the paint surface). They are always the first to attach to a surface. There are two types:
 - a. Diatomic
 - b. Non-diatomic.
2. Algae - this group is commonly known as the SEAWEEEDS. They can be broken down into three main classes (based on colour) and a minor class (based on physiological characteristics). The three classes are:
 - a. green alga - chlorophyta
 - b. brown alga – phaeophyta
 - c. red alga – rhodophyta
3. These classes will generally have a vertical distribution on panels, with the green alga at the splash zone or water-line and further down the brown alga and then red alga. The fourth class is the blue green alga (cyanophyta) which have a dark brown/black appearance very similar to slime. Animals - there are eight main classes of animals which will appear on the panels:
 - a. Tubeworm
 - b. Barnacle
 - c. Bryozoa Hydroid
 - d. Mussel

- e. Tunicate
- f. Amphipod
- g. Porifera

3.3. Results

3.3.1. Unexpected accident with the paint

As previously stated in the materials section, 5 different paints were prepared. Marine tests were performed for all the samples, but release experiments only could be performed on for 4 of them. The paint containing the PP's Cu⁰ nanoparticles suffered an unexpected violent reaction while it was stored (after the application on the panels for the marine tests and before the application on the panels for the release experiments). As a consequence, the paint was damaged preventing it to be applied on the panels and being tested. An image of the paint and its container aspect after the accident can be seen in Figure 2.

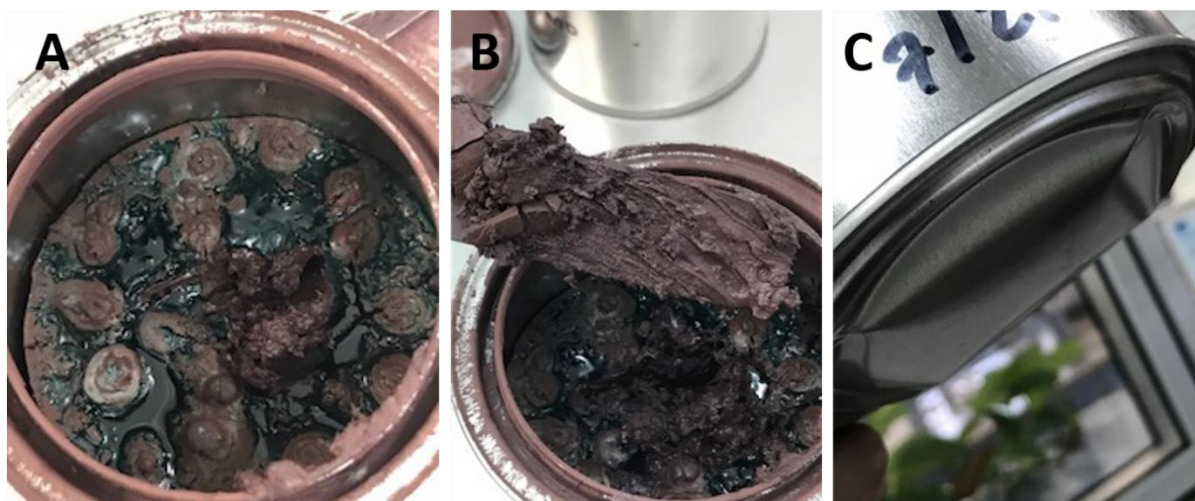


Figure 2 – Paint accident evidences. A) B) Paint aspect; C) Paint container damage.

The spill did not have any bad consequences because the paint volume was small and the container, although it was clearly damaged (Figure 2C), was able to retain the spill. However, accidents like this should be a warning of what could happen if bigger batches are prepared without previous controls and tests in a lower size scale are not performed (as it was done in NANOFASE).

Since the paint could not be tested, efforts were focused in the other four samples. Thus, the following results consider micro-Cu₂O, micro-Cu⁰, nano-Cu₂O and nano-Cu⁰, but not PP's nano-Cu⁰.

3.3.2. ENMs characterization

Electron microscopy and EDX

Micro-Cu₂O particles were initially characterized with TEM. Since they were too thick, SEM was used to complement the results. In Figure 3 electron microscopy images of micro-Cu₂O particles are observed. The sample was mainly formed by aggregated particles.

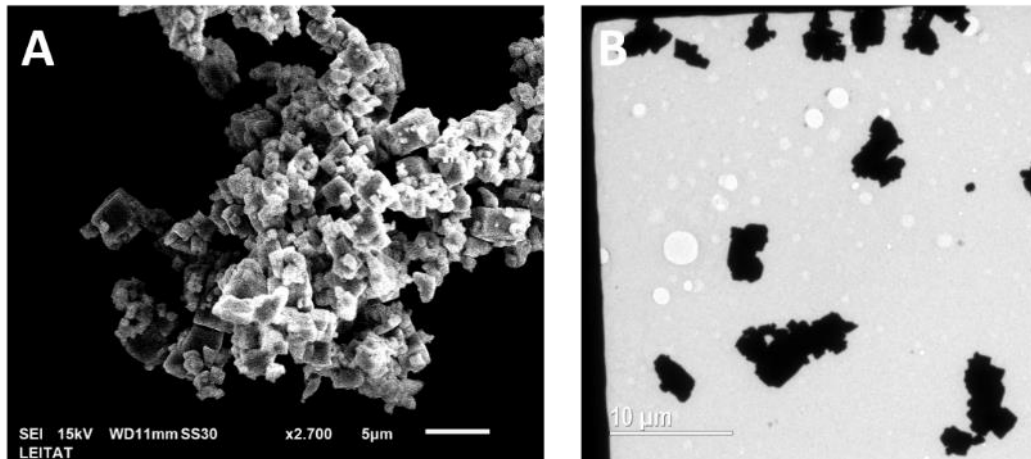


Figure 3 – A) SEM and B) TEM image of micro-Cu₂O particles.

Results from the EDX spectrum performed can be seen in Table 2. The atomic % ratio of Cu and O is around 2, what is what was expected since in the sample there were supposed to be 2 atoms of Cu per 1 atom of O (Cu₂O).

Table 2 – Results of EDX measurement on micro- Cu₂O sample

Spectrum Label	Spectrum (atomic %)
C	17.2
O	26.6
Cu	56.2
Total	100
Cu/O ratio	2.1

Micro-Cu⁰ particles were not as aggregated as micro-Cu₂O ones. Indeed, some individual particles could be seen. In Figure 4 electron microscopy images of micro-Cu⁰ particles are observed.

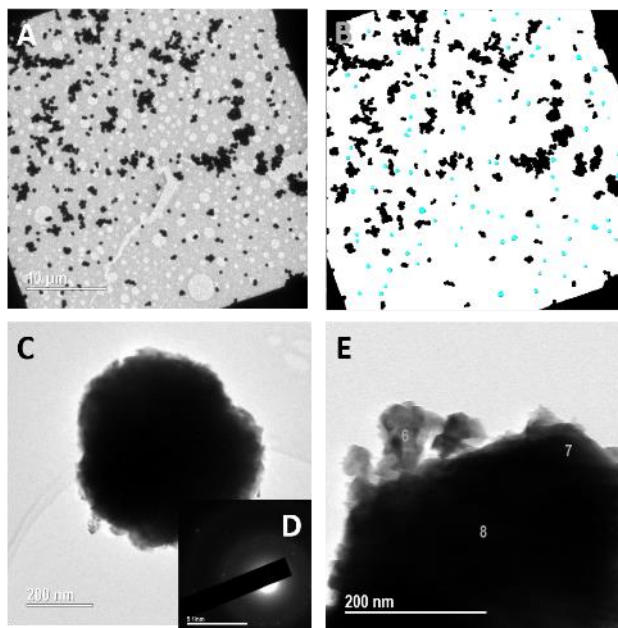


Figure 4 – micro-Cu⁰ A) TEM image; B) TEM image treated with FIJI software; C) TEM image with higher magnification; D) diffraction pattern of the particle shown in “C”; E) TEM image indicating the areas from where EDX measurements were obtained.

From Figure 4C many irregularities are observed in the particles’ surface suggesting that it could be composed by multiple crystals. However, in the diffraction pattern (Figure 4D) only few (not very intense) bright spots are seen. This means that the particle is made up of large crystallites, not many small ones. That is as expected since the particles were supposed to be in the micro range. Otherwise, the diffraction pattern would have been comparable to the one observed in nano-Cu₂O (Figure 5A) and nano-Cu⁰ (Figure 6D). The results of the EDX analysis in the areas indicated in Figure 4E are shown in Table 3. From the Cu/O ratio it is inferred that the outer parts were much more oxidized than the inner ones. Moreover, even in the outer part (spectrum 6), since the ratio is 3, not all the copper was oxidized.

Table 3 – Results of EDX measurements on micro-Cu⁰ particles.

Spectrum Label	Spectrum 6 (atomic %)	Spectrum 7 (atomic %)	Spectrum 8 (atomic %)
C	14.5	13.6	7.0
O	21.5	4.8	1.5
Si	-	-	0.3
Cr	-	-	0.4
Cu	64.0	81.7	90.8
Total	100	100	100
Cu/O ratio	3.0	17.0	62.5

In the TEM images the nano-Cu₂O particles were mostly aggregated. However, some isolated and smaller aggregates like the one shown in Figure 5B were also found. The diffraction pattern shown in Figure 5A suggests that the particle is polycrystalline. Since the particle is made of smaller crystals, which are oriented in different directions, the multiple dots seen in the image are generated.

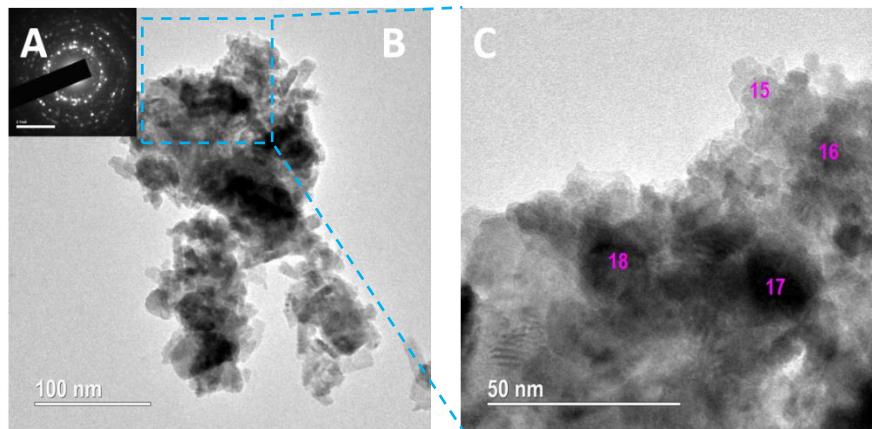


Figure 5 – nano-Cu₂O A) Diffraction pattern; B) TEM image; C) TEM image magnification from image B, indicating the areas from where EDX measurements were obtained

From the EDX analysis, again, can be observed how the outer parts are more oxidized than the inner parts. In this occasion, since the particles should be of Cu₂O, the expected Cu/O ratio would be 2. However, in the outer parts (spectrum 15 and 16) it was around 1, suggesting that Cu₂O was oxidized to CuO (which chemically is a more stable compound). In the inner parts (spectrum 17 and 18) although the Cu/O ratio was not 2 yet, it was higher than in the outer parts. Indeed, a value of around 1.5 would suggest that half of the material was Cu₂O and that the other half has been oxidized to CuO.

Table 4 - Results of EDX measurements on nano-Cu₂O particles.

Spectrum Label	Spectrum 15 (atomic %)	Spectrum 16 (atomic %)	Spectrum 17 (atomic %)	Spectrum 18 (atomic %)
C	62.8	42.5	31.8	37.1
O	19.2	29.0	27.4	26.3
Cu	18.0	28.5	40.8	36.6
Total	100	100	100	100
Cu/O ratio	0.9	1.0	1.5	1.4

Nano-Cu⁰ TEM images, like in the case of micro-Cu⁰, shown particles aggregates with some isolated particles in between. The corresponding images can be observed in Figure 6. From Figure 6D, is proved that the aggregates are made of small crystals, like in nano-Cu₂O sample (Figure 5A).

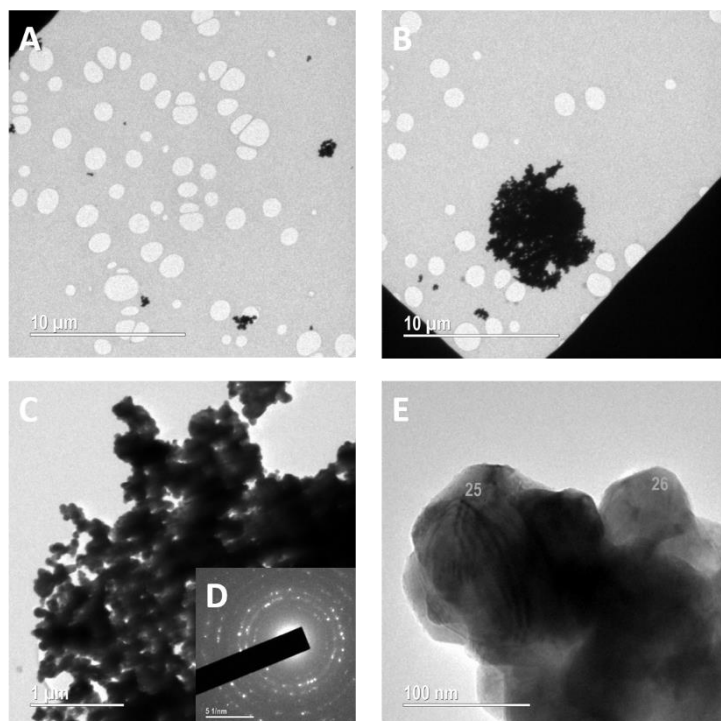


Figure 6 – nano-Cu⁰ A) B) C) TEM image; D) diffraction pattern; E) TEM image indicating the areas from where EDX measurements were obtained.

The EDX results confirmed that the particles boundaries were oxidized. Although, the ratio confirmed that pure Cu⁰ was also present in the sample.

Table 5 - Results of EDX measurements on micro-CuO particles.

Spectrum Label	Spectrum 25 (atomic %)	Spectrum 26 (atomic %)
C	1.1	9.0
O	15.4	25.9
Cr	2.1	1.6
Cu	81.4	63.5
Total	100	100
Cu/O ratio	5.3	2.4

X-Ray diffraction

XRD measurements were used to check if the materials composition were the expected ones. Moreover, it was possible to determine if the materials were oxidized (since oxide structures provide a different diffraction pattern) and in which amount.

The micro-Cu₂O sample diffraction pattern perfectly matched with the Cu₂O diffraction reference pattern from the database (Figure 7). Thus, confirming that the material presented

the expected composition. In the case of micro-Cu⁰ sample, the diffraction pattern obtained in the measurements was very similar to the one in the database for Cu⁰ (Figure 8). However, evidences of Cu₂O were also found. In this case it was estimated that 5% of the material was oxidized from Cu⁰ to Cu₂O. The peaks corresponding to the Cu₂O signal can be observed in blue in the enlarged image. Regarding the nano-Cu₂O sample, a good agreement with the expected composition is observed. However, in this case, copper oxidation from Cu₂O to CuO is observed. According to the XRD results, a 14.5% of the material was oxidized. The nano-Cu⁰ sample also presented a mixture of oxidized and non-oxidized material. As for the micro homologous sample (micro-Cu⁰), the Cu⁰ was oxidized to Cu₂O. This sample was the more oxidized one, with almost one third of the material being oxidized. The results show how the oxidation process is enhanced with smaller particle size, as is expected and is explained by its higher exposed area.

The containers containing the particles used in the different characterizations were opened some months before all the characterization concluded. Most probably, the particles' contact with air is what triggered the oxidation. However, the containers containing the particles introduced in the paints were opened just before their incorporation, which would have limited the oxidation. In any case, these analyses are useful to show what could happen to the particles if they are not properly stored.

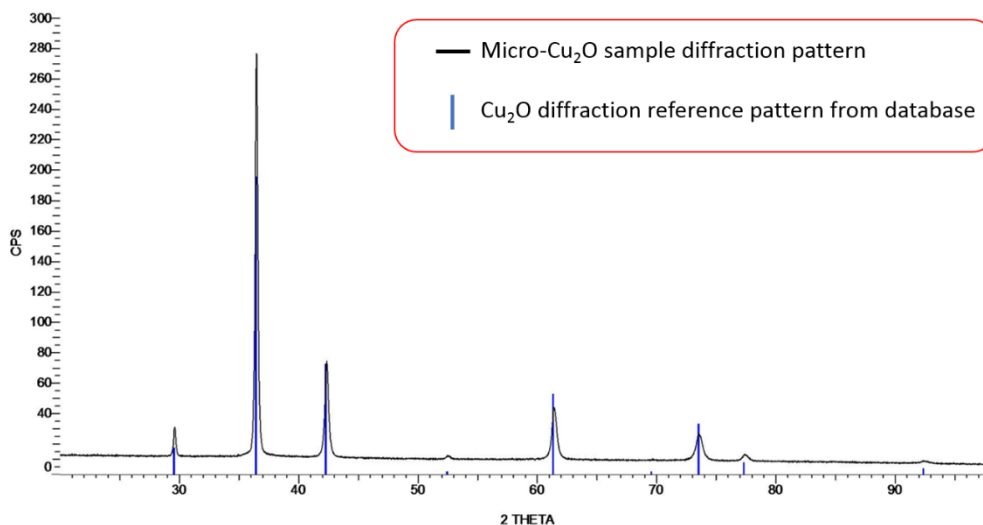


Figure 7 – XRD results of micro-Cu₂O sample

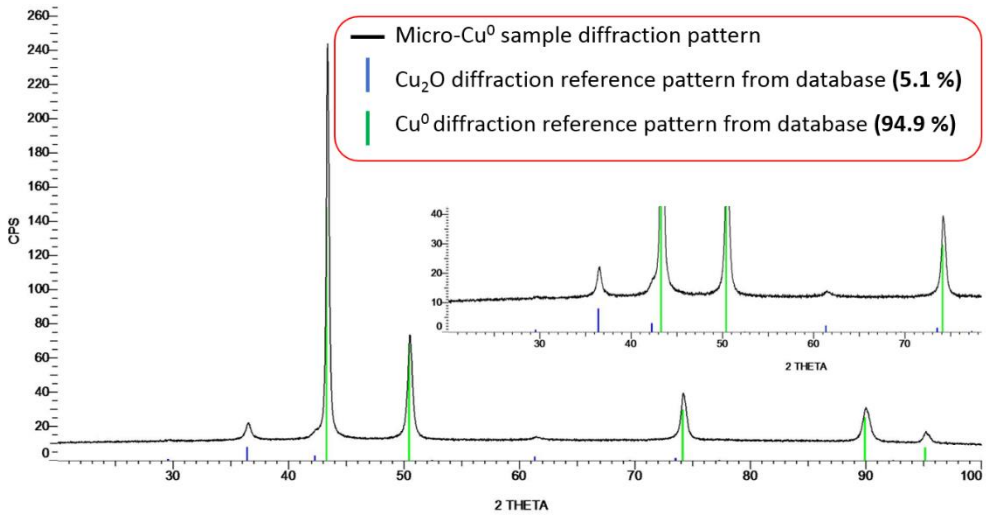


Figure 8 – XRD results of micro-CuO sample

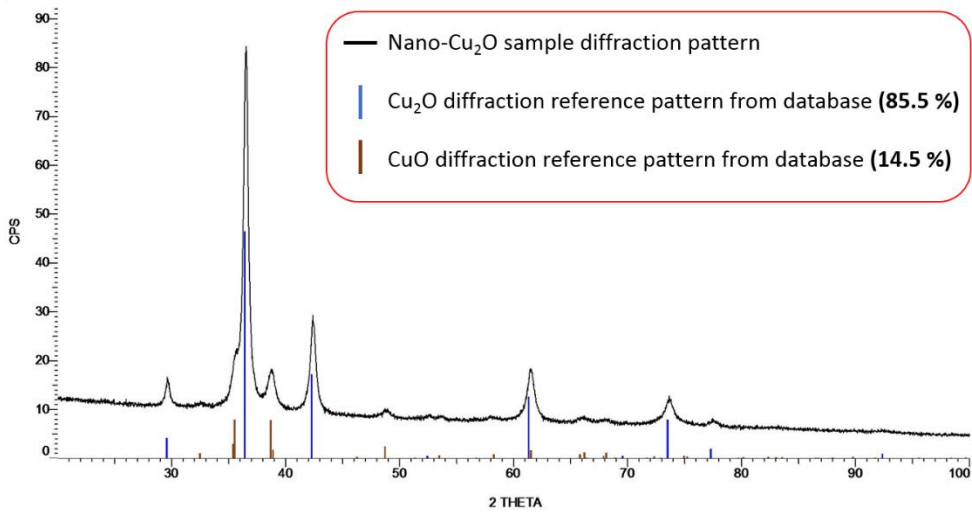


Figure 9 – XRD results of nano-Cu₂O sample

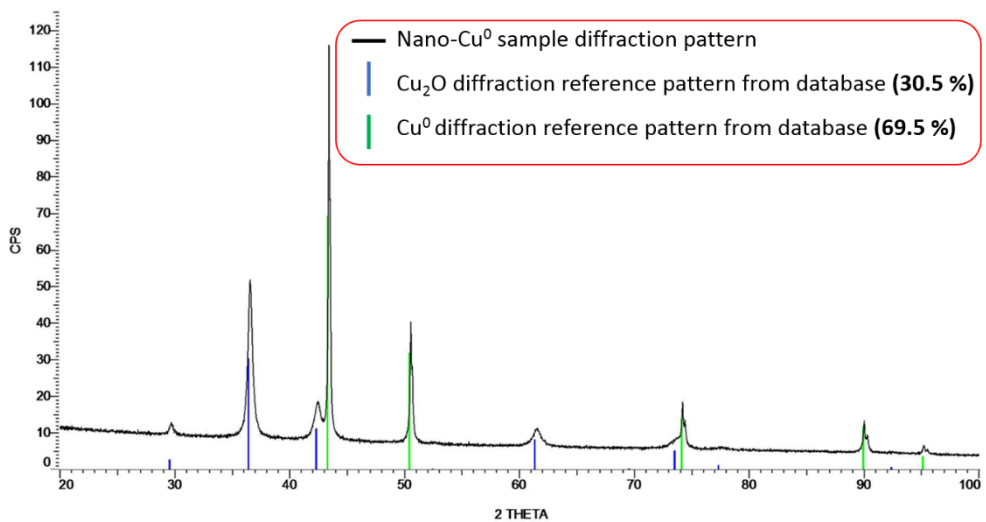


Figure 10 – XRD results of nano-Cu⁰ sample

Brunauer–Emmett–Teller (BET) surface area measurements

The BET results, as expected, shown a reduced surface area for the samples with bigger particles as expected.

Table 6 – BET measurements results

SAMPLE	SURFACE AREA (m ² /g)
Micro-Cu ₂ O	6.1
Micro-Cu ⁰	3.9
Nano-Cu ₂ O	22.4
Nano-Cu ⁰	11.4

3.3.3. Paints characterization

Inductively Coupled Plasma Mass Spectrometry

Theoretically, all the paints should have the same Cu and Zn concentration. However, paints formulation processes are quite complex, this is way small deviations are observed among samples. However, the deviation among replicates (3 per each sample) is quite small, the Relative Standard Deviation (RSD) being between 0.4% and 3.3%, what suggest that the particles were homogeneously dispersed, distributing similar amounts of Cu and Zn within the paint.

Table 7 – ICPMS paints measurements results

PAINT SAMPLE	Cu concentration (wt%)				Zn concentration (wt%)			
	AVERAGE	±	ST. DEV	%RSD	AVERAGE	±	ST. DEV	%RSD
Micro-Cu ₂ O	37.11	±	0.16	0.4	7.78	±	0.04	0.5
Micro-Cu ⁰	41.61	±	0.53	1.3	7.79	±	0.16	2.1
Nano-Cu ₂ O	33.53	±	0.20	0.6	7.97	±	0.13	1.7
Nano-Cu ⁰	36.85	±	0.95	2.6	9.32	±	0.31	3.3
PP_Nano-Cu ⁰	32.15	±	1.07	3.3	5.68	±	0.15	2.7

Electron microscopy and EDX

All the paints were observed using scanning electron microscopy. Both secondary electrons (SE) and backscattered electron (BSE) imaging modes were used together with EDX. In secondary electron mode the microscope generates the image with the electrons that are ejected from specimen atoms by inelastic scattering interactions with beam electrons, which originate from the sample surface providing a good surface resolution. In backscattered electron mode the microscope generates the image with high-energy electrons originated from the electron beam that are reflected (or back-scattered) by elastic interactions with specimen atoms. Since heavy elements (high atomic number) backscatter electrons more

strongly than light elements (low atomic number), and thus appear brighter in the image, BSE images are used to detect contrast between areas with different chemical compositions [3].

As observed in Table 7, Cu-based compounds represent a high percentage of the total paint mass. As a consequence, in the SEM images the Cu-based particles were very easily located since they covered most of the area. The distribution of the particles was uniform in all the areas of the paints observed, meaning that the dispersion method used in the preparation of the paints was optimised for a homogeneous distribution of the particles in the paints.

In the paint containing micro-Cu₂O particles both Cu and Zn were detected through EDX analysis. What could be concluded from the results was that ZnO presented a cubic shape while Cu₂O particles were spherical. Moreover, ZnO crystals were isolated and had a bigger size, while Cu₂O particles were smaller but formed big aggregates. Organic material (C and O) covering the particles was also detected.

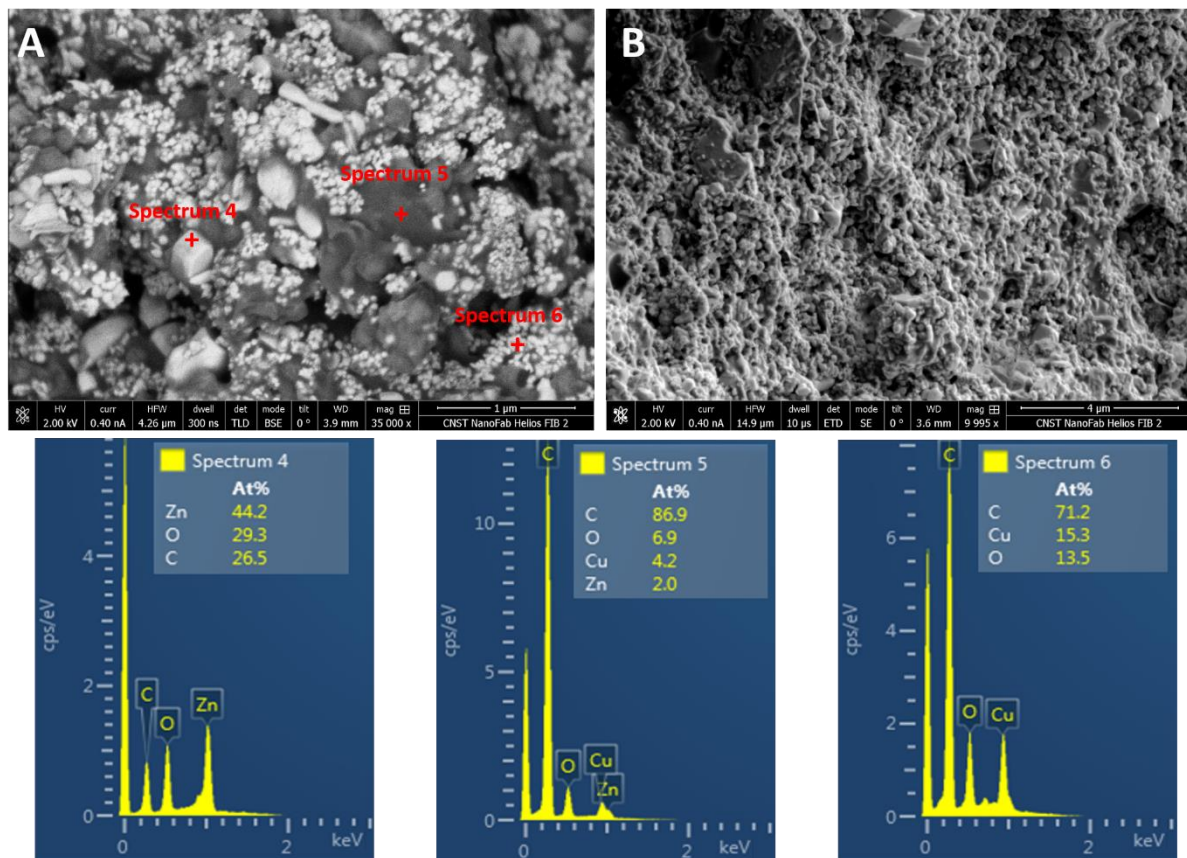


Figure 11 – SEM image and corresponding EDX spectrum of the paint containing micro-Cu₂O particles. A) Back-scattered electrons mode image; B) Secondary electrons mode image.

For the paint containing micro-Cu⁰ a similar particle distribution was observed. The images showed large aggregates of Cu particles. As seen in Figure 12A the particles size was around 470 nm. In Figure 12B, since the back scattered mode was used, the contrast between those metallic particles more exposed in the surface and those covered by an organic layer is easily recognized. In the images shown in Figure 12 wire-like structures all over the area studied are

more prominent. As proved below in Figure 14, these structures correspond to one of the compounds present in the formulation of the paints.

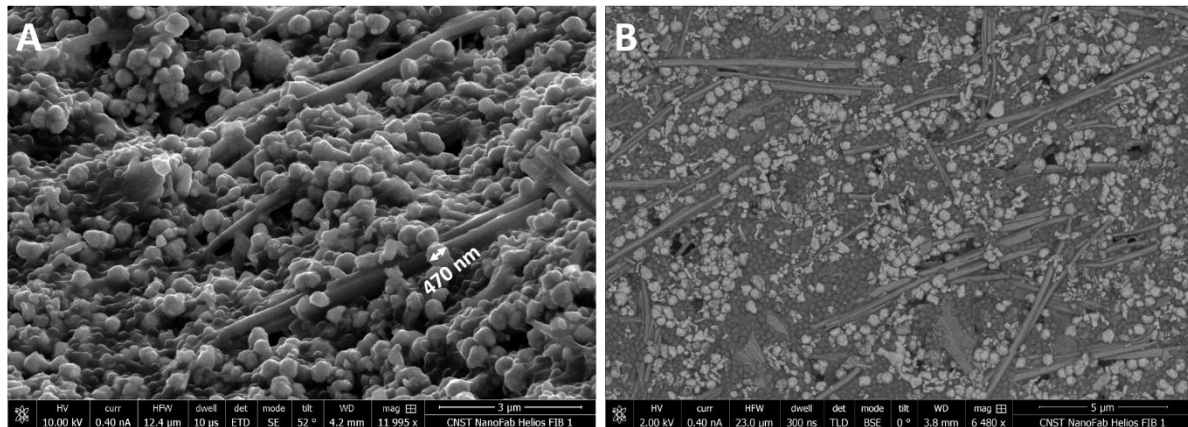


Figure 12 – SEM image of the paint containing micro- Cu^0 particles. A) Back-scattered electrons mode image; B) Secondary electrons mode image.

Again, for the nano- Cu_2O paint a similar distribution was found. However, as can be seen in Figure 13A, when images at higher magnifications were obtained, particles around 50 nm were observed. Most of them were very aggregated, but others as the one pointed with the arrow are isolated.

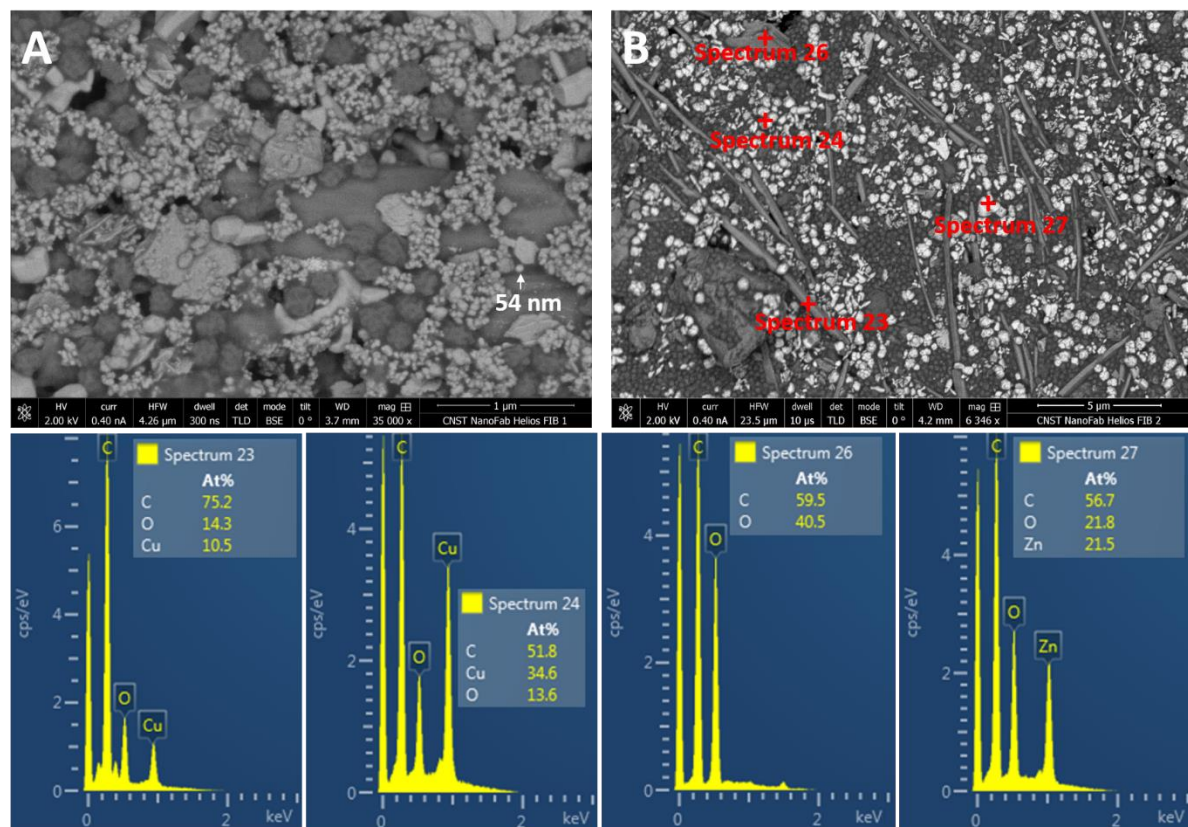


Figure 13 – SEM image and corresponding EDX spectrum of the paint containing nano- Cu_2O particles. A), B) Back-scattered electrons mode image.

The EDX spectrums provided similar conclusions to the ones obtained in the EDX analysis of the other paints. Cu (spectrum 24) is the main component in the paints presenting a rounded shape with very aggregated particles. ZnO (spectrum 27) crystals are cubic or rectangular shaped and were present in a lower amount than Cu-compounds, what was expected since the Zn concentration is lower than for Cu (Table 1 and Table 7). Organic compounds (spectrum 26), as shown by a high C peak and O are also detected. What was not previously measured was the composition of the wire-like structures. From the EDX analysis (spectrum 23) it was concluded that they were also Cu compounds. Although for both the contrast in the back scattered mode image and the EDX measurements the Cu presence was not so intense as in the particles. Thus, it was inferred that from the components of the paints (shown in Table 1), it was likely to be Cu-Pyrithione. To confirm it SEM images of Cu-Pyrithione were obtained. As seen in Figure 14 Cu-Pyrithione presents a wire-like shape, suggesting that it is the compound observed in the paints.

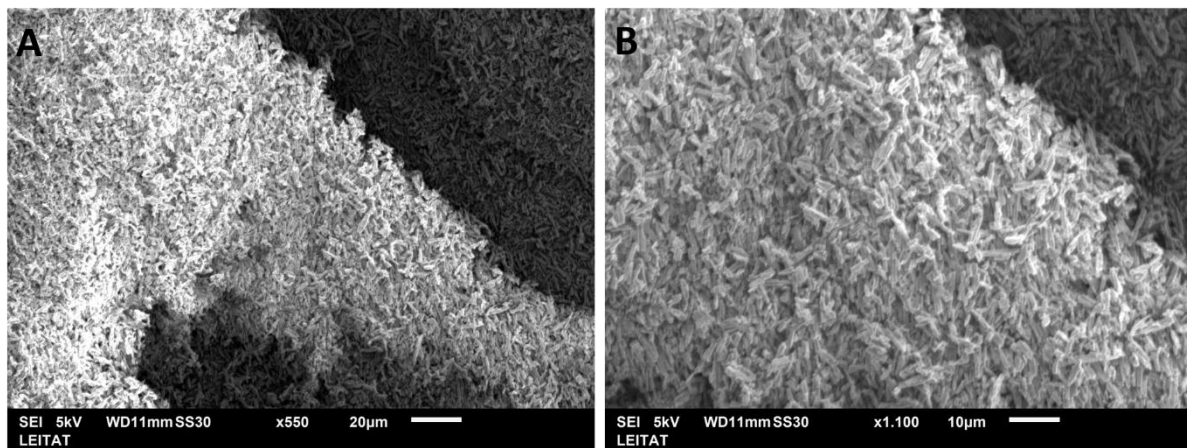


Figure 14 – Cu-Pyrithione SEM image.

In the paint containing nano-Cu⁰ particles, as in the other paints, a distribution of aggregated Cu particles with entangled Cu pyrithione was also observed.

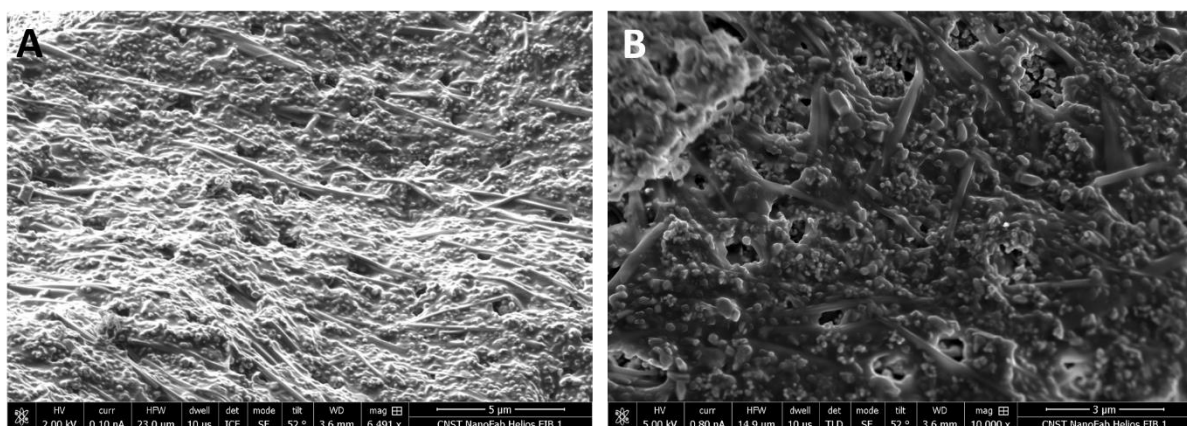


Figure 15 – SEM images of the paint containing nano-Cu⁰ particles. A), B) Secondary electrons mode image.

3.3.4. Released materials

Marine water

The pH of the marine water solution along the release test is shown in Figure 16. Each series represents one replicate. The names reflected in the legend refer to the kind of Cu-based particles that were included in the paint and the panel number inside the solution. As previously mentioned, in each vessel (replicate) two panels were included. Since there were 4 different types of paints (i.e. $n\text{Cu}^0$, μCu^0 , $n\text{Cu}_2\text{O}$, $\mu\text{Cu}_2\text{O}$), each one with three replicates, there were a total of 12 series. As the graph shows, the values fluctuated a bit but always remained in a pH range between 7.6 to 8.2. For all the samples the behaviour was similar, there was not any increase/decrease pattern exclusive for a single kind of sample. Thus, the conclusion obtained from the pH analysis is that pH is maintained constant throughout the experiment with a value around 8, which is the value expected for marine water.

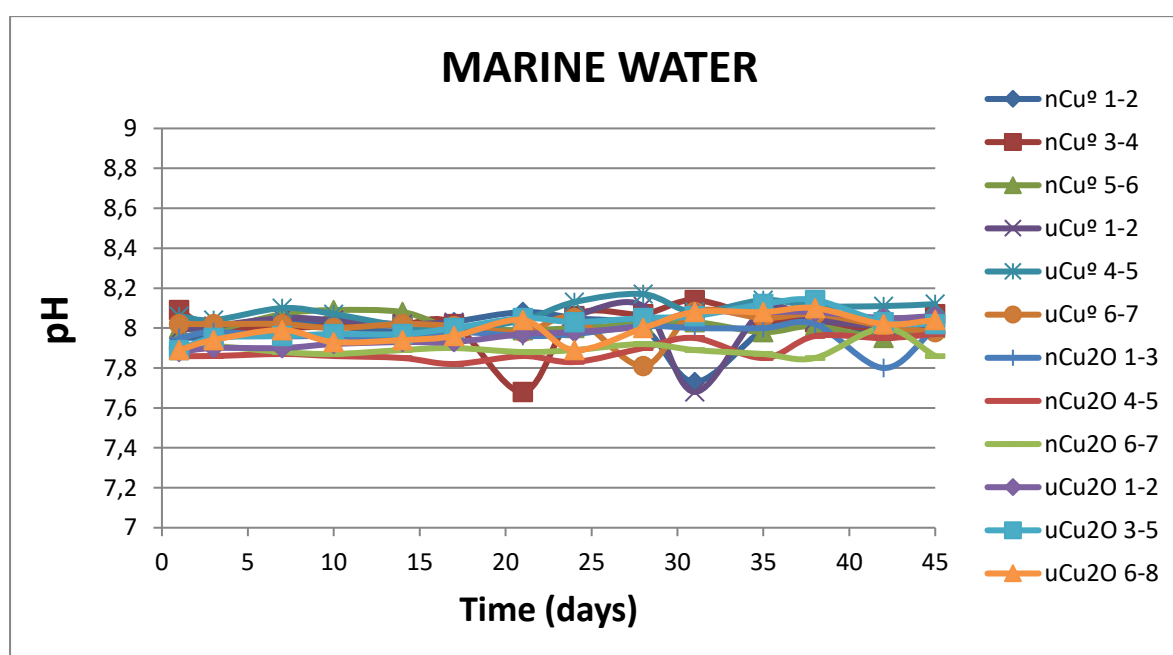


Figure 16 – pH value of the release experiment along time in marine water.

The copper and zinc concentrations released to marine water and measured by ICPMS are shown in Figure 17. Each graph corresponds to a paint, which includes the average value and the standard deviation (error bars) from the three replicates.

The paints containing micro- Cu_2O and micro- Cu^0 presented a similar behaviour, for this reason the effects observed will be explained together. For both samples the copper (red line) increased along time during the first half of the experiment. However, around the second half, instead of continue increasing, the concentration decreased. The expected release was a continuous increase in concentration. A decrease was not expected since the water is not replaced, so any Cu is removed from the solution. However, the concentration decrease was observed in both paints. This effect is probably due to the copper reaction with the marine salts, which tend to form aggregates and to stick to the beaker glass and to the paint panel surface. Thus, not being available in solution and not being possible to collect them for the

ICPMS analysis. As is shown in Figure 18, the salts formation could be observed by eye. The more days the paints were in the water, the greener the beakers glass/panels became. From the second half of the experiment a remarkable increase in the deviation among replicates was also observed. Again, this effect was attributed to the salts formation and aggregation, which differed among replicates. The Zn release (grey line) agreed with the expected release behaviour, a continuous increase along time or an increase and stabilization. According to the results, a high release of Zn occurs in the beginning and then this concentration is maintained, meaning that release does not occur or it occurs in a much smaller extent.

In the case of nano-Cu₂O paint the copper release presented a constant increase. Values among replicates did not differ a lot resulting in low deviations. The zinc presented a high release in the beginning and then the concentration was maintained. In this case, values

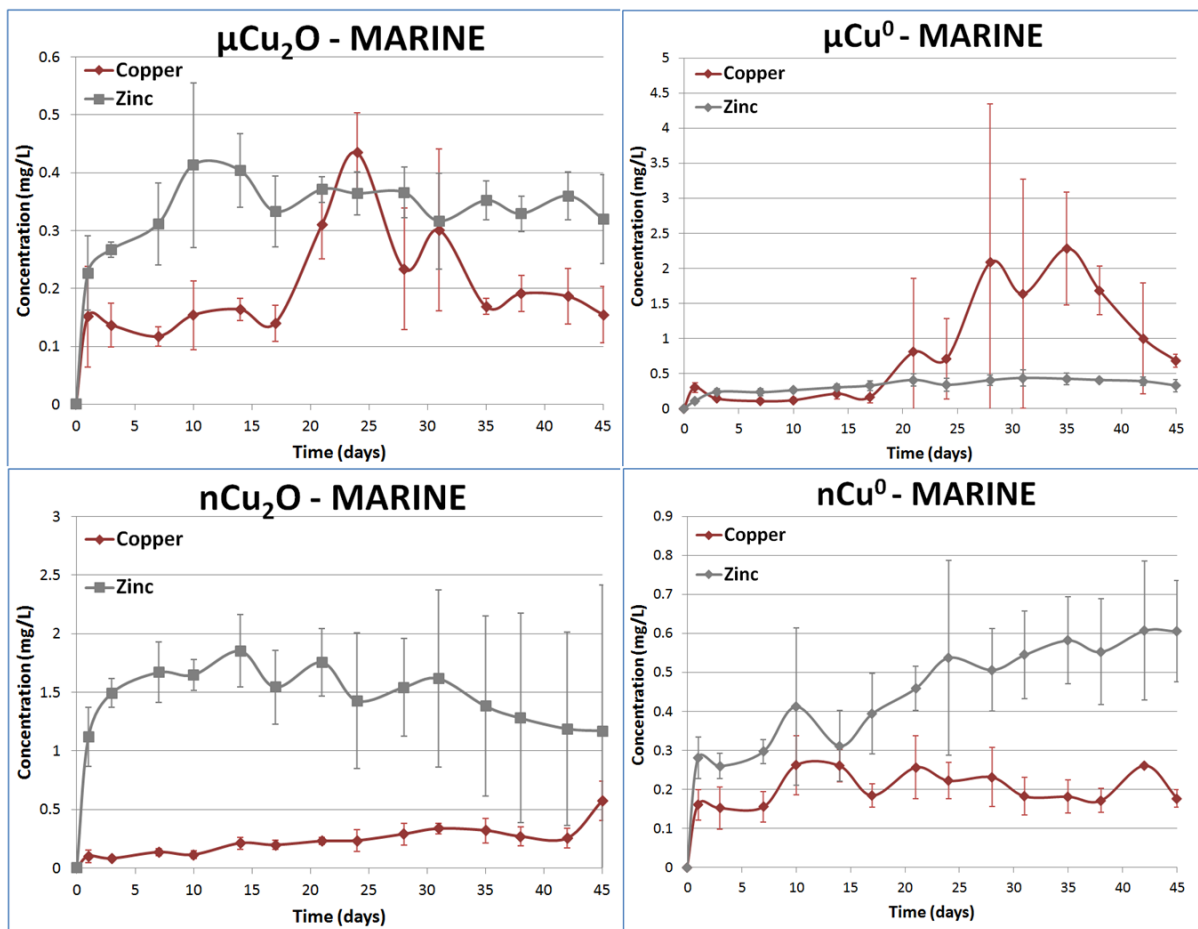


Figure 17 – Copper and Zinc concentration in marine water released from the paints along the experiment. Y axis (concentration (mg/L)) is different in each graph since it was adapted to show a detailed representation of the release rates along time. Error bars represent the standard deviation among the three replicates.

among replicates differed a lot, especially in the second half of the experiment. In nano-Cu⁰ paint the copper release increased in the beginning and then it was maintained along the experiment. Some decrease in concentration was also observed, probably due to the same effect explained for micro-Cu₂O and micro-Cu⁰, but in this case the differences in concentration were not so big. The Zn presented a high release in the beginning and then it kept increasing at a slower rate, but it did not stop increasing.

In Figure 18 the copper salts formation and their appearance is shown. Micro-Cu⁰ and nano-Cu⁰ were the paints presenting a more intense colour, although in micro-Cu₂O and nano-Cu₂O salts aggregates were also observed. As shown in the images some aggregates stuck in the panel surface, others in the glass and others remained in suspension due to the stirring force.

Eventually, some aggregates were deattached by the stirring action moving them to the solution. The longer the paints were immersed in water, the higher the release and the higher the aggregates formation. That is why depending on the replicate the concentration detected when the sample was collected could vary a lot depending on how many aggregates were attached and how many suspended and available to collect.

The characteristic green colour of the compound suggests that it was hydrated copper carbonate. In order to confirm it, an FT-IR analysis was performed on the compound. As the spectra shows in Figure 19, the peaks matched with the expected composition of copper carbonate (Cu₂CO₃(OH)₂) also known as “Malachite”.

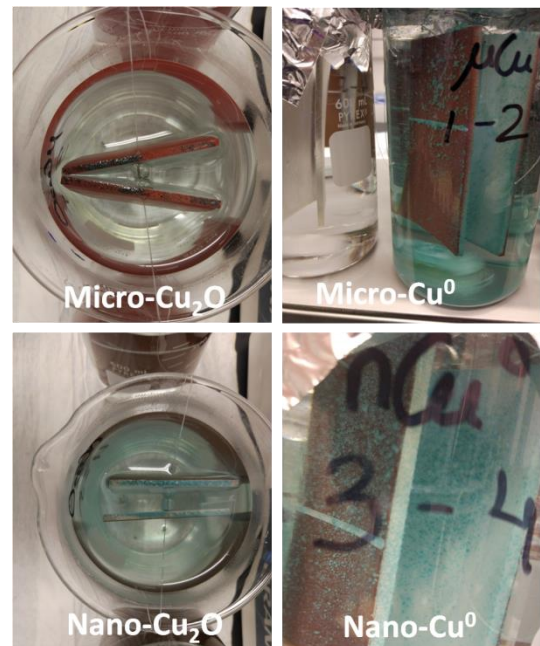


Figure 18 - Aspect of the release waters and paints in the experiment showing the formation of the salts aggregates

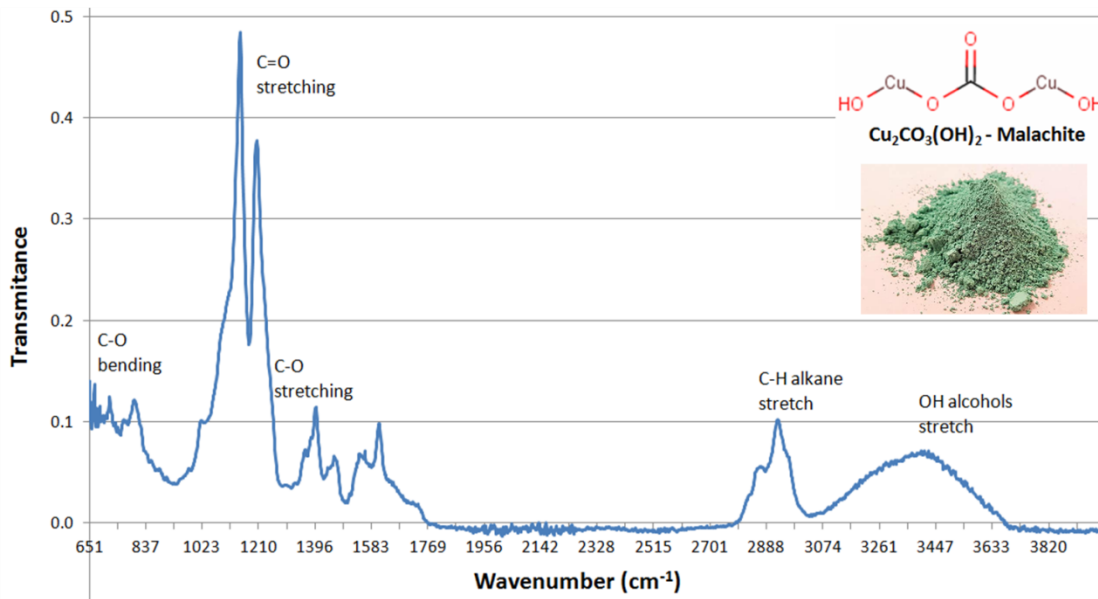


Figure 19 – FT-IR spectra of the aggregates formed during the paints release experiment in marine water.

Ultrapure water

The pH values in ultrapure water followed a similar pattern as in marine water but at a lower pH. pH was quite stable along the whole experiment, no significant deviation was observed.

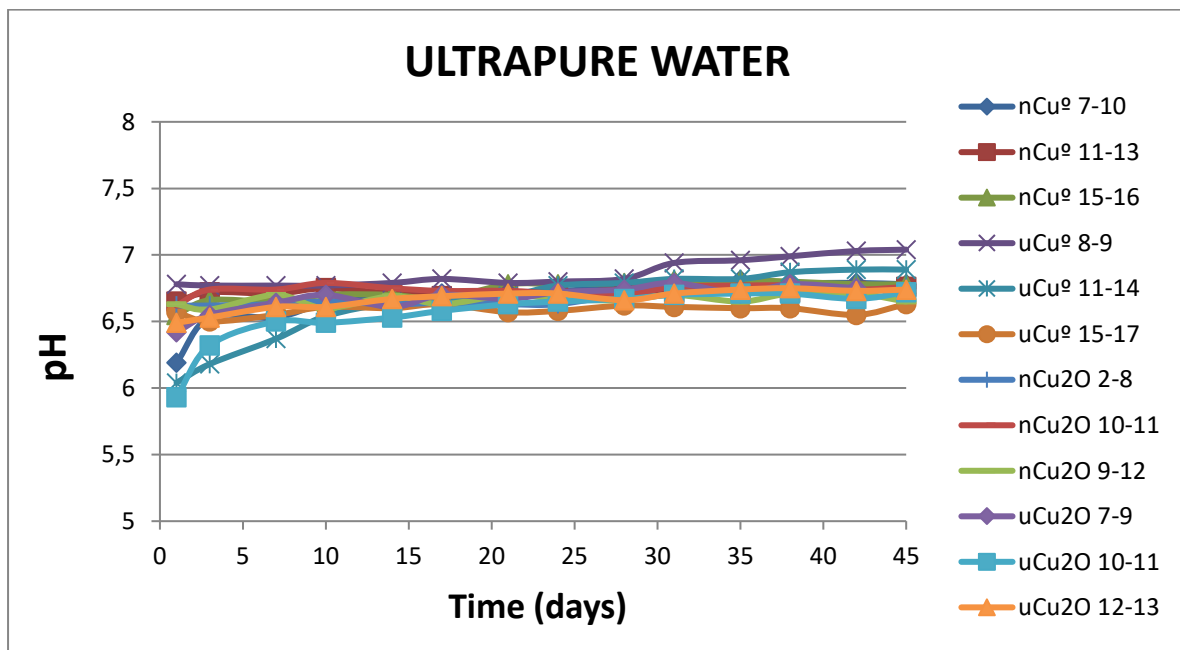


Figure 20 - pH value of the release experiment along time in ultrapure water.

The copper and zinc concentrations released to ultrapure water and measured by ICPMS are shown in Figure 21. Release in ultrapure water presented a similar behaviour in the different paints. In all the cases the Zn concentration was much higher than for Cu since the first days of the experiment. For a more detailed representation of the copper release behaviour a separate Figure (Figure 22) just containing the copper release has been included. For easier

interpretation look at

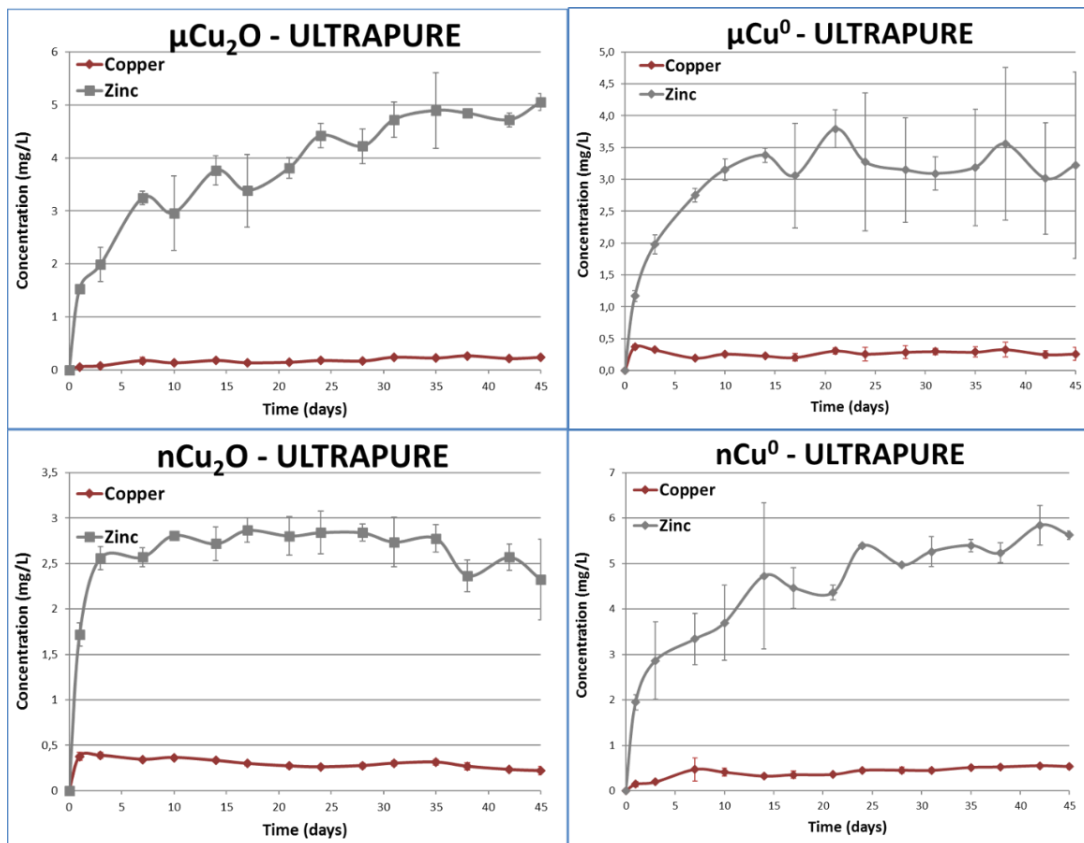


Figure 21 for Zn and to Figure 22 for Cu.

In micro- Cu_2O sample, the Cu concentration increased during the whole experiment, although the release rate (curve slope) was higher in the beginning. At the end of the experiment the copper concentration in the release solution was around 0.5 ppm. The Zn concentration, like the Cu concentration increased throughout the whole experiment reaching the highest value the last day (45th day), with a concentration of 5 ppm, one order of magnitude higher than for copper. In the case of micro- Cu^0 the copper concentration increased until the first time point (1 day) and then it decreased until it oscillated around a 0.25 ppm concentration. As in the marine water experiment, some released copper (in this case without salts) stuck to beaker walls, the stirrer and the panels, diminishing the concentration in water. As shown in Figure 23, specially for micro- Cu^0 , at the end of the experiment a high amount of copper was found stuck in the material used for the experiment. After two weeks the copper concentration started to present remarkable variations among replicates (high error bars), suggesting that the behaviour was not reproducible. Zinc concentration increased during the first two weeks reaching a stable value around 3.5 ppm. Like the copper concentration, the deviation among replicates also increased after two weeks. In nano- Cu_2O sample the copper release behaviour was very similar to micro- Cu^0 .

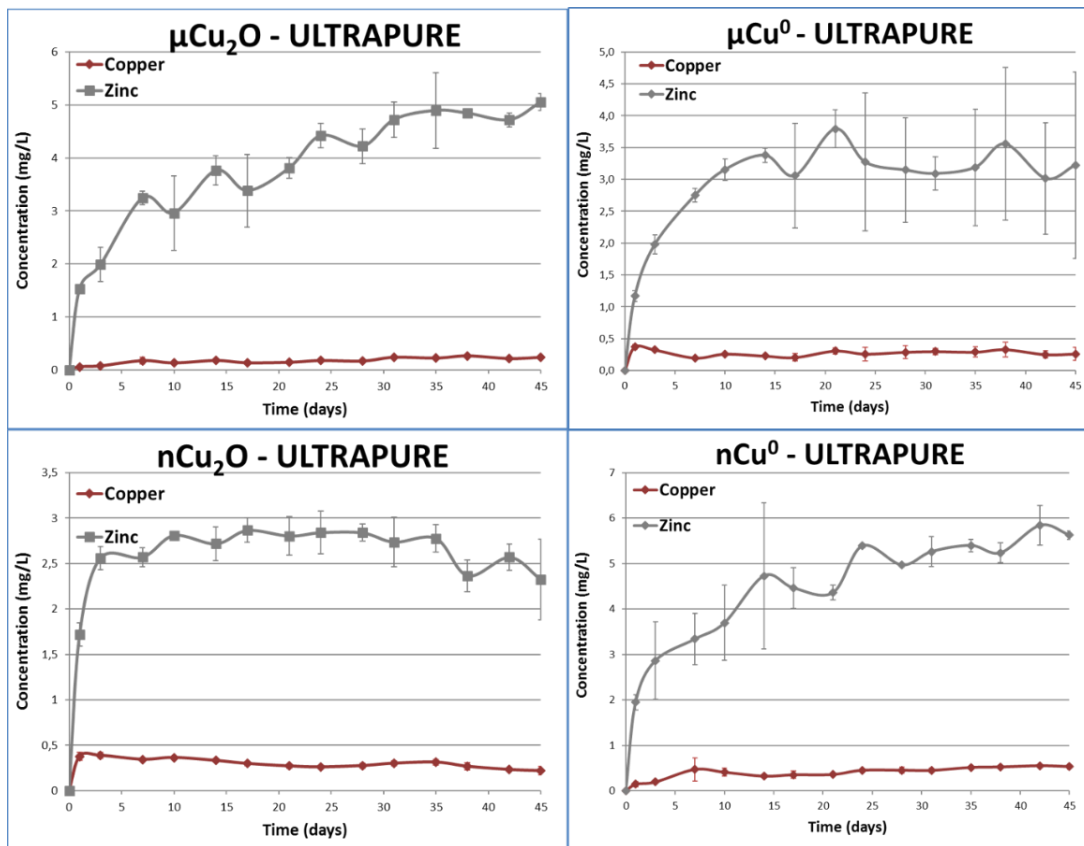


Figure 21 - Copper and Zinc concentration in ultrapure water released from the paints along the experiment. Y axis (concentration (mg/L)) is different in each graph since it was adapted to show a detailed representation of the release rates along time. Error bars represent the standard deviation among the three replicates.

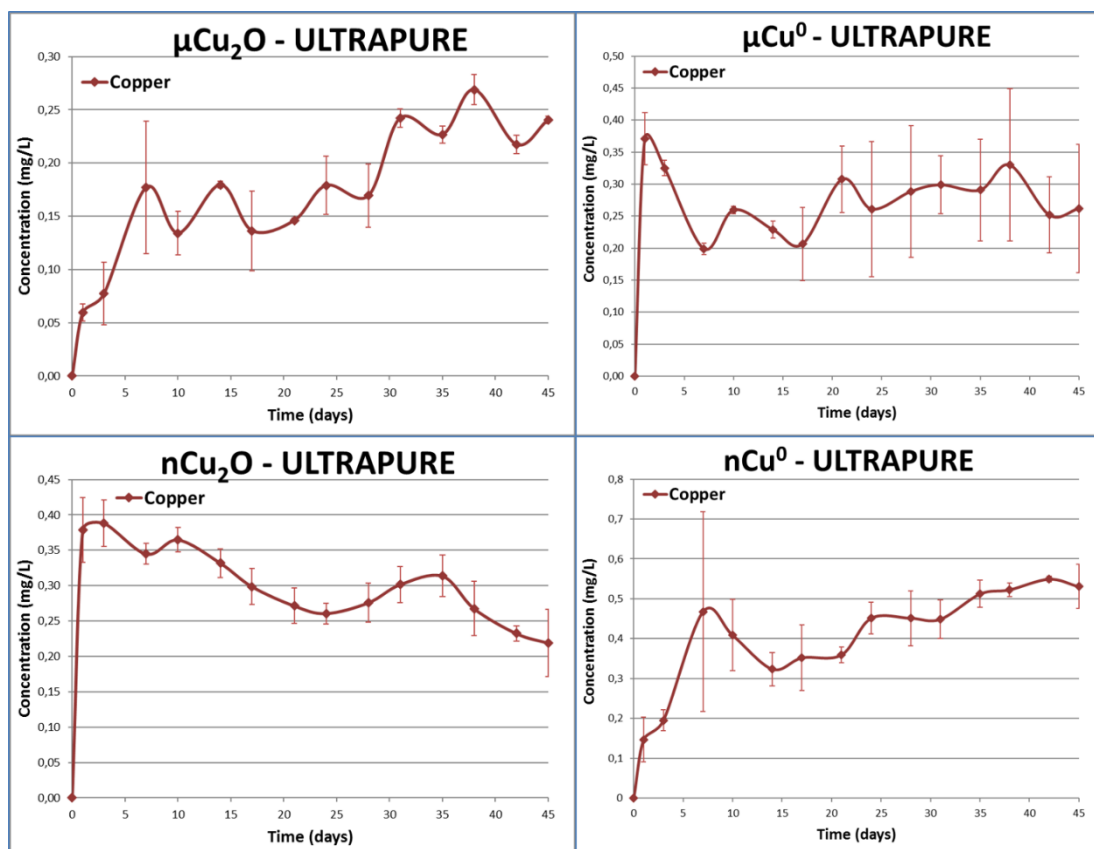


Figure 22 – Copper concentration in ultrapure water released from the paints along the experiment. Y axis (concentration (mg/L)) is different in each graph since it was adapted to show a detailed representation of the release rates along time. Error bars represent the standard deviation among the three replicates.

A high release occurred the first day reaching a concentration around 0.4 ppm and then it decreased down to 0.2 ppm. The zinc concentration also increased during the first days but after, it was maintained stable around 2.7 ppm. In nano-Cu⁰ paint the copper concentration increased gradually along all the experiment, reaching a concentration around 0.5 ppm at the end. Zinc concentration, as well as for copper, gradually increased along all the experiment reaching a final value of 5.5 ppm. For both copper and zinc, the concentration increased faster at the beginning.

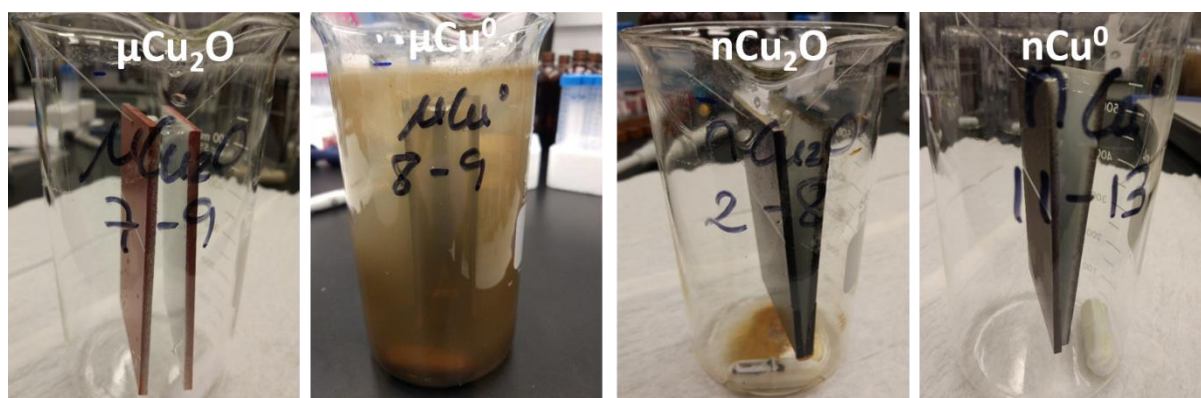


Figure 23 – Empty beakers containing the stirrer and painted panels after 45 days of release experiment in ultrapure water. As shown in Figure 23, the micro-Cu⁰ sample was the one where a higher amount of copper was attached in the experiment material (beaker walls, stirrer and paint panels). It would explain the copper concentration decrease along time of micro-Cu⁰ presented in Figure 22. The same occurs for nano-Cu₂O, where copper deposition was also observed. The paints exhibited an unexpected high release, which ended up in attachment to the surfaces. For micro-Cu₂O (currently the commercial paint) and nano-Cu⁰ copper deposition was not observed. Most probably, for this reason, concentration decrease with time was not observed.

Release rates calculation

Since the panels were weighed before and after the paint application, the exact amount of paint on each panel was known. From the paints ICPMS analysis the amount of copper and zinc was measured (Table 7), so it was possible to calculate the total amount of zinc and copper on each panel before the experiment. From the release waters ICPMS results, the released Cu and Zn in both marine and ultrapure water were calculated. Comparing the initial amount of Cu and Zn with the concentrations in released waters, release rates were calculated, these are shown in Table 8.

Table 8 – Cu and Zn release rates in marine and ultrapure water for all the samples

PAINT SAMPLE	MARINE WATER		ULTRAPURE WATER	
	Cu release rate (%)	Zn release rate (%)	Cu release rate (%)	Zn release rate (%)
	AVERAGE ± ST. DEV			

Micro-Cu₂O	0,00043% ± 0,00010%	0,00195% ± 0,00058%	0,00024% ± 0,00005%	0,02135% ± 0,00124%
Micro-Cu⁰	0,00203% ± 0,00016%	0,00208% ± 0,00084%	0,00028% ± 0,00013%	0,01509% ± 0,00070%
Nano-Cu₂O	0,00050% ± 0,00029%	0,00681% ± 0,00915%	0,00034% ± 0,00029%	0,01041% ± 0,00903%
Nano-Cu⁰	0,00026% ± 0,00004%	0,00235% ± 0,00101%	0,00050% ± 0,00004%	0,02103% ± 0,00094%

In both media, Zn generally gave higher release rates than Cu, in some cases being 2 order of magnitude higher. Higher release rates were observed in ultrapure water compared with marine as shown by the ICPMS results, although as commented before, in marine water the salts precipitation could have decreased the amount of ions available in solution.

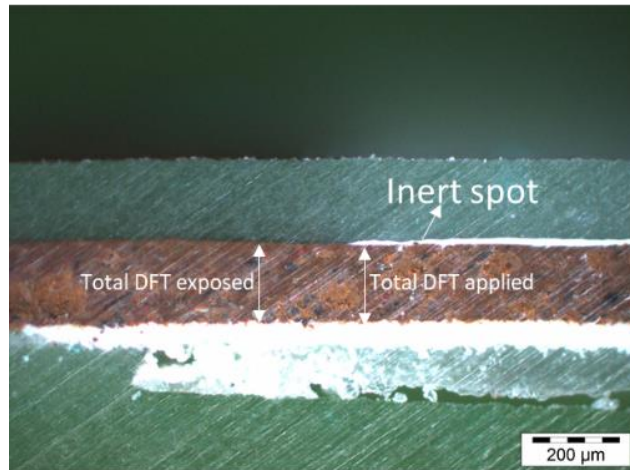
From all the results, the highest release measured was 0.02% and the lowest was 0.0002%, both for micro-Cu₂O sample immersed in ultrapure water. Although general trends were observed (the ones described above), as in this case, the same sample in the same medium can present very different release behaviours for copper and zinc, for this reason it is important to measure each specific case to determine the corresponding release rates.

The antifouling paints were investigated by optical microscopy. The intention was to determine the decrease in the DFT for the different panels after performing the release experiments and to see if some differences in the polishing mechanism or the leached layer could be found. Unfortunately, a clear decrease in DFT in any of the paints containing the different types of copper evaluated could not be determined. Most probably because the simulation time is very short compared with the typical use life of the paints (around 5 years).

Figure 24 (a) and (b) show the cross section of the paints containing Cu (I) nano and Cu (I) micro, as example. As shown in the images, the DFT of the paint below the inert point (reference white line) was equal to the DFT of the paint that was exposed to water, indicating that the paint did not experience any polishing. A leached layer was observed indicating that copper was released, but it was very difficult to evaluate accurately the microns formed.

Same results were found between different paints or exposure media (sea water and distilled water). The other paints containing the other types of copper were also measured, but images showing the cross – section are not included in the report because no difference was observed.

(a) Cu(I) nano



(b) Cu (I) micro

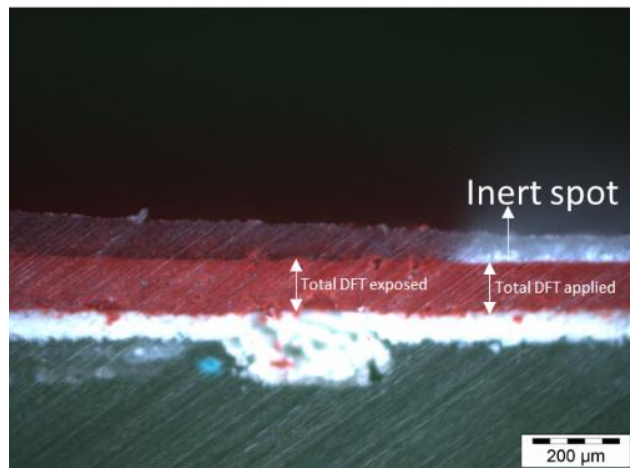


Figure 24 – Cross-section of the paints on the panels showing the paint thickness (DFT) and the inert spot (reference white line).

3.3.5. Tests in marine facilities

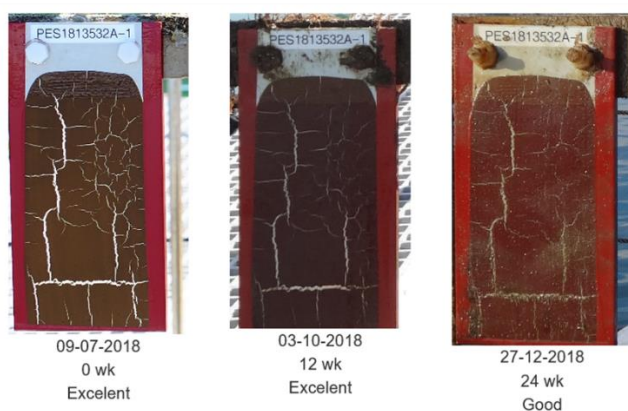
Figure 25 shows a comparison of antifouling performance between antifouling paints containing micro-Cu₂O (commercial paint) and nano-Cu₂O after 4 months immersion. The evolution of the fouling on the surface was very similar for both types of copper until 3 months of immersion. Then, a slightly better performance was observed for the paint containing nano-copper. The short algae observed was chlorophyll (green algae).

Cu (I) micro



Slime > 50% of coverage
algae coverage > 50%
Animals = 0%

Cu (I) nano



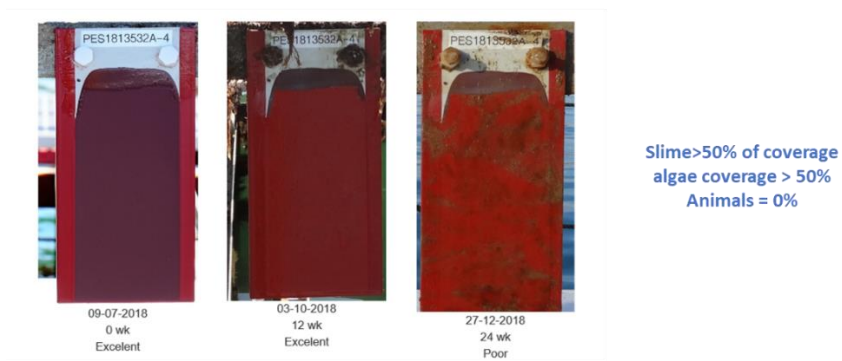
Slime > 50% of coverage
6% < algae coverage < 25%
Animals = 0%

Figure 25 – Panels with micro-Cu₂O and nano-Cu₂O paints after 12 and 24 weeks immersed in marine water.

Figure 26 shows a comparison of antifouling performance between antifouling paints containing micro-Cu⁰ and nano-Cu⁰ after 4 months immersion. The nano-Cu⁰ was incorporated into the paint in two ways: solid phase (powder) and dispersed in ethylene glycol solution (provided by PP). In Figure 26, the paint containing nano copper dispersed in ethylene glycol is labelled as Cu (0) nanodispersion.

A similar antifouling behaviour was observed for paints containing Cu (0) micro and Cu (0) nano after 4 months of immersion. For nanodispersed copper (0) the micro-organisms appearance started earlier, but after 4 months, the antifouling performance seemed to be equal for all the paints regardless of size and if the copper was previously dispersed or not.

Cu (0) micro



Cu (0) nano



Cu (0) nanodispersion

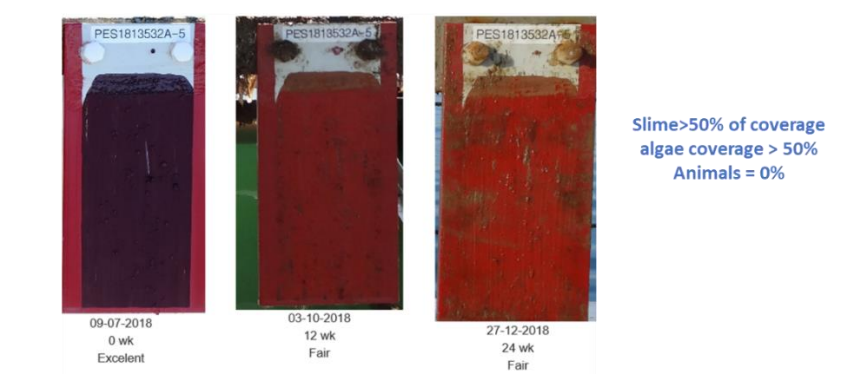


Figure 26 - Panels with micro-Cu⁰, nano-Cu⁰ and nano-Cu⁰ (from PP) paints after 12 and 24 weeks immersed in marine water. A blank panel (uncoated), shown in Figure 27, was also immersed to analyze the fouling pressure in the Mediterranean Sea. In this case, different types of animals, such as tube worms, barnacles, bryozoa Hydroid and tunicates and green algae were observed.



Figure 27 – Blank (uncoated) panel after 12 and 24 weeks immersed in marine water.

3.4. Conclusions

The raw particles composition was measured by XRD and EDX and in all the cases the expected composition was detected. Oxidation was observed on the particles surface as expected. According to the tests in marine facilities the best performing paint is the one containing nano-Cu₂O, compared with the commercial one (micro-Cu₂O). However, the formulation requires optimization since after the application cracks appeared.

In marine water the copper ions reacted with the marine salts forming hydrated copper carbonate, which tended to form aggregates and stuck to the beaker glass surface and to the paint panel surface. In ultrapure water, especially for micro-Cu⁰ and nano-Cu₂O, some copper was also stuck to the beaker glass and paint panel.

Release rates ranged from 0.0002% to 0.02% with Zn generally presenting a higher release rate than copper.

4. INOTEX: curtains with photocatalytic activity

4.1. Introduction

The present case study consists of polyester (PES) fabrics containing photocatalytic nanoTiO₂ to be used as curtain material. From the application point of view, the interest of the case study remains in that the incorporation of nanoTiO₂ provides photocatalytic activity to the textile. This property provides the curtain with the ability to degrade volatile organic compounds (VOCs) or other air contaminants that surround the fabric improving the air quality around the curtain.

From the environmental point of view potential TiO₂ NPs release from textiles should be investigated. In this case, the activity of most concern is washing the curtains, which could lead to nanomaterials exposure to the environment via wastewater treatment works. To assess this potential risk, household-washing simulations of the nano-enabled curtains in controlled laboratory conditions were performed following an adaptation of a standardized protocol (ISO 105-C06:2010 [4]) with the aim to determine TiO₂ NPs release rates and forms.

4.2. Materials and methods

The TiO₂ NPs were incorporated in the textile together with a wetting agent (Tanawet RC-N) and a siloxane-acryl urethane binder (Sipurino) by impregnation in INOTEX's facilities. The treated textile samples and the chemicals used were provided to LEITAT (WP4):

Table 9 – Samples provided to LEITAT

NOMENCLATURE	DESCRIPTION
Curb_TiO₂	PES fabric treated with TiO ₂ NPs, wetting agent and binder
Curb (control sample)	PES fabric without TiO ₂ NPs
Tiodisper NA-AS (commercial name)	TiO ₂ dispersion
Tanawet RC-N (commercial name)	Wetting agent

Multiple characterizations were performed on both starting and washed materials. The nanoTiO₂ dispersion (Tiodisper NA-AS) and washing waters were observed through high resolution transmission electron microscope (HR-TEM; JEOL JEM-2100) coupled with EDX (OI Aztec 80mm X-max) to determine the size and morphology of starting and released nanomaterials. XRD analysis (D5000, Bruker) was performed to determine the crystallographic structure of the TiO₂ NPs. The washed and unwashed textiles were characterized by SEM (JEOL JSM6500F FEG-SEM) coupled with an EDAX EDX system with Genesis software. Titanium concentration was determined in Tiodisper NA-AS solution and in washed and unwashed textiles with and without TiO₂ NPs by Inductively Coupled Plasma Mass

Spectrometry (ICPMS, Agilent 7500, Agilent Technologies) in LEITAT (WP4). Before the measurements the textile samples were digested with an acid solution in an analytical microwave digestion system (MARS, CEM, 1600W). Ti concentration in washing waters was also measured by ICPMS, but before the analysis optimization of the analytical procedure was performed in order to determine if liquid samples required digestion or not.

Washing cycle protocol

The household washings simulations were performed according to an adaptation of the standardized protocol ISO 105-C06:2010 Textiles -- Tests for colour fastness -- Part C06: Colour fastness to domestic and commercial laundering [4]. Each sample consisted in 1.00 ± 0.05 g of fabrics, which were cut in squares with approximately 15 cm side. A temperature sealing was applied on the textiles edges in order to avoid the textile fraying and yarns release in the washing waters, what would have hampered its later characterization. The washings were performed in 550 ± 50 ml stainless steel vessels with 75 ± 5 mm diameter and 125 ± 10 mm height. Each vessel contained one sample, 10 stainless steel (SS) balls of 6 mm diameter (to simulate mechanical impact) and 150 ml of detergent solution. The detergent used was a light duty detergent with anionic and non-ionic surfactants, fabric care additives and enzymes. The dose used was 4 ml of detergent per distilled water liter, what provided a washing pH of 7.4. The tests were carried out in a Linitest+ equipment (Lab Dyeing System, Atlas) at 40 ± 2 rpm and 40 ± 2 °C.

Prior to the textile washing the vessel with the detergent and the stainless steel balls were placed inside Linitest+ during 5 minutes in order to reach the desired temperature. Then the textile was also introduced and washed during 30 minutes. The textile was removed and the washing waters were collected. Then, following the ISO protocol, two rinsing cycles of 1 minute at 40 ± 2 rpm, 40 ± 2 °C and using 100 ml of distilled water were performed [4]. The rinsing solutions (distilled water) without the textile was also introduced in Linitest+ during 5 minutes for temperature conditioning and after rinsing the waters were collected for further characterization. After the washing cycle the samples were dried at ambient temperature.

Two different textile samples were tested: 1) PES fabric treated with TiO₂ NPs, wetting agent and binder (Curb_TiO₂¹); 2) PES fabric without TiO₂ NPs (control sample, Curb¹). TiO₂ concentration in textiles was analyzed at 1; 3; 5 and 10 washing cycles including three replicates per sample. When a sample reached the expected number of washings it was digested and analyzed through ICPMS, so a new textile was used for the following washings, meaning that it was needed to start washing the new textile from the beginning (0 washings). Thus, multiple washing waters were obtained since every time that a washing started, new washing waters were produced. To avoid release differences due to different concentrations in textiles, all the washing waters analyzed belonged to the textile washed 10 times. From the

¹ Sample's name

textile washed 10 times, washing waters from the 1st, 2nd, 3rd, 5th, 7th and 10th washing cycles were analyzed by ICPMS.

Liquid samples ICPMS analysis optimization

ICPMS is an analytical technique which ionises chemical species in a plasma then detects the ions by their mass to charge ratio. Some materials such as TiO₂, depending on the concentration, can be difficult to ionise. In these situations acidic digestion can be used, which dissolves the sample which is then introduced into the ICPMS equipment. However, this means the liquid sample is diluted and therefore the limit of detection is increased. Since we suspected that some of our liquid samples contained a relatively low concentration of Ti, acid digestion was avoided where possible in order to keep the limit of detection as low as possible.

To determine the capacity of the ICPMS equipment to ionize the sample without previous digestion, known concentrations of 1, 10 and 20 ppb of the original TiO₂ dispersion (Tiodisper NA-AS) were measured. For each of the concentrations three replicates were tested.

4.3. Results

4.3.1. ENMs

Electron microscopy

From the TEM images (Figure 28) it was confirmed that the Tiodisper NA-AS dispersion contained nanomaterials. Although some nanoparticles were isolated, most of them were forming aggregates that ranged from around 100 nm to few micrometers. Although spherical NPs were also observed, most of the NPs presented irregular shape. From the diffraction pattern shown in Figure 28A it was concluded that the sample was polycrystalline which provided diffraction in multiple directions thus generating the observed pattern. Due to the elevated amount of aggregates in the dispersion it was difficult to determine where a particle started and ended. For this reason, a particle size distribution could not be measured. High magnifications images (as the one shown in Figure 28D) showed it was not possible to distinguish discreet nanoparticles and therefore measure the size of the NPs present in the aggregates however the interplanar distances of the TiO₂ crystal could be distinguished and measured at around 3.5 Å which matches the (101) plane of anatase TiO₂.

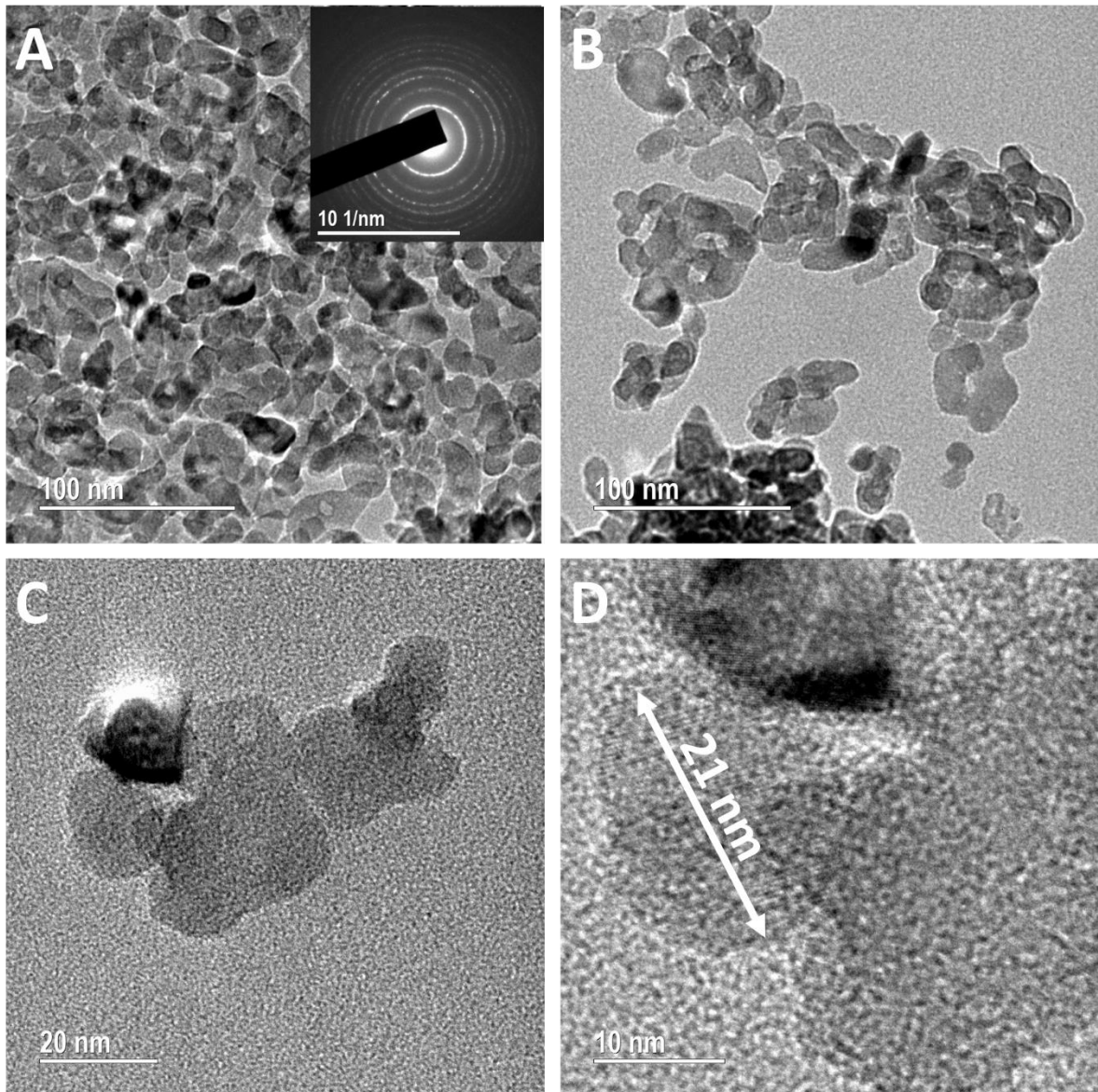


Figure 28 – TEM images of TiO₂ nanoparticles before being impregnated in the textile.

X-Ray Diffraction

The XRD measurement performed on the TiO₂ NPs dispersion (Tiodisper NA-AS) are shown in Figure 29. The results match the ICDD (International Centre for Diffraction Data) database entry for anatase TiO₂, as expected since that crystal form is the more photocatalitically active form of TiO₂ [5].

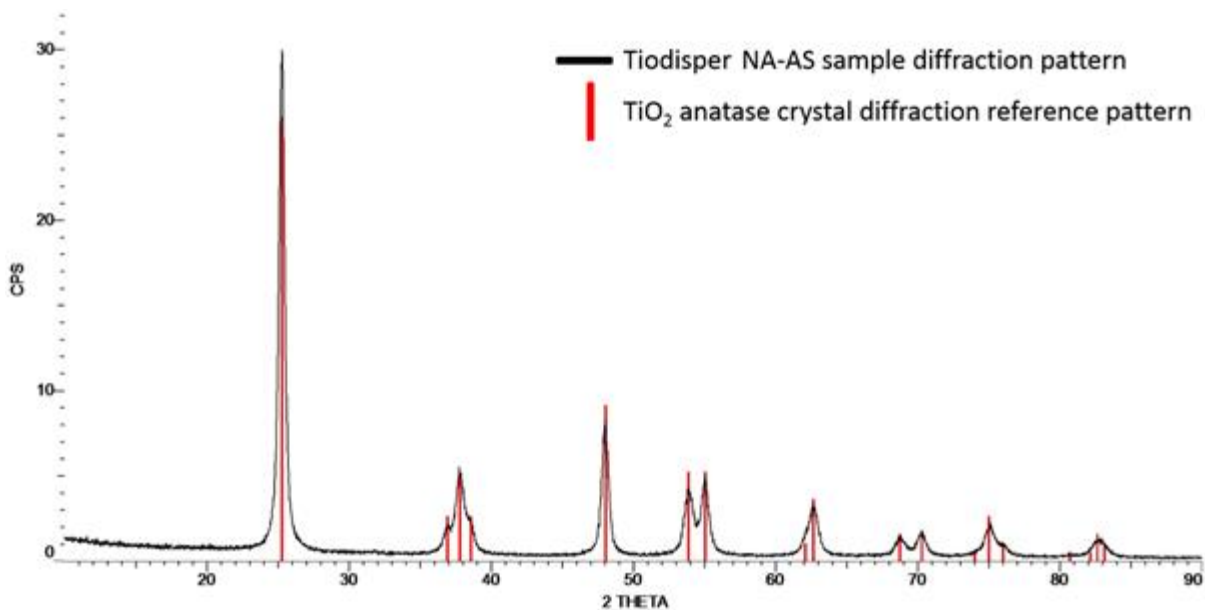


Figure 29 – Tiodisper NA-AS sample diffraction pattern

Inductively Coupled Plasma Mass Spectrometry

The ICPMS results obtained from the starting materials are shown in Table 10. It was concluded that the PES textile already contained Ti even before the incorporation of the nanoTiO₂. The reason could be the extensive use of TiO₂ as a delustering agent in synthetic fibres. A delustering agent is a substance added in synthetic fibres to reduce the lustre (sheen) and transparency of the fibre. Commonly, powdered anatase TiO₂ is used for that purpose. In any case, after the Tiodisper NA-AS addition, the amount of Ti increased significantly; by 1000 ppm, 50% of the original concentration. This means that in the textiles containing nanoTiO₂ two kinds of TiO₂ will be present, 1/3 of the TiO₂ will come from the Tiodisper NA-AS and 2/3 from the TiO₂ previously present in the textile. This fact shows the difficulty of working with real materials, since as in this case, the matrix can produce interferences with the materials of interest.

Table 10 - Ti concentration determined by ICP-MS in the samples provided by INOTEX.

SAMPLE	Ti CONCENTRATION (ppm)	RSD (%)
Control sample (Curb)	2111 ± 44	2.1
Textile with NPs (Curb_TiO ₂)	3095 ± 123	4.0
NPs dispersions (Tiodisper NA-AS)	193847 ± 2691	1.4

4.3.2. Unwashed textiles characterization

Electron microscopy and EDX

In Figure 30A an SEM image of the Curb textile sample yarns is shown. On the yarns multiple particles can be seen, which are distributed along the entire surface. From the magnified

image shown in Figure 30B is concluded that while some of the particles are a few micrometers in size, others have submicron size. The platinum in the EDX spectra of both background and particles is from a thin Pt coating applied to the sample to minimize sample charging problems. The large low energy peak (0.277 keV) is the C K α characteristic X-ray and most of this signal comes from the textile (polyester). The oxygen K α electron transmission has an energy of 0.525 keV and the titanium L α emission has an energy of 0.452 keV but this is a much less intense X-ray line than the K α line at 4.088 keV, which does not overlap with any of the elements of interest. For these reasons this peak is used for TiO₂ identification. Much of the oxygen peak will be signal from the PET however it is reasonable to assume when Ti is detected the particles are made of TiO₂.

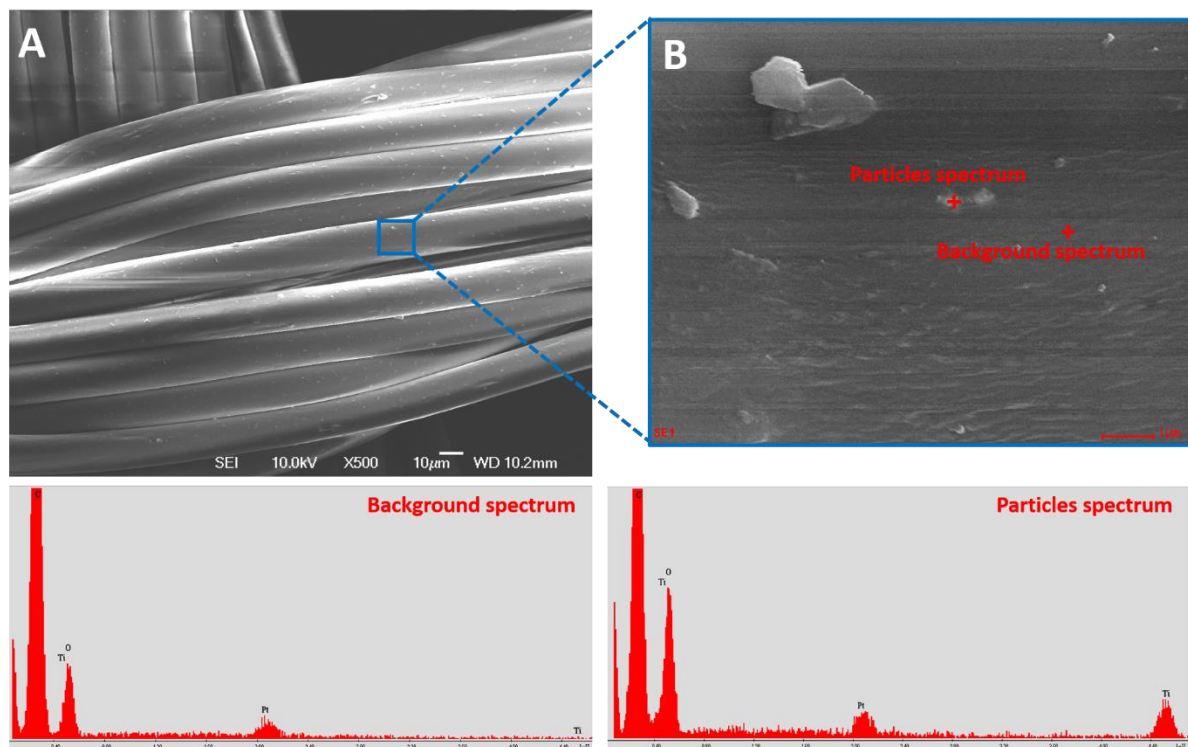


Figure 30 – SEM images and corresponding EDX spectra of Curb sample.

For the Curb_TiO₂ sample a similar conclusion is obtained. In Figure 31A multiple particles can be seen in the yarn's surface. In the EDX analysis performed from Figure 31B again in the background there is no Ti presence while in both particles (big and smaller) TiO₂ was detected.

Although the elemental analysis (EDX) of both samples lead to similar results, when the surface images of Curb and Curb_TiO₂ samples are compared some differences are apparent. When Figure 30B and Figure 31B are compared it is clearly seen that in Curb_TiO₂ sample there is a higher number of particles. Comparing Figure 30A and Figure 31A, although it is more difficult to detect, it is useful to realize that this is a general trend, it happens in all the yarns. Moreover, in Curb_TiO₂ sample there is a higher number of smaller particles forming aggregates, which is not seen in Curb sample. Most probably these small particles are the ones from the Tiodisper NA-AS that have attached to the textile during the impregnation process. Thus, it is possible to differentiate among the two TiO₂ particles distribution present

in the samples. The bigger one originally coming from the textile and the second one lately added by impregnation.

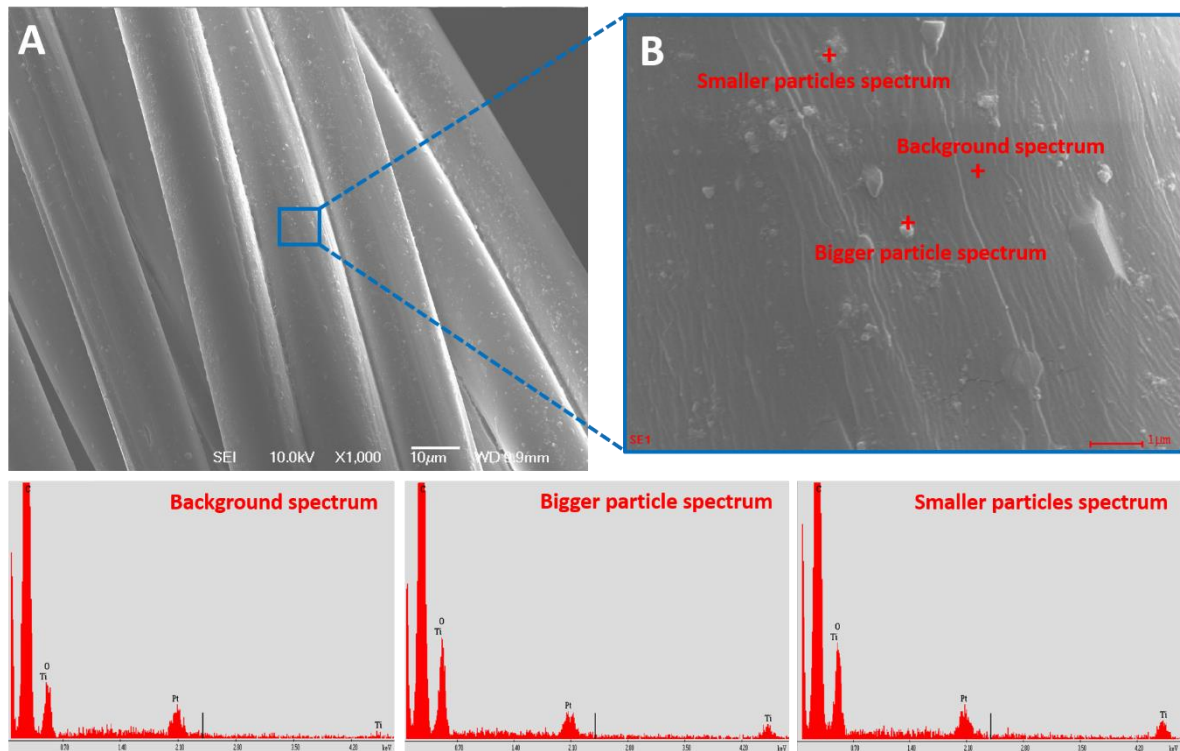


Figure 31 – SEM images and corresponding EDX spectrums of Curb_TiO₂ sample.

4.3.3. Washed textiles characterization

Electron microscopy and EDX

The main difference between washed and unwashed textiles observed by SEM was that in the former a large amount of detergent partially covering the yarns was observed. As mentioned in the methods section the textiles are submitted to two rinsing processes after every washing. However, as demonstrated in the images it was not enough to rinse off all the detergent. In any case, the detergent present on the textile should not have a direct impact on the release, so its presence is not highly relevant for our study. The aim of observing the textiles through SEM was to determine how the particles on the surface are affected by the washings. In previous studies with other materials (not involved with NANOFASE) aggregation of all the particles between yarns has been observed, giving an idea of how well attached they were in the textile and consequently how likely release was to occur. In this particular case study, as seen in Figure 32 and Figure 33 the particles distribution on the textiles was very similar to the one observed for unwashed textiles, suggesting that they are well attached (which has been confirmed with ICPMS). For washed textiles, like for unwashed textiles, the number of particles on the yarns surface of Curb_TiO₂ sample was greater than for Curb, meaning that the TiO₂ concentration was higher, which was also later confirmed with the ICPMS analysis.

In Figure 32 SEM images of Curb_W5 (washed 5 times) are shown. In Figure 32A it is clearly seen how part of the yarns are covered by detergent and others are not. In Figure 32B EDX analysis was performed on different areas where particulate-like matter was found. However, in none of the spectra was Ti signal detected. There could be two reasons. First, that the particles on which the analyses were performed were organic, probably from the detergent. If they were made of other elements apart from Ti the EDX would have also detected it, which was not the case. The second possibility is that the detergent layer on the particles is hampering the detection of Ti. As can be seen in the upper right side of Figure 32B, the area where the EDX was performed was covered by detergent, providing more arguments to think that the second possibility is what is actually happening.

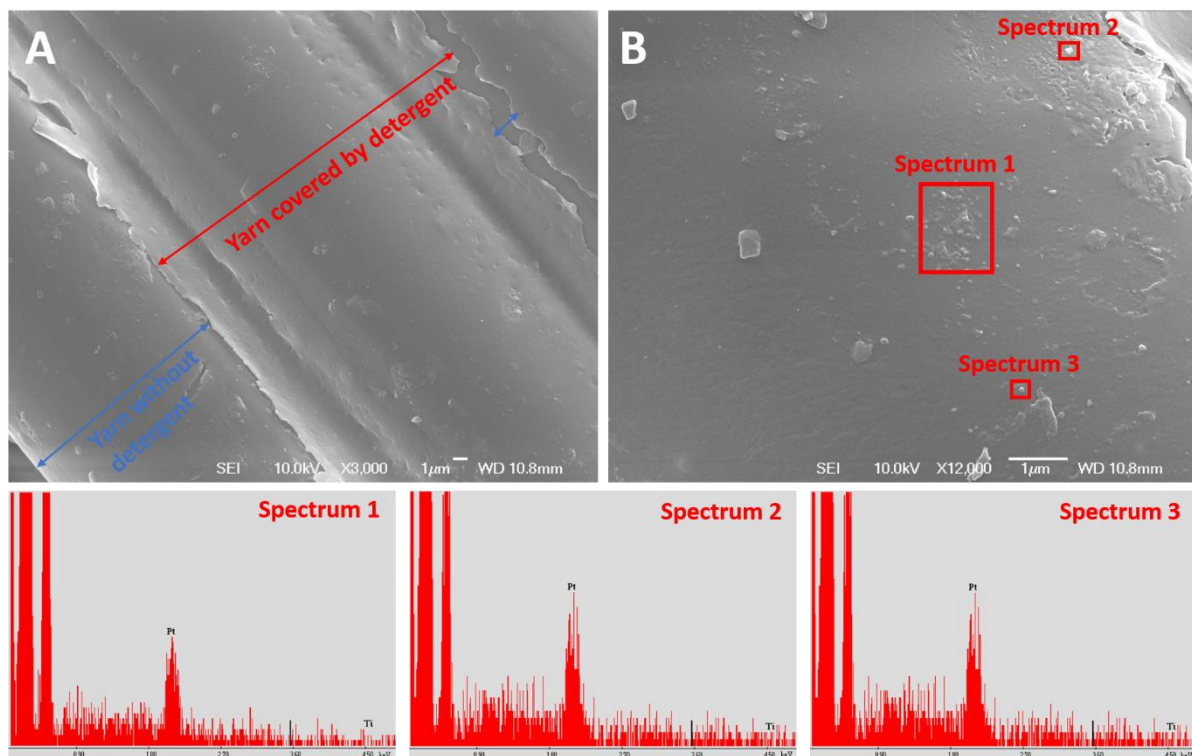


Figure 32 – SEM images and corresponding EDX spectrums of Curb_W5 (washed 5 times) sample.

Looking at Figure 33, the Curb_TiO₂ sample has a higher number of particles than in Curb. In the image with higher magnifications (Figure 33B) the nanoparticles aggregates can easily be seen. There are also some individual nanoparticles as the one pointed with the arrow, others are forming aggregates smaller than 100 nm, but most of them are forming bigger aggregates containing a high number of NPs. In the EDX analysis of Curb_TiO₂_W5 samples Ti was detected, most probably because the area wasn't covered by detergent, making its detection easier.

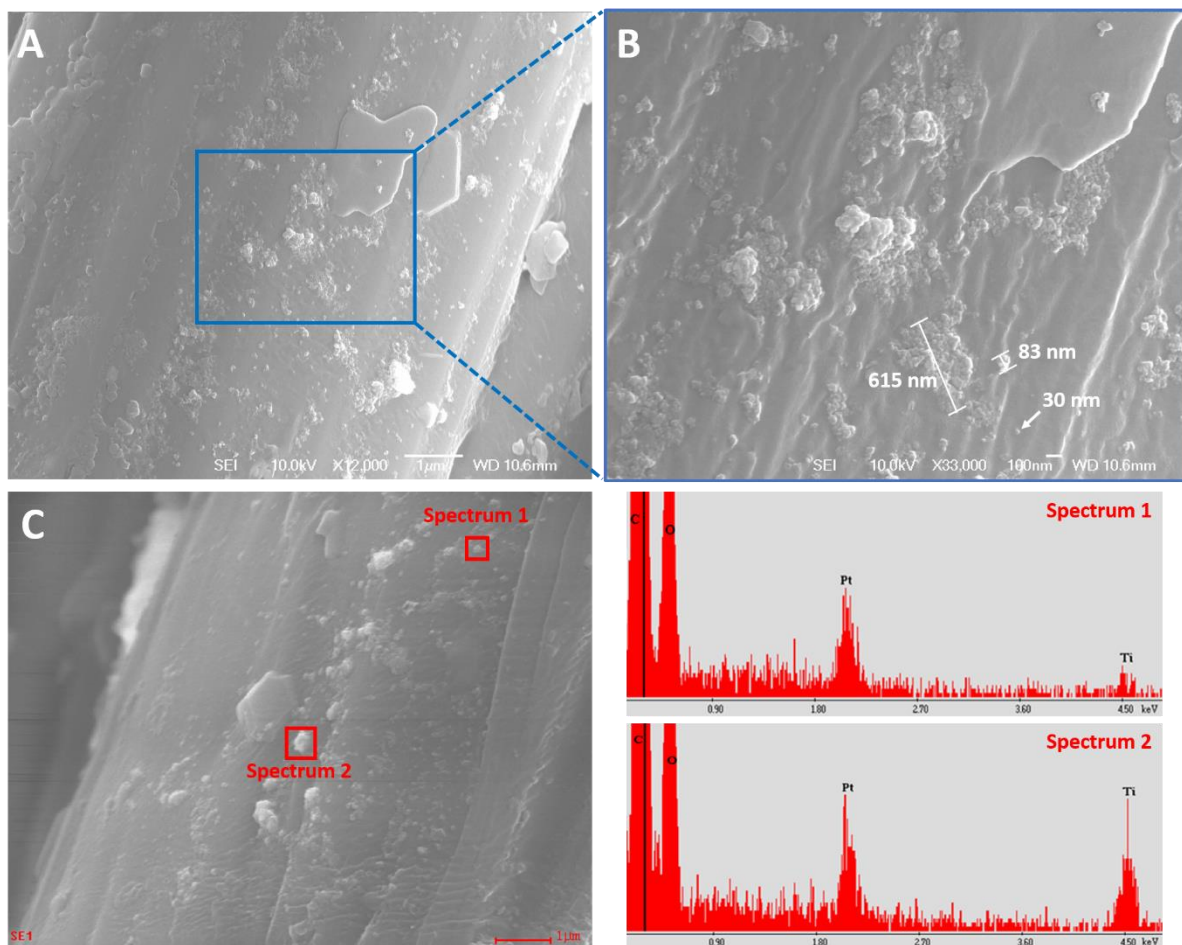


Figure 33 – SEM images and corresponding EDX spectra of Curb_TiO₂_W5 (washed 5 times) sample.

Inductively Coupled Plasma Mass Spectrometry

The Ti concentration in Curb and Curb_TiO₂ textiles with washings was measured by ICPMS, the results are shown in Figure 34. The height of the bars represents the mean value from the three replicates, while the error bars correspond to their standard deviation. In the left-side chart, the Ti concentration in textiles is shown while in the right-side chart the TiO₂ (or Ti) remaining percentage is plotted considering the unwashed textile concentration as a 100%. Both charts are built with the same data, but the different representations to clarify the observation of different conclusions.

From the left-side chart is clearly seen that the Ti concentration of the textiles where the TiO₂ NPs dispersion was applied (Curb_TiO₂) is higher than in the control (Curb). Since the lower concentration found in Curb_TiO₂ washed textiles is higher than the maximum (unwashed) Curb sample, the results suggest that TiO₂ NPs are still present in the textile after 10 washings. It is also remarkable that for both samples the concentration decrease is approximately the same. From around 3100 ppm to 2800 ppm for Curb_TiO₂ (300 ppm decrease) and from 2100 ppm to 1800 ppm for Curb (300 ppm decrease). However, since Curb sample has less TiO₂ than Curb_TiO₂, these 300 ppm decrease means a higher released percentage. This fact is easily appreciated in the right-side chart, where the released percentage in each sample is

shown. After 10 washings around 90% of TiO₂ remains in Curb_TiO₂ sample and 80% in the case of Curb sample. Meaning that Curb TiO₂ release is approximately 10% lower.

The Ti concentration decrease statistical relevance has been evaluated through an Analysis of Variance (ANOVA) data treatment with an α value equal to 0.05. For both Curb and Curb_TiO₂ samples the conclusion was the same. There is a significant Ti concentration decrease from the unwashed textile (0 washings) in comparison with the washed textiles (1, 3, 5, 10 washings). However, there is not a statistically relevant difference among washed textiles. Meaning that Ti concentration after 1 washing is not statistically different after 3, 5 or 10 washings. These results could be explained by the small decrease in concentration along washings compared with the Ti concentration variance among replicates. In other words, the concentration decrease after the first washing is so small that the standard deviation among replicates has a higher impact hiding it.

Considering that the Ti concentration in all the washed textiles is the same, the release percentage for Curb and Curb_TiO₂ can be determined as an average from the 1st, 3rd, 5th and 10th washings. For the Curb sample $17 \pm 2\%$ of Ti is released, while for Curb_TiO₂ only the $9 \pm 2\%$. It is surprising that in Curb_TiO₂ sample, even though it has a higher concentration of TiO₂, the amount released is smaller. This effect is probably produced by the substances included in the nanoTiO₂ formulation to improve the attachment, as binders and wetting agents. However, it must be emphasized that the TiO₂ released in Curb sample, since it is the control, does not come from the TiO₂ nanodispersion, it is the background TiO₂ used in the fibre as delustering agent. The same can be applied for Curb_TiO₂ sample. It doesn't mean that all the TiO₂ released was in the nanometer range. Most probably, part of it, belonged to the TiO₂ present in the textiles before the nanoTiO₂ incorporation.

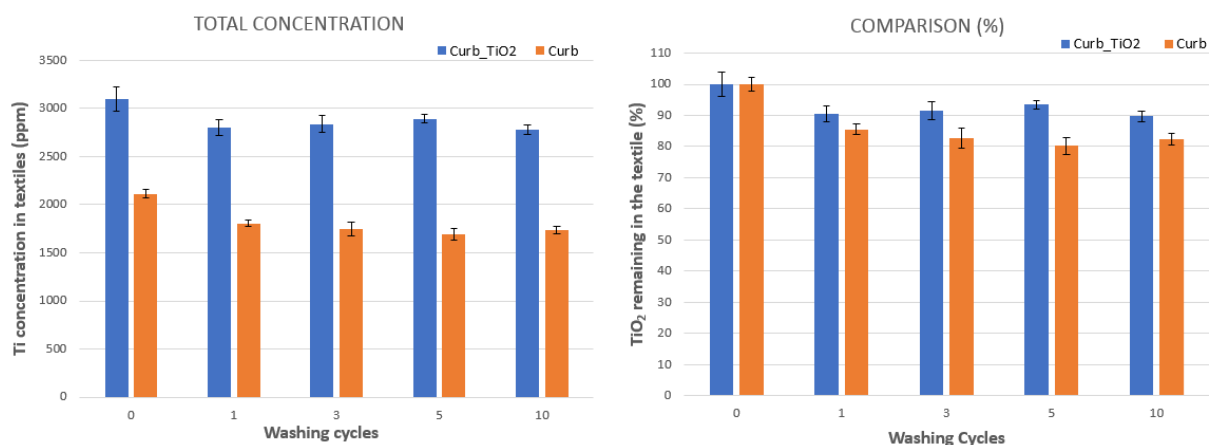


Figure 34 – Curb_TiO₂ and Curb samples Ti concentration in textiles along washings.

4.3.4. Washing waters characterization

Liquid samples ICPMS analysis optimization

From the results obtained in the ICPMS measurements without acid digestion of the known concentrations, shown in Figure 35, it is clearly observed that the ICPMS plasma ionization it is not enough to ionize all the titanium in the sample. For the three concentrations tested the measured concentration differs from the known concentration, a trend that is more noticeable as the Ti concentration increases. Therefore, even though it leads to an increase in the detection limit, acid digestion is needed before ICPMS measurements of the textiles washing waters.

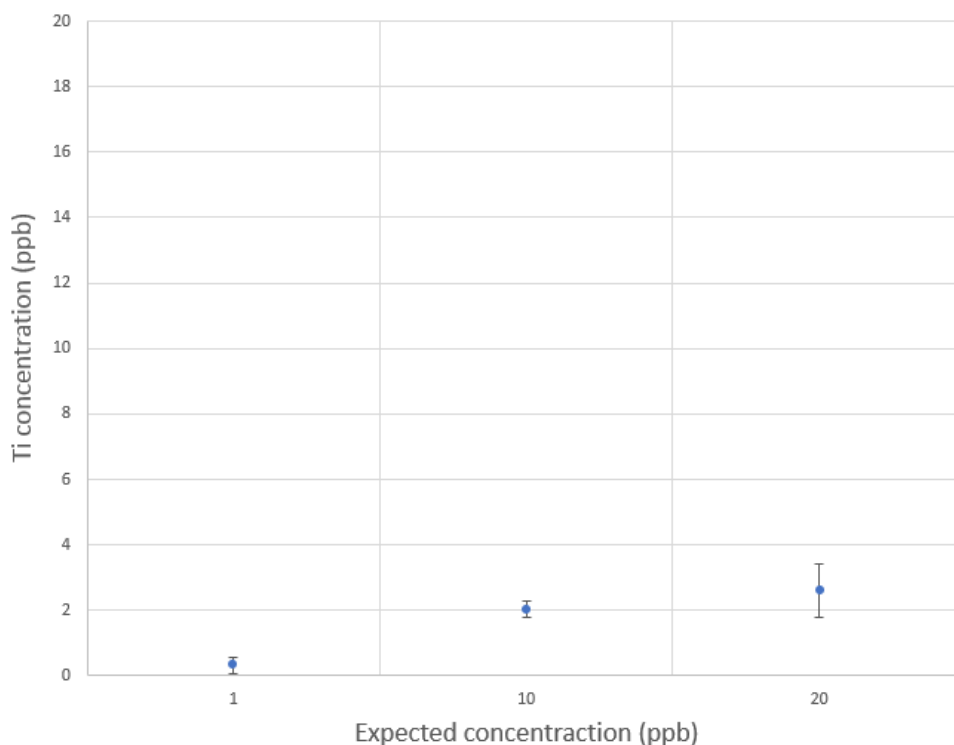


Figure 35 – ICPMS plasma ionization test.

Inductively Coupled Plasma Mass Spectrometry

The washing waters collected during the washing experiment were analyzed through ICPMS. Ti concentration in water was higher for Curb_TiO₂ sample than for Curb. Differences around one order of magnitude were measured.

For Curb sample, due to the low amount of Ti, concentrations above the limit of detection were only found for the first and second washing waters. Concentrations around 20 ppb were measured. Ti concentration in the second washing waters were lower than in the first, suggesting that release decreases along washings.

For Curb_TiO₂ a decrease of Ti concentration along washings was also observed in washing waters. As can be seen in Figure 36, the release trend is exponentially negative, what means that during the first washings there is big difference in concentration along washings, whether

for the last ones the difference is smaller. Indeed, from 7th to 10th washings a concentration difference was not observed. As shown in Figure 36, for Curb_TiO₂ sample, an exponential equation trendline was calculated to describe the release behavior (red dashed line):

$$y = \frac{291.03}{x^{0.466}}$$

Where:

y = Ti concentration in washing waters (ppb)

x = The number of washings performed, should be a natural (\mathbb{N}) number.

The previous equation could be useful to predict the amount of Ti that could be found in washing waters if more washings were performed (e.g. 20, 30, 50 washings).

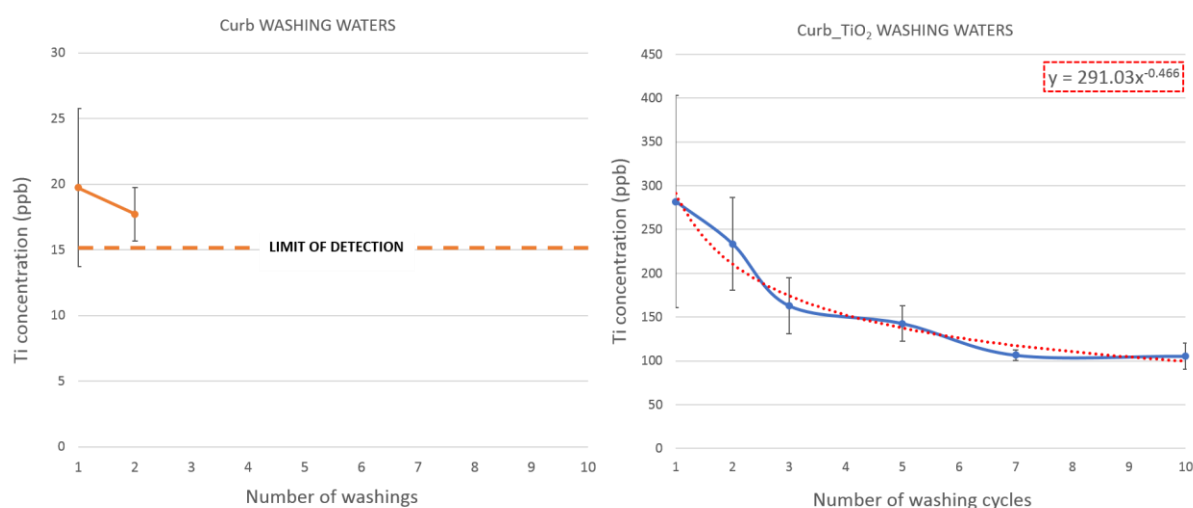


Figure 36 – Ti concentration in washing waters of Curb and Curb_TiO₂ samples. Orange and blue solid line representing washing waters Ti concentration experimentally determined by ICPMS for Curb and Curb_TiO₂, respectively. Red dashed line showing the exponential equation trendline (theoretical approach).

Electron microscopy

In order to not only determine the amount but also the form of TiO₂ released from the curtains, TEM images of the washing waters were obtained. In Figure 37, TEM images from a small amount of white sediment found in the vessel which had been used to store one of the water from the first washing of Curb_TiO₂ are shown. As seen in Figure 37 the nanoparticles released formed big aggregates surrounded by organic matter, most probably coming from the detergent. From the EDX results (Figure 37D) it was confirmed that the components observed were TiO₂. From the diffraction pattern obtained from the sample, which is shown in Figure 37C it was confirmed that the released TiO₂ was in anatase form since the pattern exactly matched with the one previously measured in Tiodisper NA-AS (Figure 28A). Curb washing waters were also observed by electron microscopy but no released TiO₂ was found.

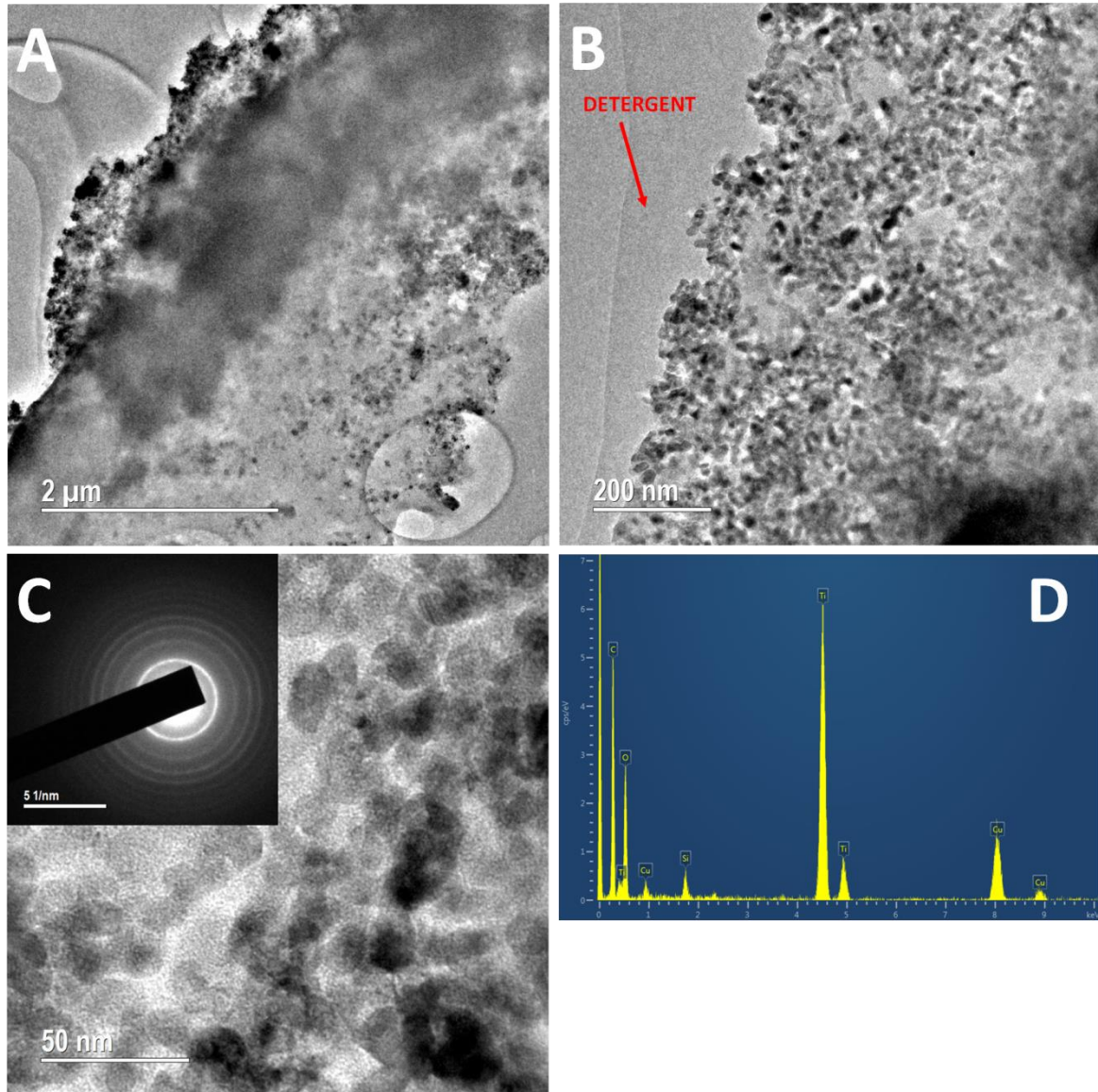


Figure 37 – TiO₂ NPs released from Curb_TiO₂ sample.

4.4. Conclusions

For both control (Curb) and nano-enabled curtains (Curb_TiO₂) a high release was observed for the first washing while statistically relevant difference in concentration for the following 9 washings was not measured.

In previous published studies, release of TiO₂ from textiles during household washings ranged from 0.01% to 3.4% of the initial elemental Ti concentration in the first washing and rinsing process [6], meaning that releases of $17 \pm 2\%$ and $9 \pm 2\%$ are relatively high. However, although in other published studies the release in the first washing is lower, in the present case study the release is very low during the following 9 washings. In order to do a relevant comparison, the current textiles should be compared with other textiles also washed 10 times.

Release forms were determined by electron microscopy, where large TiO₂ aggregates were observed.

5. INOTEX: camping tents with antibacterial activity

5.1. Introduction

Nowadays, in the textile industry there is interest in introducing silver NPs into products due to their well-known antibacterial properties [7]–[12]. However, one of the inconveniences they are facing is the weak NPs attachment in the textiles. The textile manufacturers are aware of the problem and are looking for alternatives to ensure the maximum attachment of the nanoparticles, not only to achieve a long-term effect of the treatment but also to minimize nanoparticles release to the environment. The present case study is one of many examples of efforts to improve NPs attachment. It was proposed by INOTEX, who participated in a project where the product was developed by a third party.

5.2. Materials and methods

The case study consists of a cotton fabric modified with a fluorocarbon based thin water repellent layer in both sides. In addition, a watertight impermeable layer of polyacrylic coating paste containing Ag nanoparticles, stabilized with polyethylenimine (PEI) polymer through a coordinate-covalent bond, was applied to one of the sides. The resulting textile-based composite is intended to be used as a material to fabricate camping tents. According to INOTEX, the Ag presence diminishes the potential harmful effect of bacteria on the fabric, avoiding undesirable effects such as mould or the appearance of bad odours.

Four different samples were tested, all of them exemplified in Figure 38 and shown in Figure 39. All the samples of the cotton tent cloth were treated with a fluorocarbon finish preventing the coating paste penetration, and coated by one-side single or double polyacrylic coating with or without Ag-PEI NPs content. The four samples together with the Ag-PEI dispersion and the polyacrylic paste containing the Ag-PEI dispersion were sent to LEITAT (WP4). The Ag-PEI dispersion was also sent to UoB for characterization.

From the environmental point of view, in WP4 there is an interest of testing the potential release of Ag NPs to the environment. During the use phase the textile will be exposed to weathering effects. However, for Ag to be released the cotton textile would need to be destroyed first, which is not likely to happen in normal use. For this reason, the main release scenario and therefore the one studied in NanoFASE is during the end-of-life stage, more specifically during landfilling. The leaching of silver nanoparticles from the textiles was studied simulating an accelerated end-of-life process according to the standardized protocol EN – 12457-4: Test for leaching of granular waste materials and sludges [13].

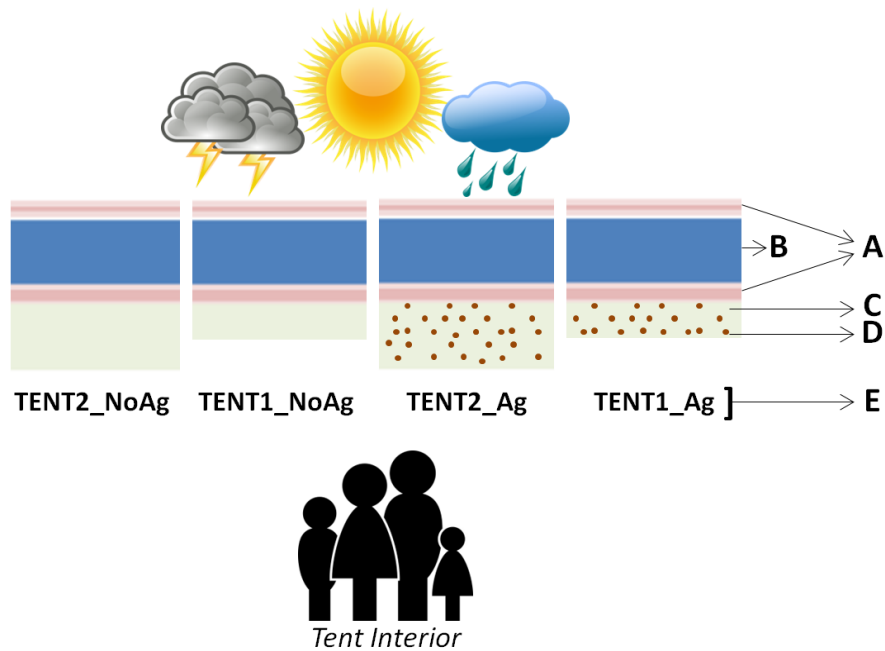


Figure 38 – Case study composition, textile for camping tent applications. A: Fluorocarbon based thin water repellent layer; B: Cotton fabric; C: Mixed dispersion of synthetic copolymers (acrylics and polyurethanes) impermeable layer; D: Ag nanoparticles coated with Polyethylenimine (PEI); E: Samples code.

The samples containing Ag NPs (both with 1 or 2 polyacrylic coating layers) are the ones intended for commercial applications, while the non-containing Ag were specifically designed for the test as control.

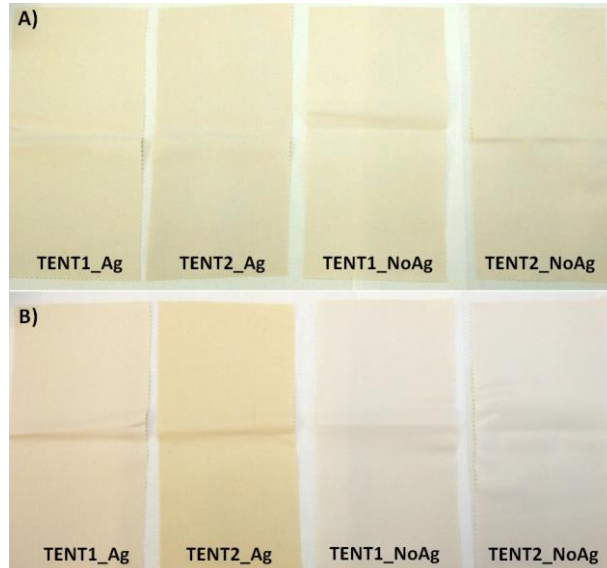


Figure 39 – Visual aspect of the 4 samples. A: Tent exterior side; B: Tent interior side (showing the polyacrylic coatings, see Figure 31 for the meaning of the codes).

In Figure 39A it is observed that the exterior side of all the textiles look the same, while the tent interior side showing the polyacrylic coating (Figure 39B) presents some differences from one sample to others. When the polyacrylic coating does not contain Ag-PEI NPs the samples are whitish. However, since Ag-PEI NPs dispersion presented a brownish colour, the more silver the sample contains, the more brown-coloured the tent interior side looks.

The density of each sample, which was used in a later stage to calculate the release rate per area, was measured by weighing three replicates of the Ag containing samples in a 0.1 mg precision balance (Ohaus Adventurer SL, AS214). In order to precisely measure the area of each textile, a photo of the weighted textiles was taken and the images were processed with FIJI software [14] as can be seen in Figure 40.

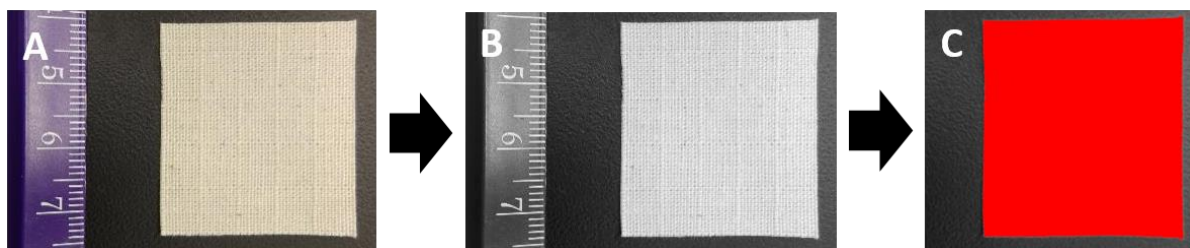


Figure 40 – A) Original picture; B) Image conversion to greyscale; C) Textile recognition and area measurement by the software.

The Ag-PEI dispersion was diluted to 100 ppm with ultrapure water and observed through high resolution transmission electron microscope (HR-TEM; JEM 2010, JEOL Ltd.) to determine the size and morphology of the nanomaterials (Figure 42). The TEM images were analysed using FIJI software [14] to obtain its size distribution. The four textile samples plus the original Ag-PEI NPs dispersion were digested in an analytical microwave (CEM, Mars) and analyzed through Inductively Coupled Plasma Mass Spectrometry (Agilent, 7500) to determine the Ag content. In addition, the textiles surface was observed with scanning electron microscopy (JEOL 6500F FEG-SEM).

Once the raw materials were characterized, they were submitted to the leaching test following the protocol specifications [13]. The textiles were cut into fragments ≤ 10 mm as seen in Figure 41A. They were cut with a Pinking shears (zig-zag scissors) because textile edges that are unfinished can easily fray and the threads pull out easily, the saw-tooth pattern does not prevent the fraying but limits the length of the frayed thread minimizing the damage and helping to obtain less threads in the leaching waters, easing their further analysis and treatments. Once the textiles were cut, 3 g were introduced in 50 ml polypropylene vial with 30 mL of ultrapure water (maintaining the 10 L/kg liquid to solid ratio proposed by the protocol). Then, the samples were shaken with an end-over-end shaker (OVAN, NR50 E) at 10 ± 3 rpm during 24h at ambient temperature (25°C). Three replicates were tested for each textile ending up with a total of 12 samples. After the landfill simulation the respective leaching waters were collected. In each vial 30 mL were introduced, but after the experiment, due to the textile water absorption, only around 25 mL could be collected. 5 mL were directly collected for Ag

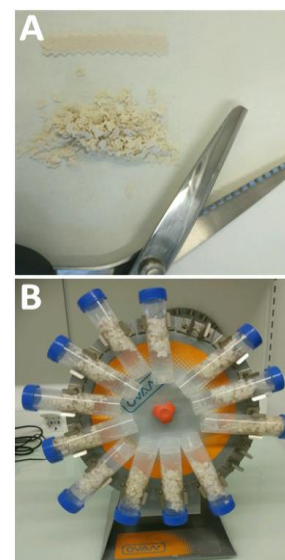


Figure 41 – A) Textile fragments. B) Fragments in contact with water being shaken.

determination through ICPMS; 5 mL were filtered through a filter paper of approximately 20 - 25 μm pore size (Filter-Lab quantitative filter paper, ANOIA); 5 mL were centrifugated with 3kDa centricons (Amicon Ultra-15 Centrifugal Filter Units, Millipore) and the remainder was collected, freeze-dried and observed through HR-TEM (JEOL JEM-2100).

5.3. Results

5.3.1. Starting materials

Transmission Electron Microscopy

The TEM images of the Ag-PEI dispersion show two differentiated size population of silver particles, which present a spherical shape. One of them is in the micro range and the other in the nano range. Figure 42A shows the bigger particles, Figure 42D shows the smaller ones and in Figure 42B, C the two different sizes populations can be appreciated. Moreover, especially in Figure 42A, the polyethylenimine coating can be observed as a darker substance surrounding the particles.

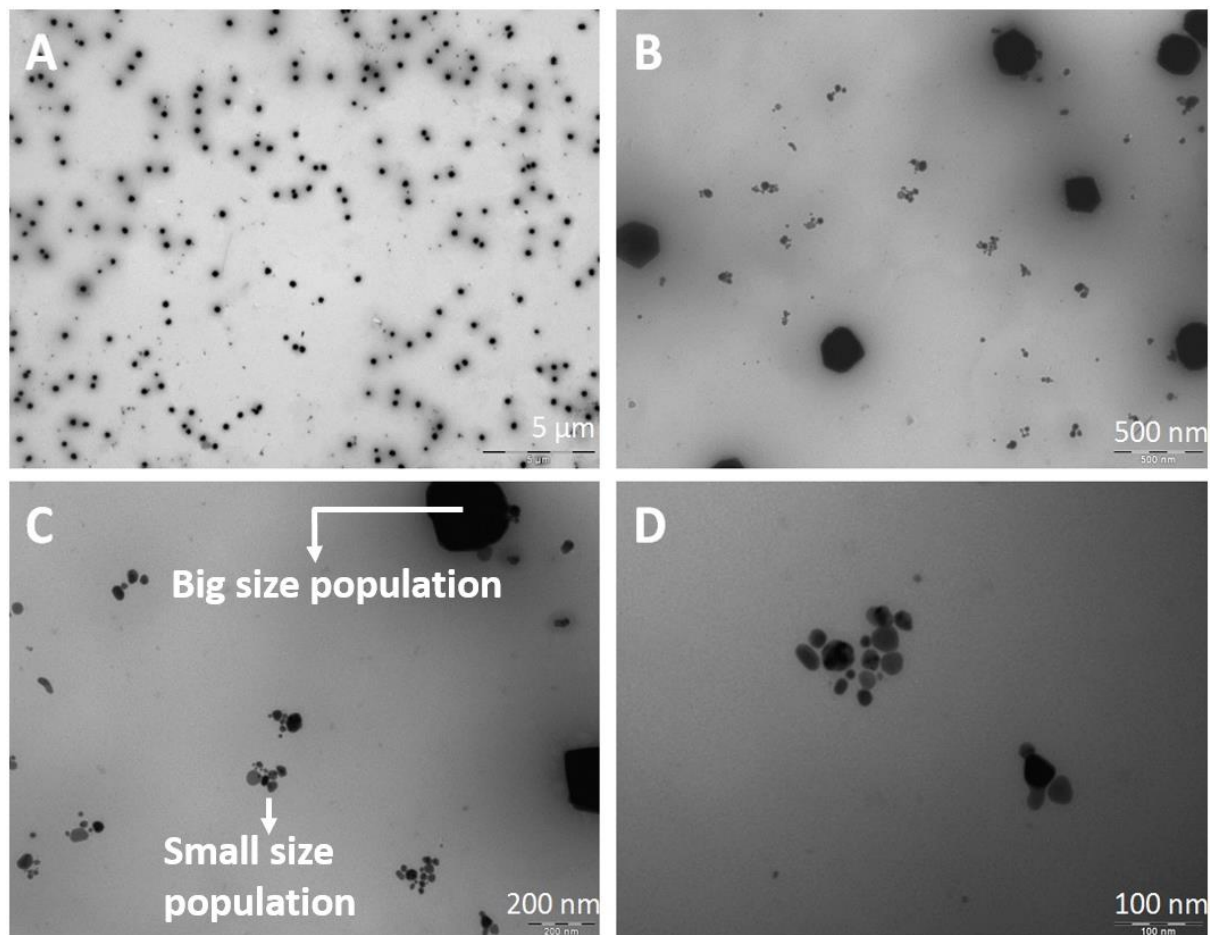


Figure 42 – HR-TEM images of Ag-PEI dispersion where the two size populations can be observed.

The size distributions of the two populations are presented in two different graphs for an easier interpretation. As can be seen in Figure 43 there is around one order of magnitude of difference between the two populations. The bigger particles presented a more uniform distribution (lower RSD%) while the smaller ones were more disperse.

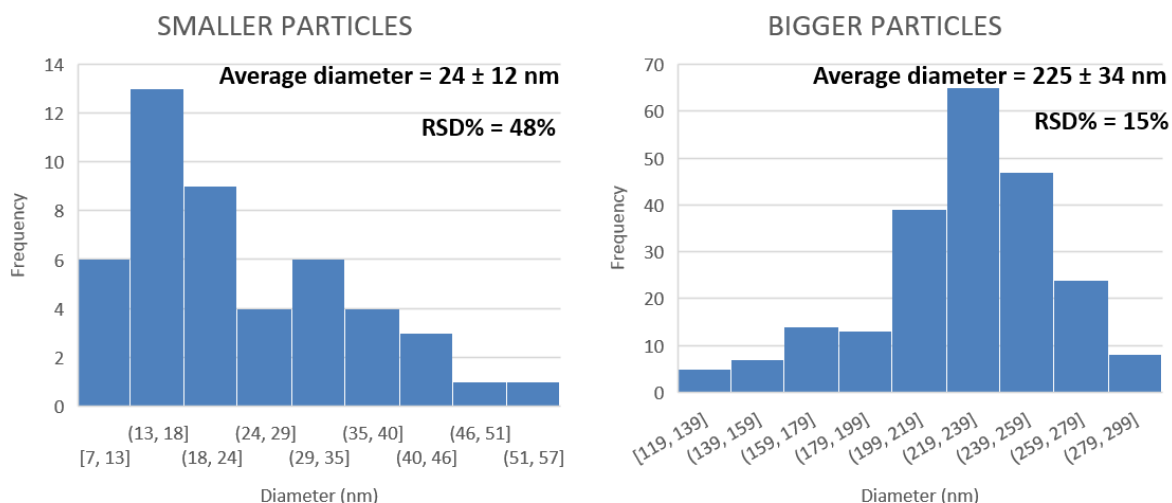


Figure 43 – Ag-PEI dispersion size distribution.

Scanning Electron Microscopy

From the SEM images of the camping tent samples before performing the leaching experiment a clear difference between the interior and exterior side of the textile sample was observed (Figure 44). While in the exterior side a regular textile pattern is seen, in the interior side containing the polyacrylate coating, a layer recovering the whole surface is clearly seen.

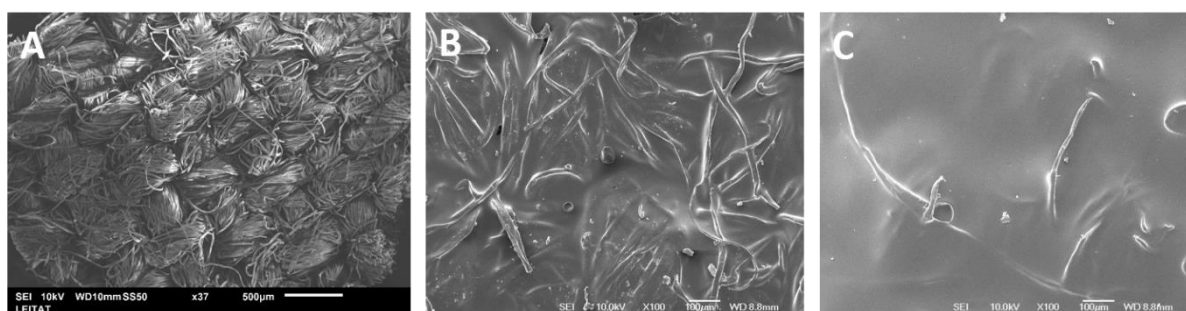


Figure 44 – SEM images of the camping tent samples before the leaching experiment. A) Tent exterior side, magnification: x37; B) tent interior side with one coating, magnification: x100; C) tent interior side with two coatings, magnification: x100.

A significant difference was found between samples with one and two coatings. While with one layer the textile fibres can be seen underneath the coating, with two layers, although some fibres can also be seen, most of the area is only covered by the coating providing a much more homogenous appearance.

Inductively Coupled Plasma Mass Spectrometry

The ICPMS results are shown in Table 11. As expected, in TENT2_NoAg and TENT1_NoAg silver was not detected, while in TENT2_Ag and TENT1_Ag it was. Moreover, the uncertainties (coming from three replicates) are very low, which suggests that the sample is quite homogeneous. As expected, the silver concentration in TENT2_Ag was higher than in TENT1_Ag. Since TENT2_Ag present one layer more than TENT1_Ag, the density measured also was higher, 24.9 ± 1.3 mg/cm² for TENT1_Ag and 27.0 ± 0.6 mg/cm² for TENT2_Ag.

Table 11 - Ag concentration in the original textiles and Ag-PEI dispersion determined by ICPMS.

SAMPLE	Ag CONCENTRATION (ppm)	RSD (%)
TENT2_NoAg	< 0.7 (not detected)	-
TENT1_NoAg	< 0.7 (not detected)	-
TENT2_Ag	111.9 ± 2.0	1.79
TENT1_Ag	68.9 ± 0.2	0.29
Ag-PEI dispersion	5000 ²	-

5.3.2. Aged materials and leaching waters

Electron Microscopy

In Figure 45 the samples surface after the leaching experiment are shown. No significant differences before and after the leaching experiment were found. The exterior side (made of cotton) looked a bit worn away. More yarns were protruding from the surface as a consequence of the mechanical wearing, but since this side does not contain any nanomaterials it doesn't have any effect on the release. Regarding the interior side, for both samples containing one and two coatings, the visual aspect was the same as for unwashed samples. In the images (both in Figure 45 B and C) small holes or area without coating were observed. However, these areas were also detected before the experiments and are probably due to the application method of the coating, they were not caused by the leaching experiment. Most probably, the leaching produced some damage in the outer layers of the coating, but the damage was not enough to be observed through electron microscopy.

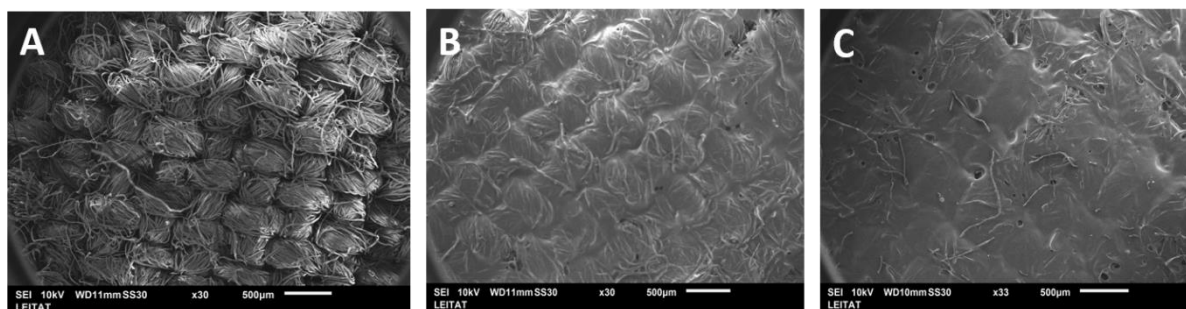


Figure 45 – SEM images of the camping tent samples after the leaching experiment. A) Tent exterior side, magnification: x30; B) tent interior side with one coating, magnification: x30; C) tent interior side with two coatings, magnification: x33.

As previously mentioned in the methodology section, part of the leaching waters were freeze-dried in order to obtain a solid residue to observe through SEM. The images corresponding to the freeze-dried residues are shown in Figure 46. In the residues, small fragments of the samples were found, which looked similar to the previously analysed fragments. Again, the same pattern was observed, for samples containing only 1 coating the yarns were more easily

² Information provided by INOTEX

visualized than for those samples containing 2 coatings. Multiple EDX measurements were performed in different areas of all samples but Ag was not detected in any of them.

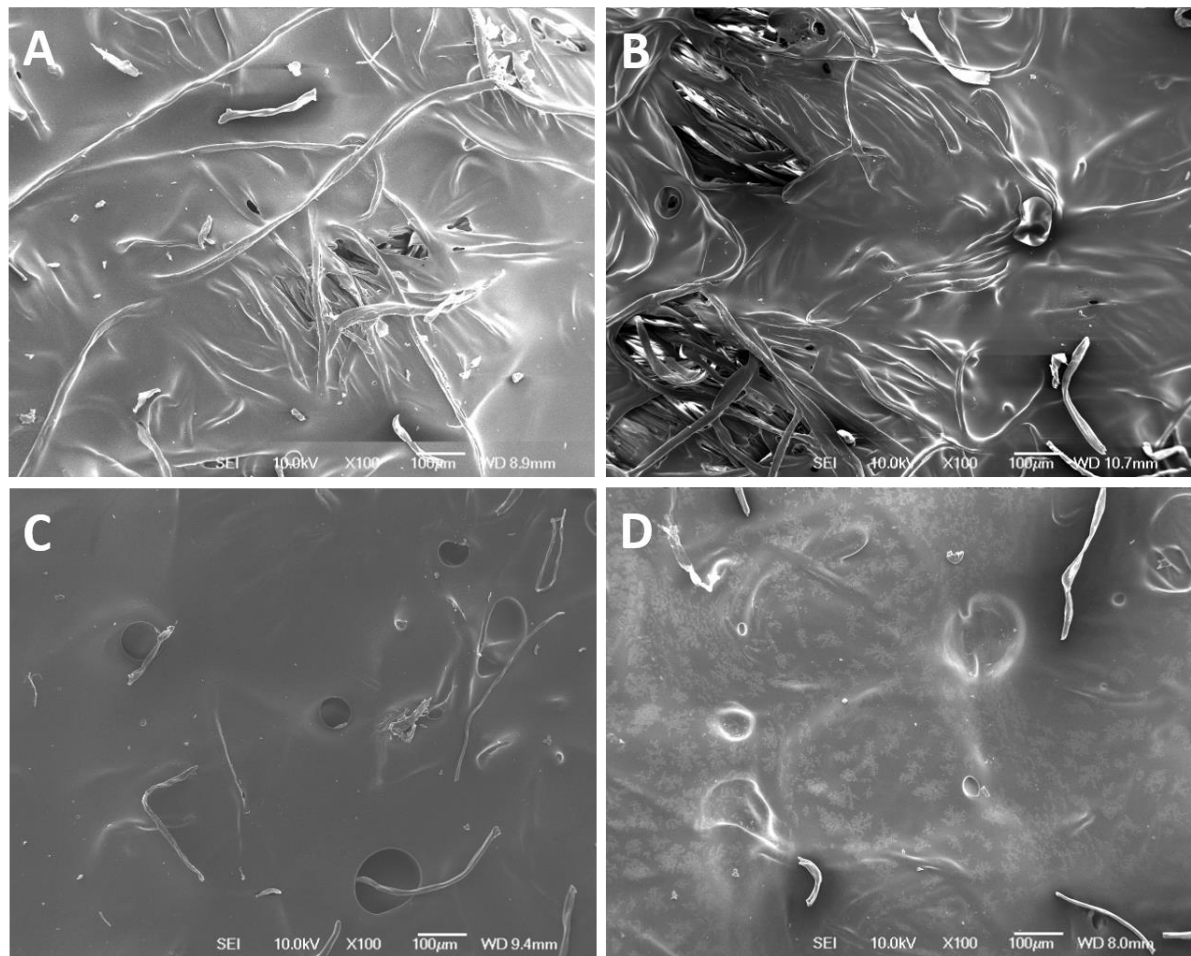


Figure 46 – SEM images of the residues from freeze-dried leaching waters of samples A) TENT1_NoAg; B) TENT1_Ag; C) TENT2_NoAg; D) TENT2_Ag.

Inductively Coupled Plasma Mass Spectrometry

Ag concentration in washing waters determined by ICPMS is shown in Figure 47. In the chart the total silver concentration is divided in three categories: (i) unfiltered water, (ii) filtered water with paper filter of 20 µm pore size and (iii) water filtered with 3 kDa centricons corresponding to the ionic content. For each of them, the corresponding standard deviations coming from three replicates were also included. Released waters of non Ag containing control samples (TENT1_NoAg and TENT2_NoAg) in all the cases presented Ag concentration values below the limit of detection (0.2 ppb). Thus, for simplicity, they were not included in the chart.

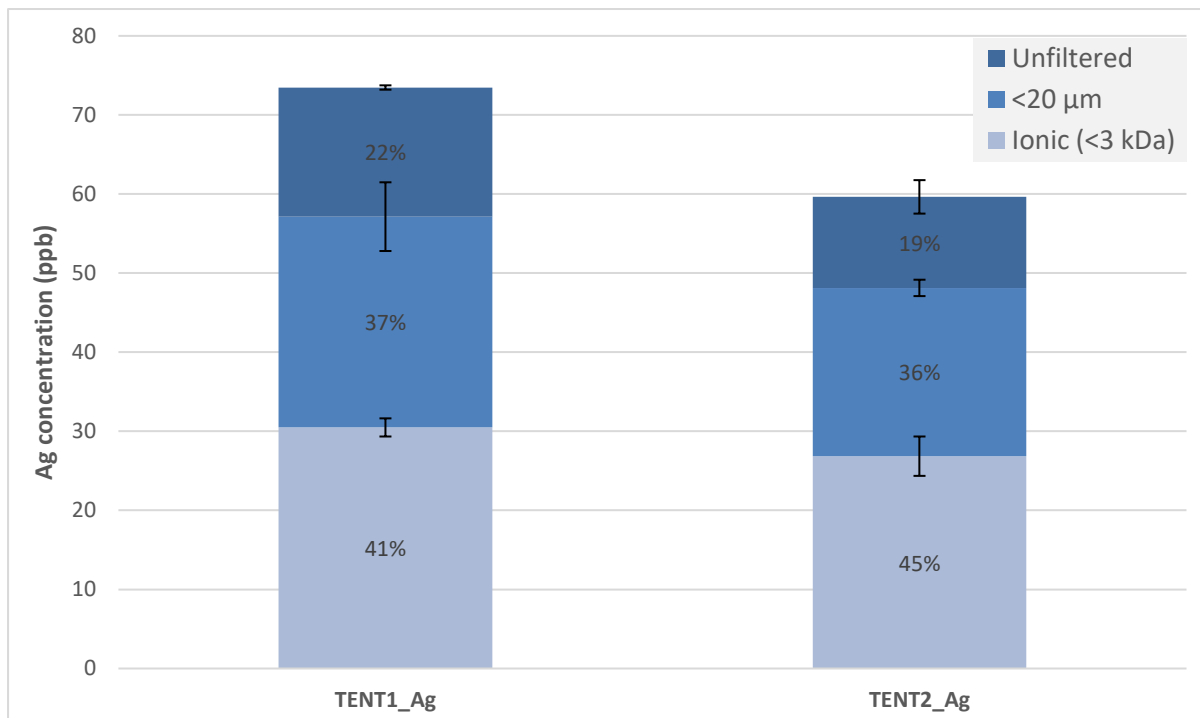


Figure 47 – Ag concentration in camping tents leaching waters.

For both samples (TENT1_Ag and TENT2_Ag) the results obtained were quite similar. Around 20% of the released silver was present in fragments bigger than 20μm, probably Ag that was embedded in released coating fragments or attached to released yarns bigger than 20 μm. 36% – 37% of the released silver was smaller than 20μm but it was not ionic (>3 kDa). In this category are included small coating fragments containing Ag, small cotton yarns with Ag attached and maybe freely released NPs, although no evidence for this was found in electron microscopy. The ionic content was higher than 40%, being the main Ag release form for the camping tents in the leaching study.

The total concentration of released Ag for both samples was relatively low, 73.5 ± 1.1 ppb for TENT1_Ag and 59.6 ± 2.5 ppb for TENT2_Ag. A fact that can seem surprising is that TENT1_Ag (which contains less silver) presents a higher Ag concentration than TENT2_Ag. However, it must be considered that for both samples the weight tested was the same. Thus, since TENT2_Ag density is higher, in order to have the same weight the volume tested was lower, so the coating area from where the release was coming from was smaller too. To delete the area factor release rates were normalized with the area and are presented in Table 12.

Table 12 – Camping tent case study release rates

RELEASE RATE (Ag μg / textile m ²)	
TENT1_Ag	183 ± 3
TENT2_Ag	161 ± 7

With the area correction TENT1_Ag still presents a higher release. In any case, the release rate difference between both samples is very small suggesting that, as expected, their release behaviour is very similar. Indeed, since only the superficial layers of the coating containing the Ag-PEI NPs are being released, there should not be difference on the release rate per area.

Considering that the starting concentrations were 68.9 ± 0.2 ppm for TENT1_Ag and 111.9 ± 2.0 ppm for TENT2_Ag (Table 11) and knowing the total amount of Ag released, the released percentage can be determined. The values obtained are $1.07 \pm 0.02\%$ and $0.53 \pm 0.02\%$ released of total silver for TENT1_Ag and TENT2_Ag respectively. Since TENT1_Ag sample presents almost the same release than TENT2_Ag sample although it had almost the half of initial silver content, it makes sense that the total release percentage is the half than for TENT2_Ag.

5.4. Conclusion

Leaching experiments proved that silver is released from camping tents, although the amounts were relatively low. Electron microscopy helped in understanding the impact of the experimental conditions on the samples. This was so small that changes before and after the leaching experiment were not observed. As proved by the ICPMS analysis, the Ag amount (%) released was $1.07 \pm 0.02\%$ for TENT1_Ag and $0.53 \pm 0.02\%$ for TENT2_Ag. With such small releases as expected no significant changes in the coating surface were observed and no Ag NPs were detected. Moreover, 40% of the silver released was in ionic form, which decreased even more the chances of finding Ag NPs in leaching waters since dissolution of any released silver NPs could have occurred. In addition, release of Ag embedded in the coating and/or attached to fibres is also a possibility, what would explain why 36% – 37% of the released silver was smaller than $20\mu\text{m}$ but it was not ionic, and that 20% of the released silver was present in fragments bigger than $20\mu\text{m}$.

6. INOTEX: cotton textiles with antibacterial activity

6.1. Introduction

The case study on antibacterial textiles was newly proposed at July 2017. It develops the experiments done within the GUIDEnano project [15], where promising results were obtained. Within NanoFASE, the attachment on cotton textile of silver nanowires with different lengths compared with silver nanoparticles was evaluated. It must be emphasized that while textiles with Ag NPs are commonly developed in INOTEX, textiles with Ag NWs were just synthesised for the NanoFASE project.

6.2. Materials and methods

The Ag nanoparticles coated with PVP were provided by a project partner (APP NANO) and the Ag nanowires (also coated with PVP) were provided by an external producer (NANOGAP), both dispersed in water. Both were characterized by ICPMS (Agilent 7500, Agilent Technologies) and electron microscopy to determine the concentration in dispersion and its morphology. Ag NPs were characterized by TEM (JEM-2100) while Ag NWs were characterized by SEM (FEI Helios Nanolab 660) using the STEM (Scanning Transmission Electron Microscopy) detector. Due to their spherical shape, nanoparticles could be measured using the automatic counting method included in FIJI Software [14]. However, nanowires were more complex to measure due to their linear shape. Thus, the same automatic counting method used for the nanoparticles was not feasible. Diameter and length of the nanowires were counted manually one by one. The longer nanowires, due to their size usually presented as curved and this feature hindered measurement because the measurement tool uses a straight line. For these cases an specific plugin for FIJI able to determine the length of curvilinear structures was used [16], [17]. An example can be seen in Figure 48.

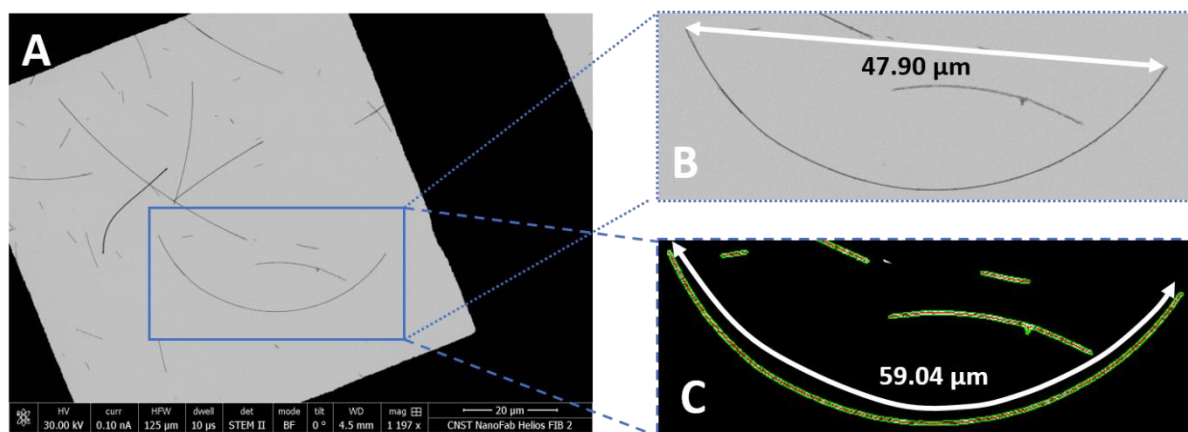


Figure 48 – A) STEM image; B) NW length using predetermined FIJI software; C) NW recognition and length measurement using FIJI plugin.

After characterization all the Ag nanomaterials were sent to INOTEX, who impregnated the cotton fabrics with the different nanomaterials (one nanomaterial in each fabric) together with a wetting agent and a binder. The theoretical final concentration of Ag in textiles was expected to be around 25 ppm.

Since the intended use of the textiles used in the case study is clothing, household washings present the most critical exposure scenario of Ag nanomaterials to the environment. For this reason, this was the process evaluated. After the cotton fabrics were impregnated they were sent to LEITAT (WP4) to perform the household washing simulations. Four different samples were provided: one containing the Ag NPs, one with the longer Ag NWs, one with the shorter Ag NWs and one without Ag for control. All the samples contained the same amount of binders and wetting agents. Textile samples were digested with acid in an analytical microwave digestion system (MARS, CEM, 1600W) and analysed through ICPMS (Agilent 7500, Agilent Technologies) to determine the Ag concentration. Electron microscopy images were obtained with SEM (FEI Helios Nanolab 660) to observe the nanomaterials distribution in the textiles. Since the concentration in released waters was expected to be quite low, a centrifugation step (clinical centrifuge, International Equipment Co.) at 1700g (3450 rpm) for 2h was applied on the released water samples before the collection for the deposition on TEM grids. Released waters sediments from the centrifugation process were observed through SEM (FEI Helios Nanolab 660) with STEM detector and EDX (Oxford Instruments X-Max 80 mm² SDD-EDS detector) for the elemental analysis.

Washing cycle protocol

The procedure is similar to the one used for curtains, described in section 4.2. The household washings simulations were performed according to an adaptation of the standardized protocol ISO 105-C06:2010 Textiles -- Tests for colour fastness -- Part C06: Colour fastness to domestic and commercial laundering [4]. Each sample consisted of 2.95 ± 0.05 g of fabrics, which were cut in squares with approximately 14 cm side. All the samples were sewn with a cotton thread to avoid the textile fraying and yarns release in the washing waters, which would have hampered later characterization. The washings were performed in 550 ± 50 ml stainless steel vessels with 75 ± 5 mm diameter and 125 ± 10 mm height. Each vessel contained one sample, 10 stainless steel (SS) balls of 6 mm diameter (to simulate mechanical impact) and 150 ml of detergent solution. The detergent used was a light duty detergent with anionic and non-ionic surfactants, fabric care additives and enzymes. The dose used was 4 ml of detergent per distilled water liter giving a washing pH of 7.4. The tests were carried out in a Linitest+ equipment (Lab Dyeing System, Atlas) at 40 ± 2 rpm and 40 ± 2 °C.

Prior to the textile washing the vessel with the detergent and the stainless steel balls were placed inside Linitest+ for 5 minutes in order to reach the desired temperature. Then the textile was also introduced and washed for 30 minutes. The textile was retrieved and the washing waters were collected. Then, following the ISO protocol, two rinsing cycles of 1 minute at 40 ± 2 rpm, 40 ± 2 °C and 100 ml of distilled water were performed [4]. The rinsing solutions were also introduced in Linitest+ without textile for 5 minutes for temperature conditioning and waters were collected for further characterization. After the washing cycle the samples were dried at ambient temperature. Four different samples were tested:

Table 13 – Samples tested in the cotton textiles with antibacterial activity case study.

NOMENCLATURE	DESCRIPTION
C_SW (control)	Cotton fabric with wetting agent and binder but without Ag
AgNP_SW	Cotton fabric with Ag NPs, wetting agent and binder
AgNWL_SW	Cotton fabric with the longer Ag NWs, wetting agent and binder
AgNWs_SW	Cotton fabric with the shorter Ag NWs, wetting agent and binder

Ag concentration in textiles was analyzed at 1; 3; 5 and 10 washing cycles including three replicates per sample. When a sample reached the expected number of washings it was digested and analyzed with ICPMS, so a new textile was used for the following washings. All the washing waters analyzed belonged to the textile washed 10 times. Washing waters corresponding to 1, 2, 3, 5, 7 and 10 washing cycles were analyzed by ICPMS.

Dissolution experiment

To obtain a better understanding of the nanomaterials behaviour once they are released, a dissolution experiment was performed. 100 ppb dispersions of each nanomaterial were prepared in triplicate. The solutions were prepared in topaz glass bottles to protect them from light. All the bottles were placed inside an orbital shaker (MaxQ 4000, Barnstead) during 24h at 25°C and with a shaking speed of 80 rpm. Samples were collected at 0h, 2h, 6h and 24h. Ionic content of the different samples collected along time was determined by centrifuging the samples with 3kDa centricons (Amicon Ultra-15 Centrifugal Filter Units, Millipore) at 6000 rpm with a centrifuge (J2-HC, Beckman) and analyzing the filtrate by ICPMS (Agilent 7500, Agilent Technologies).



Figure 49 – NMs dispersions inside topaz glass bottles being shaken in the orbital shaker during the dissolution experiment.

6.3. Results

6.3.1. ENMs characterization

Electron microscopy characterization

Electron microscopy images of each NM can be observed in Figure 50. The Ag NPs presented a circular shape, a homogeneous size and big NPs aggregates were not found. In Figure 50B it is clearly seen how the PVP covered all the nanoparticles. The amount of PVP was so high that

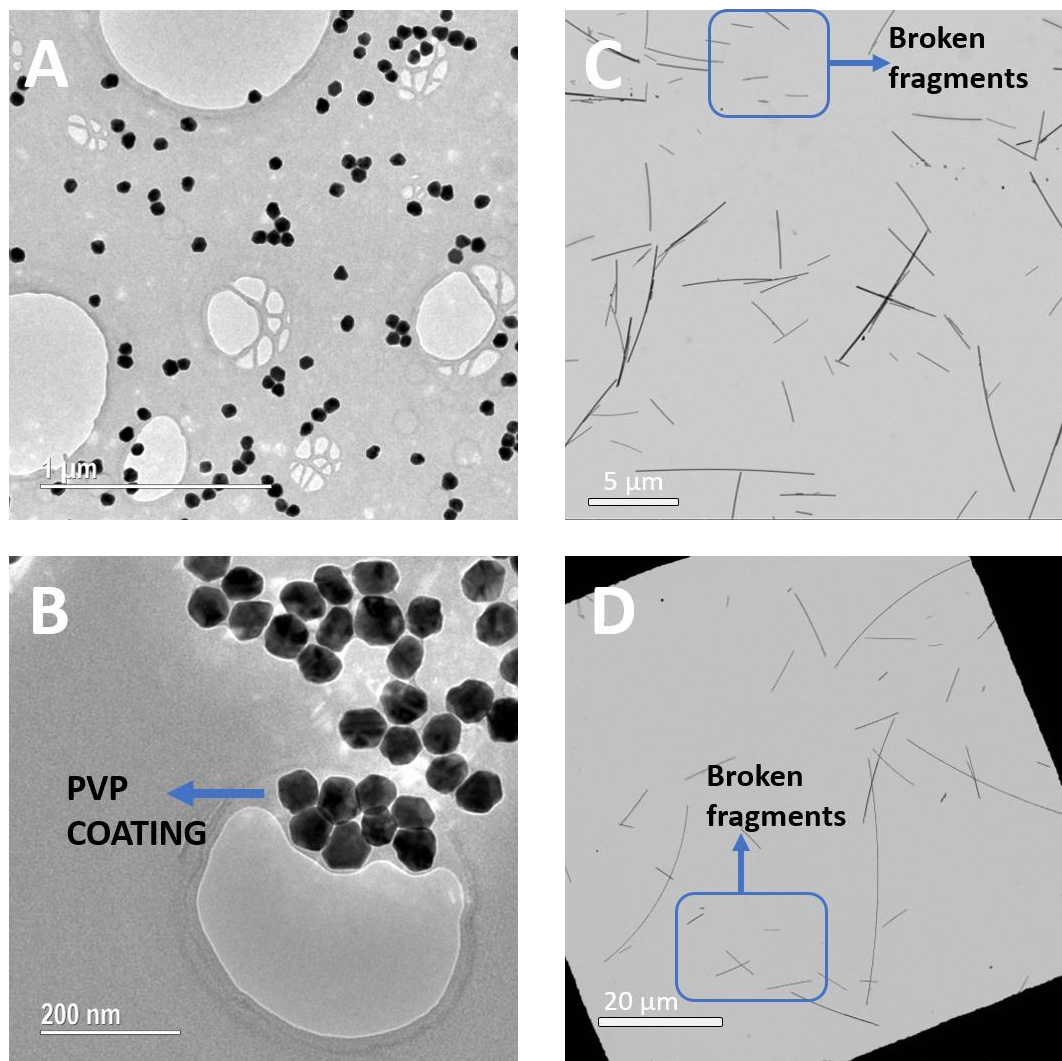


Figure 50 – Ag NMs electron microscopy images: A), B) Ag NPs; C) AgNWs_s; D) AgNWs_L

it looked like a film covering most of the grid. Both nanowires dispersion presented a clear wire shape with a high aspect ratio (length-to-diameter ratio $\gg 1$). A clear difference in length between the longer and shorter nanowires was also observed (note change in scale of Figure 50 C and D). Longer nanowires were more difficult to measure because their size was close to that of the mesh holes in the TEM grid. As a consequence, some of the nanowires were partially laying in the copper grid framework, which prevented its measurement.

Electron microscopy images enabled the determination of a particle size distribution for the dispersions of the different Ag NMs. Results are shown in Figure 51. The size characteristics

of the different nanomaterials were evaluated by means of frequency distributions (histograms). For each set of measurements the corresponding average size with standard deviation and Relative Standard Deviation (RSD) are also shown. RSD, which is usually expressed as a percentage (RSD%), is a standardized measure of dispersion of the frequency distributions that is commonly used for comparing the uncertainty between different measurements. For Ag nanoparticles, due to their spherical shape, the diameter is the only size parameter considered, while for nanowires the length, diameter and length-to-diameter ratios are plotted.

The Ag nanoparticles presented a normal distribution with an average diameter of 64 ± 6 nm. The minimum and maximum diameters measured were 49 nm and 82 nm, respectively. This small difference between maximum and minimum values together with a low RSD% of 10% (the lowest for all the sets of measurements) suggests that Ag-PVP NPs dispersion was very monodisperse. For both nanowire samples the RSD% of the diameter measurements was around 3 times higher than for the Ag NPs, suggesting that the diameters size is more diverse. A clear difference was observed with both samples. In the case of the nanowires expected to be shorter the average diameter was 44 nm, while for the longer ones it was 151 nm. This last value, according to the ISO definition [18], would invalidate the consideration of the longer wires as “nano” since none of their external dimensions is ≤ 100 nm.

The length measurements of both nanowires samples confirmed what was inferred just looking at the images, there was a significant difference between the length of the two samples. The ones expected to be shorter had a 3.5 ± 2.4 μm average length, while the ones expected to be longer 15.1 ± 13.9 μm . In the two cases the histograms high frequency bins were mainly in the lower length range (left size of the graph), which means that in both dispersions there were more nanowires of small length than with long length. This fact can be easily appreciated in Figure 50C and Figure 50D, where the small fragments were indicated. One reason could be that the nanowires had different lengths from the production process. However, it is unlikely to observe such a big difference in chemical synthesis, and if that was the reason, the diameter variability (RSD%: 27% for shorter and 32% for longer NWs) would be similar to the length variability (RSD%: 67% for shorter and 92% for longer NWs), which was not observed. In addition, the small fragments diameter was similar to that of bigger NWs, what leads to the conclusion that they were just broken fragments. In the case of the longer nanowires the histogram is even more shifted to the left and the RSD% is much bigger (67% for the shorter ones and 92% for the bigger ones). The reason could be that the longer the NWs the more likely it is that they break in smaller fragments, which can break again in even smaller fragments, ending up with a very disperse distribution and with most of the measurements reflecting nanowires of smaller length. The breakage could occur during the dispersion handling, the redispersion or during the sample preparation for microscopy. In any case, it gives information of how sensitive they are to breaking, something to consider when working with these kinds of samples, especially if as in our case they must be manipulated to be impregnated in textiles.

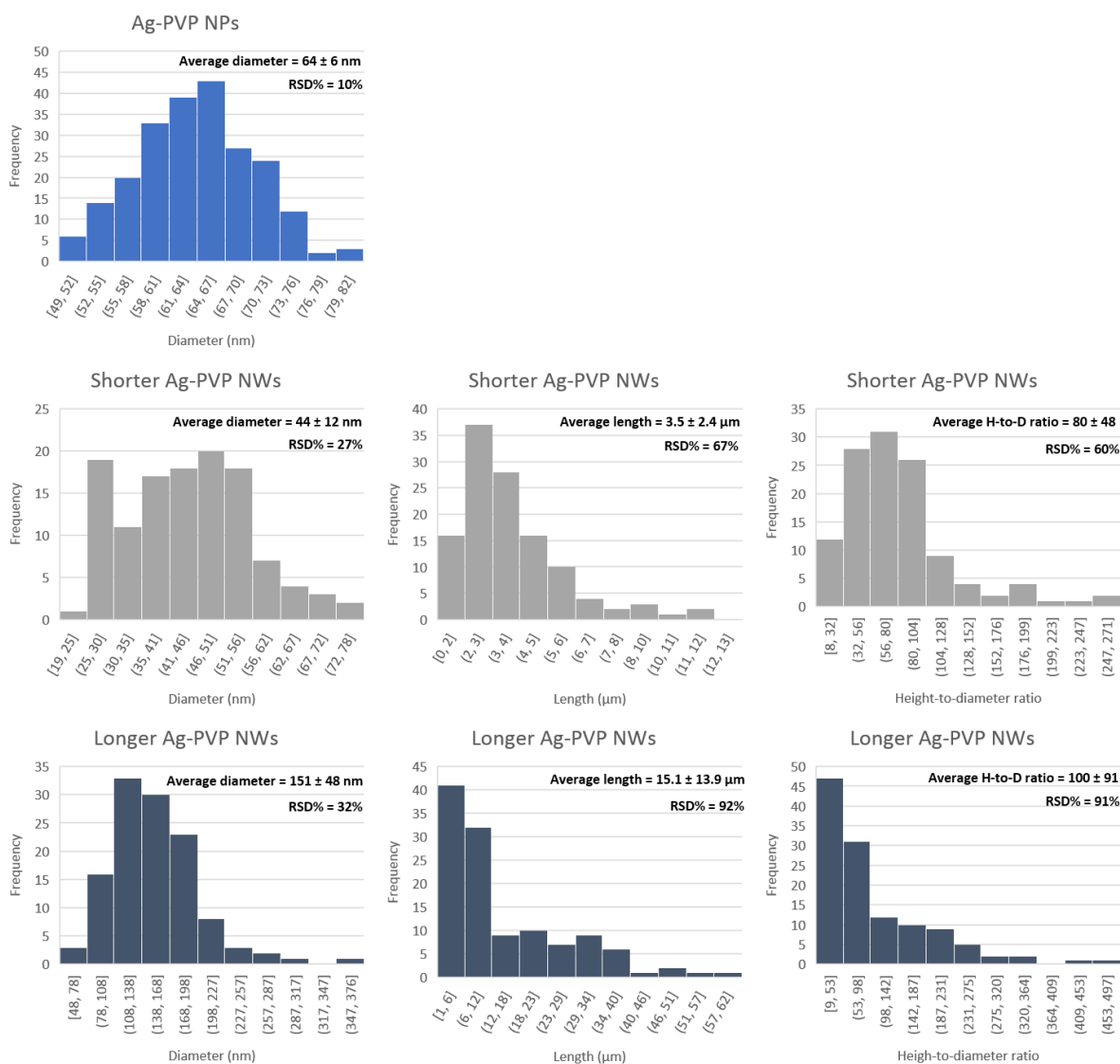


Figure 51 – Size distribution of Ag NMs

Inductively Coupled Plasma Mass Spectrometry

The Ag concentration in the different dispersions, determined by ICPMS, were used by INOTEX as a guidance to achieve the desired concentration in the textiles.

Table 14 – Ag concentration in the Ag dispersions determined by ICPMS.

SAMPLE	Ag CONCENTRATION (g/L)
AgNP_Dispersion	16.2 ³
AgNW_L_Dispersion	35.0 ± 1.6
AgNW_s_Dispersion	102.2 ± 8.5

³ Information provided by AppNano

6.3.2. Textiles characterization

Electron microscopy characterization

The textiles after the nanomaterials impregnation were observed with SEM to determine the distribution in the unwashed textiles.

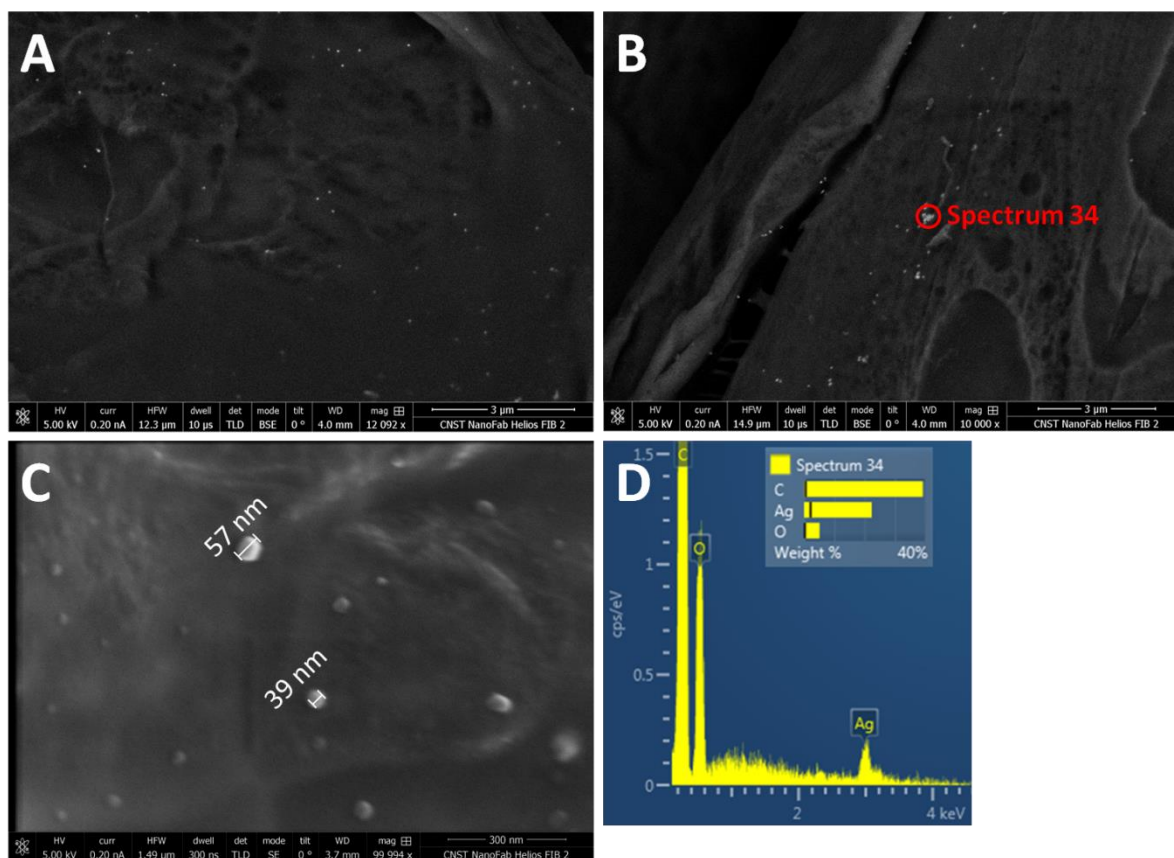


Figure 52 – SEM images and corresponding EDX analysis of unwashed textile containing Ag NPs.

For the sample containing Ag NPs the best way to detect them was using backscattered electron imaging (BSE) mode. Silver, due to its higher atomic number, was observed brighter than textile yarns, organic components or other common salts (e.g. KCl or CaCO₃) making its detection easier. In Figure 52A, B the Ag NPs presence along the textile yarns is observed. The nanoparticles were uniformly distributed and generally isolated, although some small aggregates were also found (Figure 52B). The area with the aggregate was used to perform an EDX analysis, which confirmed that the brighter dots observed were Ag (Figure 52D). Secondary electron imaging (SE) mode was used in higher magnification images. In Figure 52C the NPs size was measured. The diameter values (57 nm – 39 nm) were slightly smaller to the one measured in the raw NPs dispersion (64 ± 6 nm; Figure 51). During the impregnation process, since they were dispersed in water, part of the NPs could have dissolved removing some solid material, which would explain the size decrease. In any case, the diameter of the NPs in the textile was very close to the ones measured in the raw dispersion.

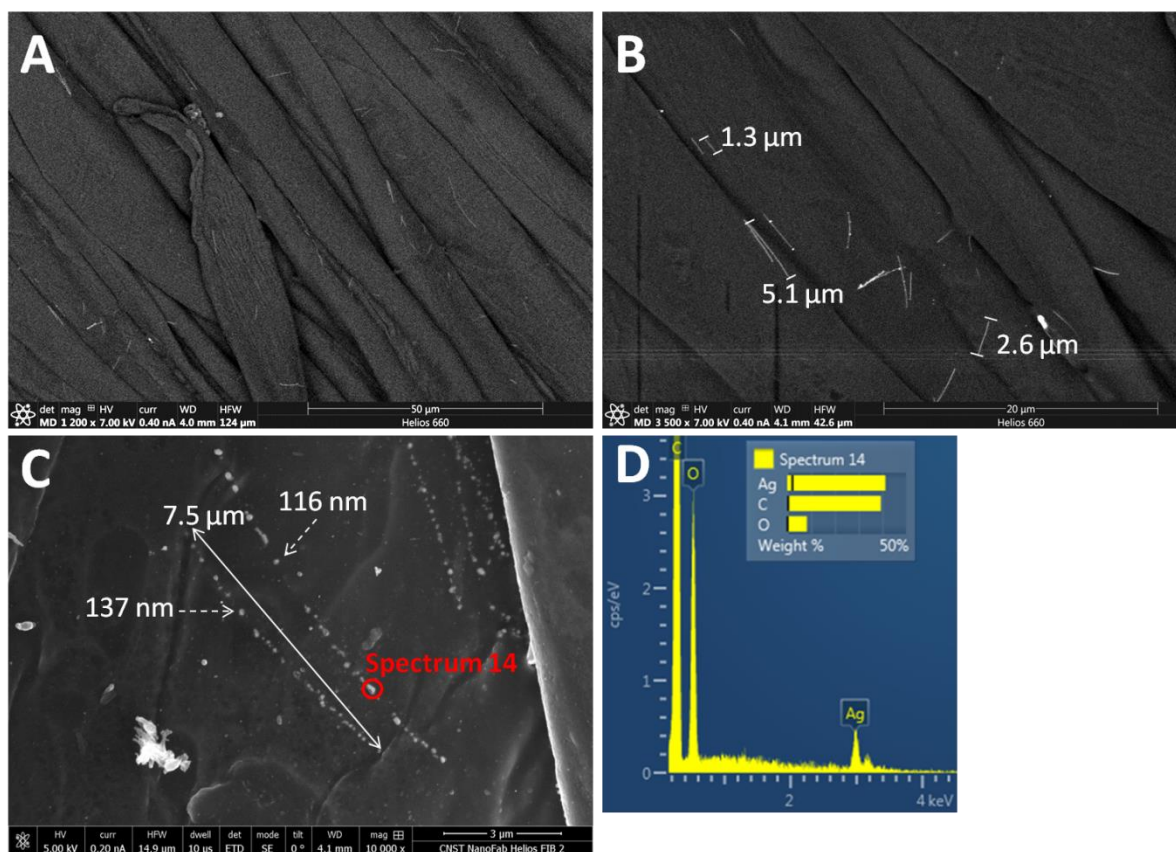


Figure 53 - SEM images and corresponding EDX analysis of unwashed textile containing the shorter Ag nanowires.

For the samples containing Ag nanowires, since they were easily recognized due to the wire shape, secondary electron (SE) mode was used. In Figure 53A,B the shorter nanowires on the textiles are observed. They were uniformly distributed along the textile and isolated, like the NPs. Although some overlapping nanowires were also found. The nanowire sizes measured were in the same size range in the raw dispersion (3.5 ± 2.4 nm; Figure 51). In some nanowires fragmentation was observed at higher magnifications (Figure 53C). The wire shape was still visible but not as a continuous line. The wire was formed by individual spherical particles around 100 nm one next to the other with a space between them. A length increase, compared with the compact nanowires, was also observed. These results were very significant since the nanomaterial characteristics on the textile were completely different from the one expected. It was not clear why the fragmentation phenomenon occurred, but water contact together with exposure to high temperatures (drying at 120°C and curing at 140 °C) during the impregnation process could have caused this effect. What was clear is that fragmentation occurred once the nanowires were on the textile surface, otherwise the wire shape would not have been maintained. EDX analysis confirmed that the fragmented wires were made of Ag (Figure 53D). A high number of nanowires observed were fragmented but not all of them.

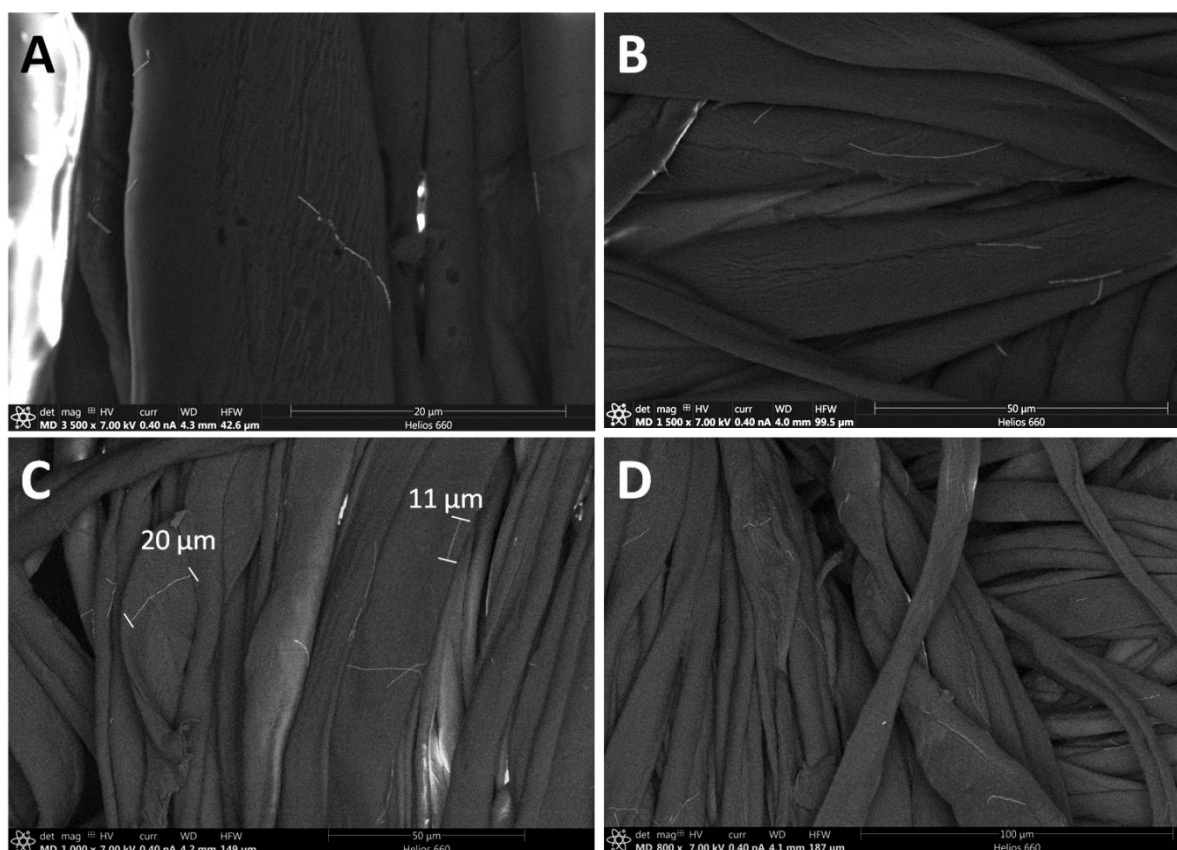


Figure 54 - SEM images and corresponding EDX analysis of unwashed textile containing the longer Ag nanowires.

The results obtained for the longer nanowires were similar to the shorter ones. Multiple nanowires were observed on the textile surface. Some of them were isolated while others were overlapping one onto the other. Their length was in agreement with the lengths measured for the raw dispersion. Again some of the NWs observed were fragmented (Figure 54A).

The control sample, although it did not contain any NMs, was also observed with SEM. On the surface multiple particulate matter was observed. However, from the EDX analysis it was confirmed that they mainly were common salts like calcium carbonate (CaCO_3) probably coming from the water used in the impregnation process. No Ag NMs were observed in the control sample. Particulate matter in some occasions can have a similar size to engineered nanomaterials causing confusion. For this reason EDX analysis is an indispensable technique to prove the nanomaterials presence in the sample.

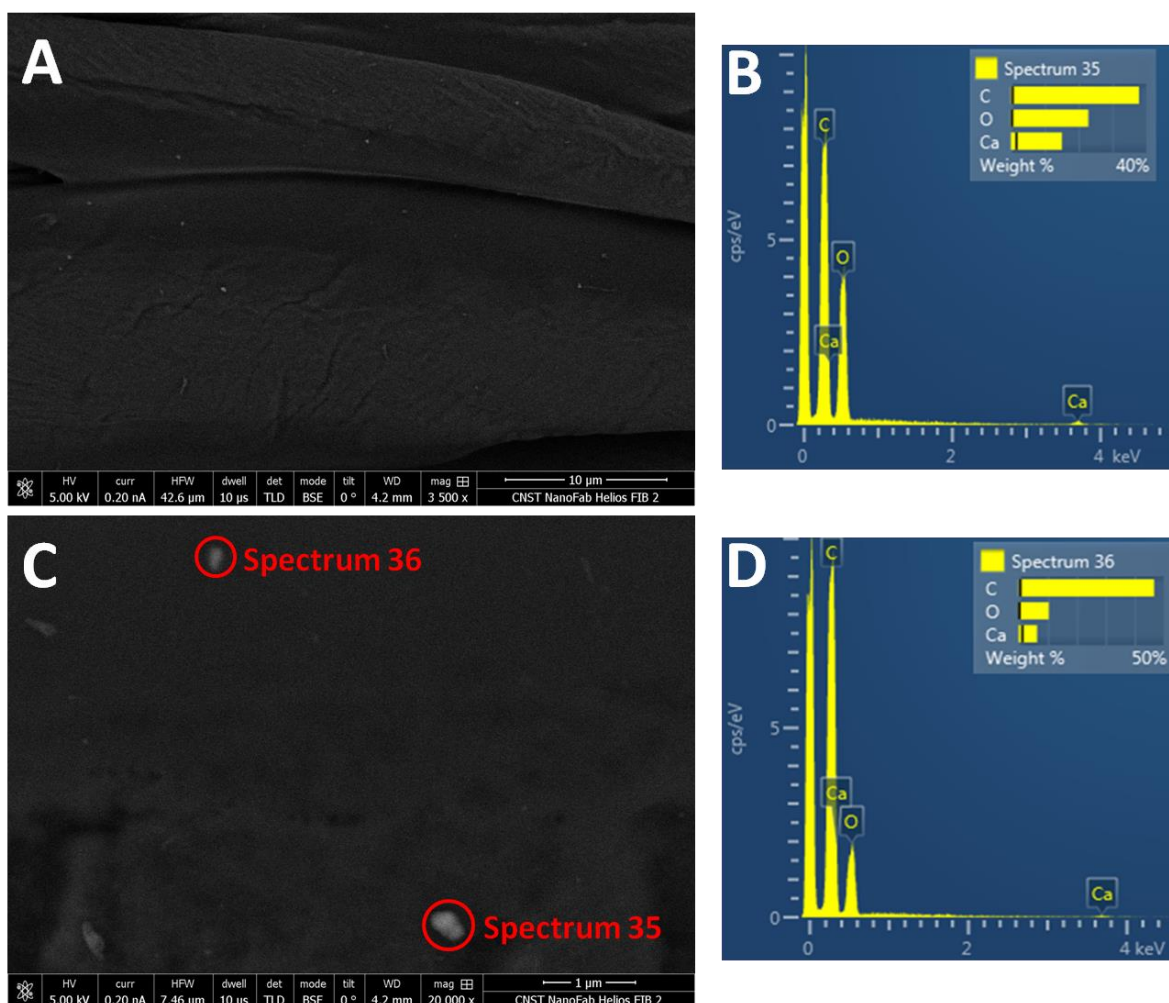


Figure 55 - SEM images and corresponding EDX analysis of unwashed control textile.

Inductively Coupled Plasma Mass Spectrometry

The Ag concentration in the different textiles samples with washings was measured by ICPMS, the results are shown in Figure 56. The height of the bars represents the mean value coming from the three replicates, while the error bars correspond to their standard deviation. In Figure 56A, the Ag concentration in textiles is shown while in Figure 56B the Ag remaining percentage is plotted considering the unwashed textiles concentration as a 100%. Both charts are built with the same data, but the different representations ease the observation of different conclusions. Control samples without silver were also washed and analysed through ICPMS but Ag was not detected. Thus, for simplicity, it was not included in the chart.

Looking at Figure 56A, the values for the unwashed textiles show starting concentration values of 22 ppm, 19ppm and 18 ppm respectively. As previously mentioned in methodology section, the textiles expected concentration was around 25 ppm. In none of the cases was the exact concentration achieved but very close values were obtained. For the different samples different concentrations were achieved and RSD% values from 2% in AgNP_SW to 25% and 12% in AgNW_s_SW and AgNW_L_SW were obtained, what gives an idea of the heterogeneity

that the textiles can present. Impregnation is a common and cost effective method used in the textile industry to impart additional functionality. Some heterogeneity is expected and does not impact on the quality of the product.

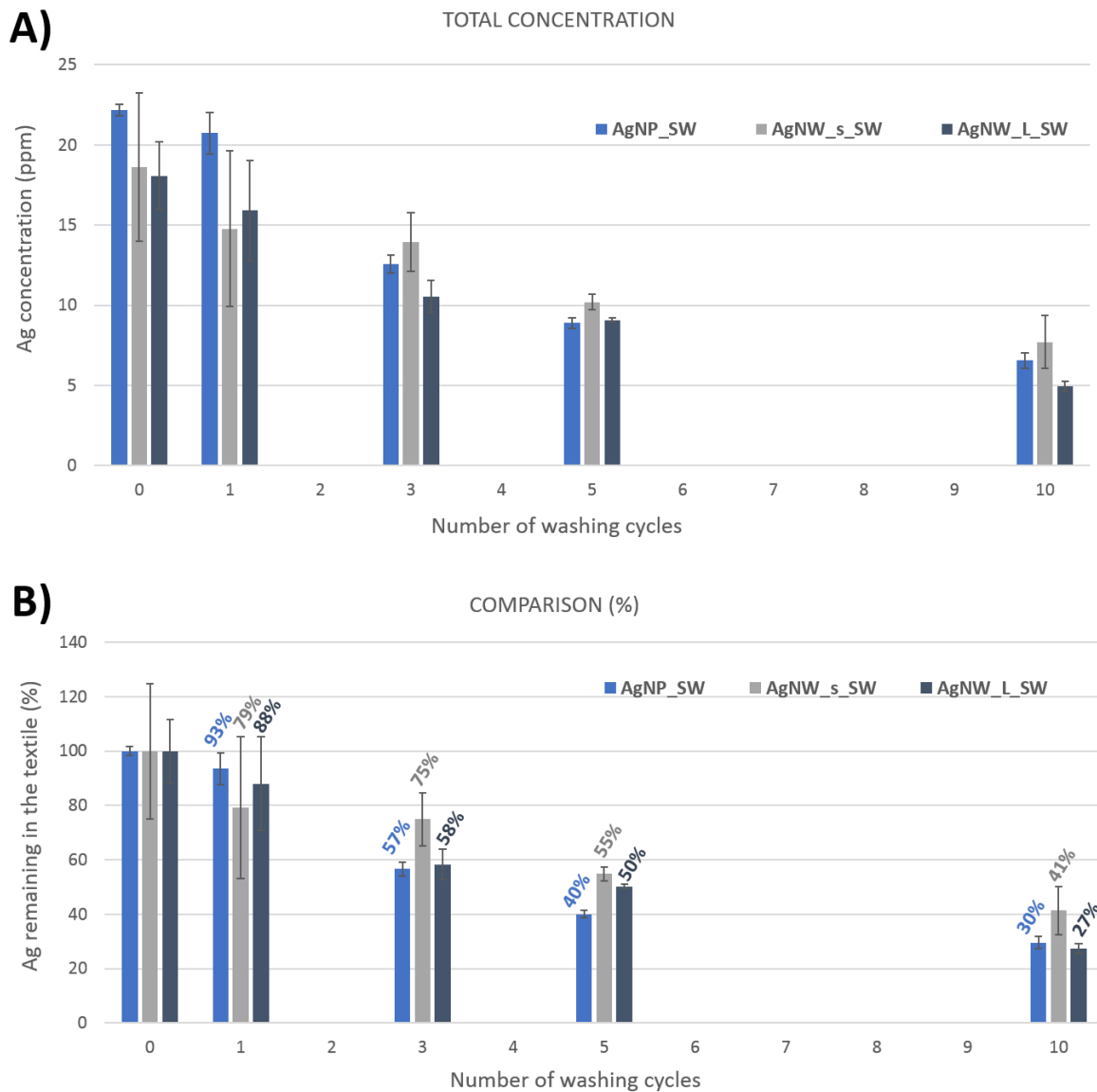


Figure 56 – ICPMS results of Ag concentration in textiles along washings. A) Total concentration; B) Comparison (%).

Looking at Figure 56B can be concluded that for all the samples the concentration decreased with washings. Moreover, in all the cases, release was higher in the first washings and decreased as more washings were performed. According to the results, the sample with lowest release contained the shorter Ag NWs (AgNW_s_SW) with 41% of Ag remaining. The sample containing Ag NPs (AgNP_SW) presented almost 10% more release, only 31% of Ag remained. Finally, the sample presenting a higher release was the one containing the longer nanowires (AgNW_L_SW), in which only 27% of the silver remained after 10 washings. For all the samples, almost the half of the silver had been released after only five washings, meaning that the attachment was not very effective.

6.3.3. Released materials characterization

Electron microscopy characterization

In the AgNP_SW released waters no silver was detected. As shown in Figure 57 micrometric round shaped particles were found, but the EDX determined these were salts probably coming from the water, not silver.

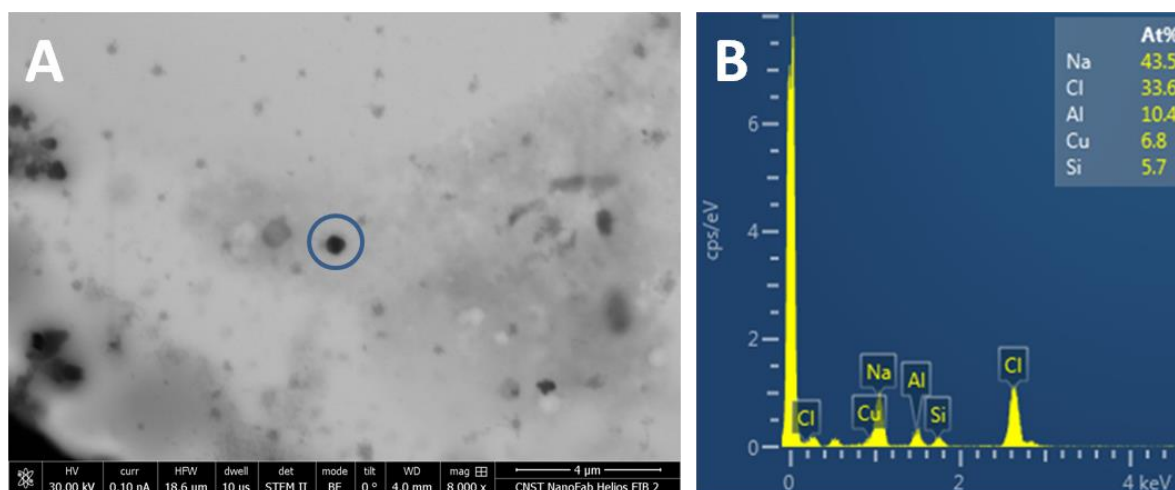


Figure 57 – STEM image and corresponding EDX analysis of the AgNP_SW release waters.

In the case of AgNW_s released waters, a nanowire fragment was found together with detergent residues. As shown in Figure 58C, the background contained C, O, Si, Cu and Al. The Cu and some C probably come from the TEM grid, Si and Al from the detergent and O is highly abundant in the environment. In the EDX analysis of the nanowire, apart from the background elements, a high amount of Ag was detected confirming that it was a Ag nanowire. Sulphur was also detected suggesting that part of the silver could be sulphurized, most likely in the surface. However, the intensity of the peak was so small that it could not be confirmed. Even more interesting is the fragment to which the spectrum 29 refers to (Figure 58E). In this occasion the EDX analysis confirms that it is Ag but from the magnified image (Figure 58B) is seen that the wire shape is not maintained. Most probably what is being observed is the nanowire being dissolved. In this spectrum the S/Ag ratio ($1.0/7.4=0.14$) is higher than in the previous spectra ($0.9/8.2=0.11$), suggesting that the sulphurized silver amount is higher. Another important observation is that in the lower part of the nanowire an agglomerated structure similar to the one observed in the top is also present, suggesting that the nanowires start dissolving mainly from the ends as would be expected. Small fragments protruding from the middle section of the wires are also seen, but they are not as abundant as the ones in the tips. Moreover, the diameter size of the nanowires was 40 nm, very close to the diameter size measured in the raw nanomaterials 44 ± 12 nm (Figure 51), meaning that silver was not released in a high amount in the inner sections of the nanowire.

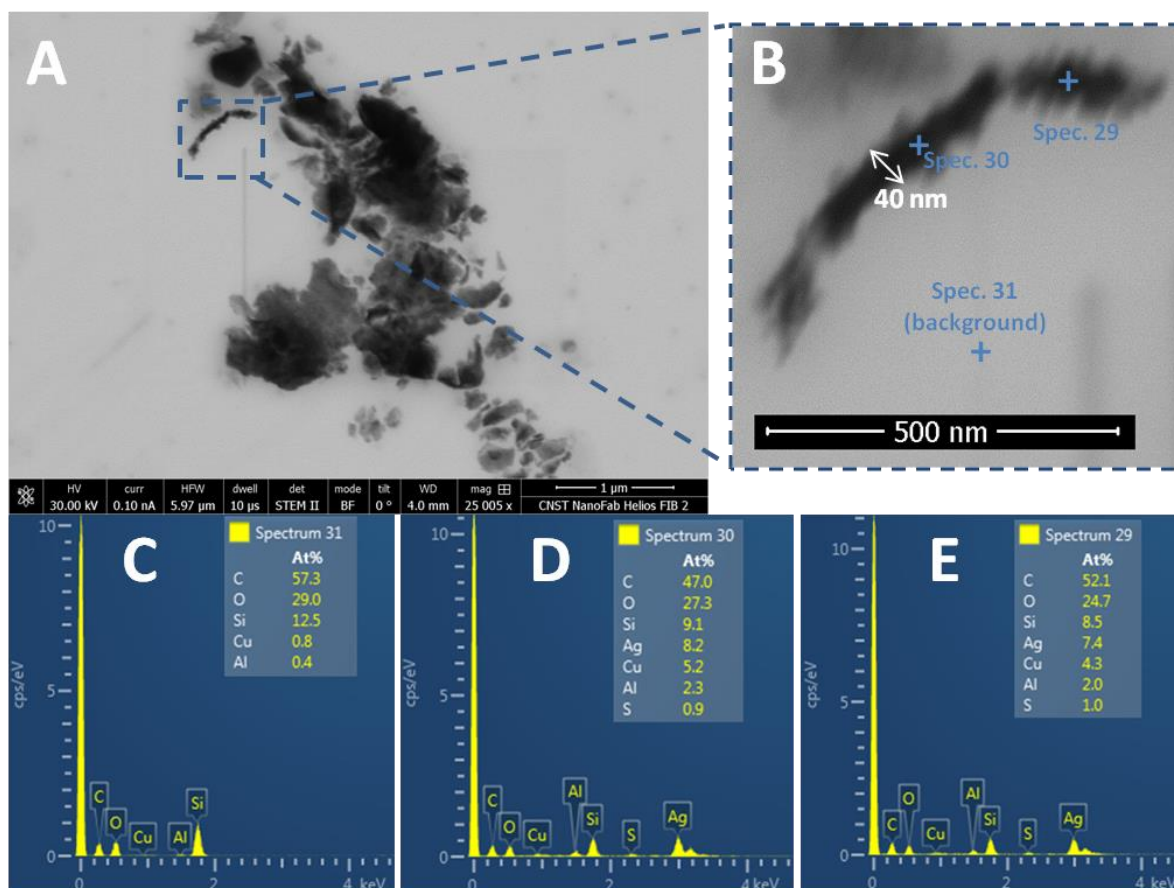


Figure 58 – STEM image with corresponding EDX analysis of AgNW_s_SW release waters.

In the released waters of Ag_NW_L_SW a high amount of nanowires were found. In this case, not only fragments were found as in the case of AgNWs_SW, but also nanowires of the same length of the original dispersions. In Figure 59 some of the fragments are shown. In all the images the nanowires appear next to detergent residues, to which they probably were adhered. In Figure 59C part of the nanowire can be seen without detergent. However, in Figure 59D, it can be seen how small residues of detergent are attached all along the nanowire.

In Figure 60 a higher magnification image of the nanowires with the corresponding EDX spectrum is shown. On this occasion, small particulate matter surrounds the nanowire not only in the tips but also in the central area. The information provided by the EDX is very similar to the one obtained from the shorter nanowire (Figure 58). The background spectra, as in the previous case, shows C, O, Si, Cu, Al. While the spectrum from the middle of the nanowire, apart from the background elements also detects Ag. When the EDX analysis was performed in the small particulate matter surrounding the nanowire Ag was also detected together with S. Again it could be Ag dissolving from the nanowires, which was partially sulphurized.

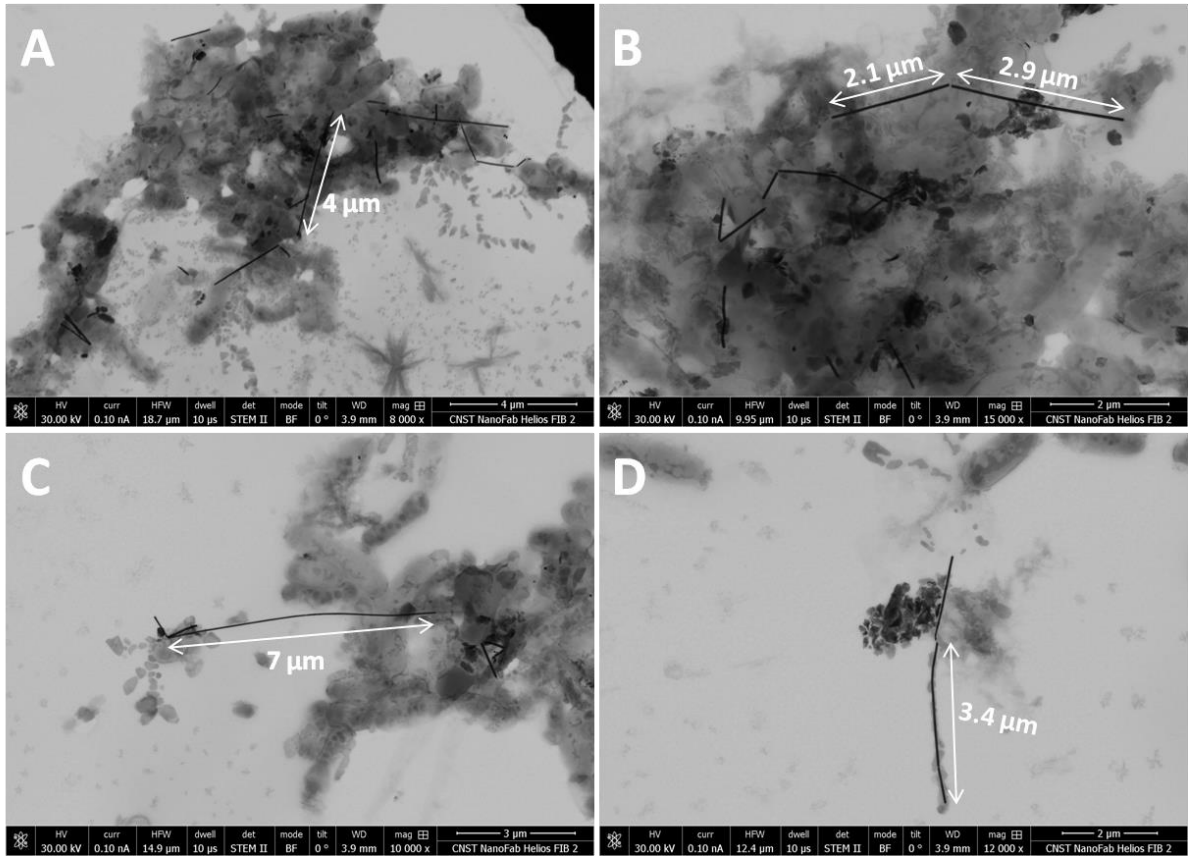


Figure 59 – STEM images of AgNW_L found in the release waters.

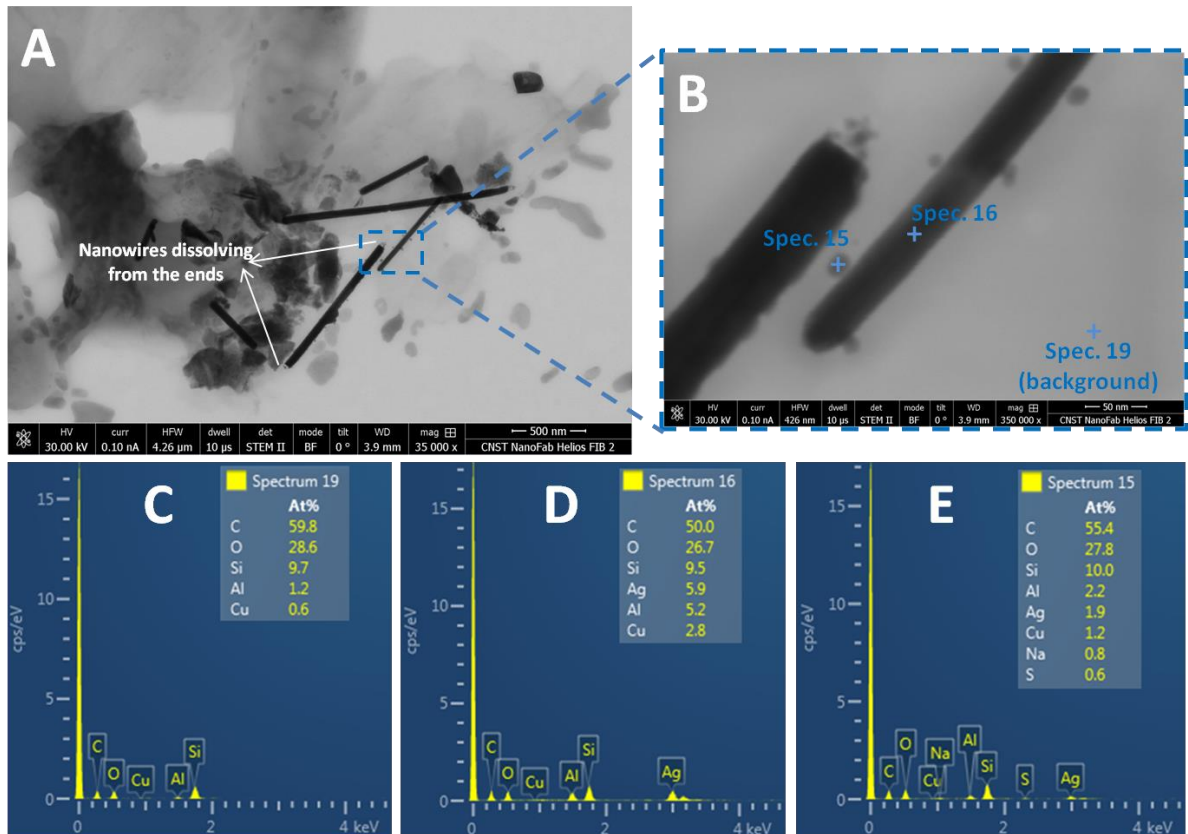


Figure 60 - STEM image of AgNW_L found in the release waters with its corresponding magnification and EDX spectrums.

Inductively Coupled Plasma Mass Spectrometry

In Figure 61 the Ag concentration in washing waters measured by ICPMS is plotted. The trend observed was to measure higher concentrations in the first washing waters and a decrease along washings, which agrees with the trend observed in textiles (Figure 56) where release also decreased with washings. During the first washings, especially in the first, there are relatively big concentration differences among the samples. However, as more washings are performed the closer the values are. Indeed, for ten washings, the Ag concentration for all the samples was almost the same, all the samples being in a range of 3.5 to 7.0 ppb.

Rinsing waters were also measured but the concentration of Ag was not high enough to be detected. The reason why the washings compared to the rinsing waters present a higher concentration is because the washing time was 30 minutes while the rinsing was only 1 minute. In any case, most probably, the rinsing also produced some release, although it was very small compared to the washings.

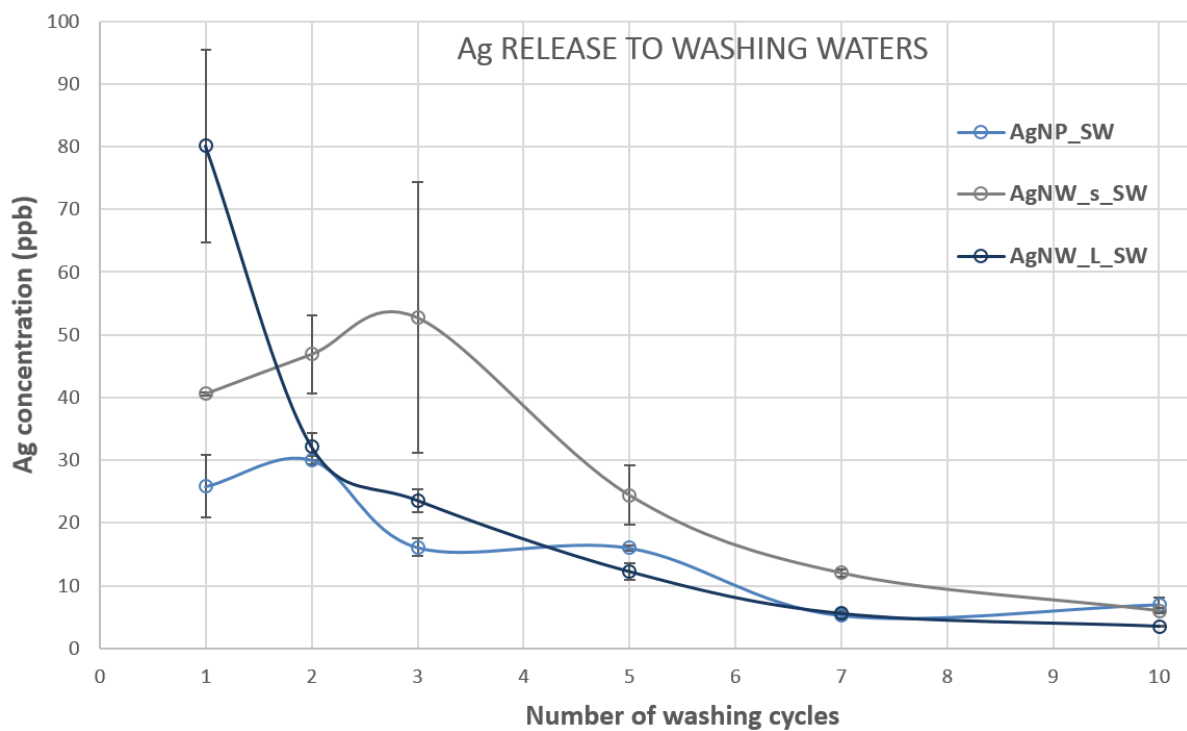


Figure 61 – Ag release to washing waters along washing cycles for the three different samples.

The concentrations measured in released waters can be related to the textiles concentration decrease along washings. For example, the concentration difference in the unwashed AgNP_SW textile compared to the one time washed sample is 1.4 ppm. Considering that the textile weight was 2.95 g and that the Ag was released to 150ml of water with detergent, the following calculation can be performed to estimate the Ag concentration in the released waters:

$$Ag \text{ concentration in released water} = \frac{1.4 \frac{mg \text{ Ag}}{kg \text{ Textile}} \cdot 2.95 \cdot 10^{-3} \text{ kg Textile}}{0.15 \text{ L}} = 28 \text{ ppb}$$

In this particular case it exactly matches with the concentration found in released waters. However, for the rest of the cases there is no equivalence since as explained in the methodology section, once a textile reached the planned amount of washings it was digested and analyzed by ICPMS to determine the Ag concentration, so a new piece of textile was washed again to reach the next number of washings. The variability in the textiles does not allow making precise calculations, but it allows knowing if the range of concentrations found in release waters is in agreement with the Ag released from the textiles determined from the ICPMS values from the textiles. In this case, for all the samples, the values found in released waters were in the same range as the expected concentrations coming from the textiles analyses, what means that both results are in agreement.

6.3.4. Dissolution experiment

The ICPMS results obtained from the dissolution experiment are shown in Figure 62. The different Ag nanomaterials presented different dissolution behaviours. The longer Ag NWs were the ones had a higher ionization rate with around 17% of the silver ionized at the end of the experiment. More than half (10%) of the ionization occurred in the first two hours, meaning there was a higher ionization rate initially. In addition, the trend followed suggested that the ionized Ag would continue to increase. For AgNW_s the higher ionization rate also occurred in the beginning, presenting almost the half of the ionized silver (4%) in just 2h. However, in this case, it looked like the ionized material plateaued since the concentration at 6h and 24h were very similar. For the AgNPs, unlike the other two nanomaterials, no ionized material was detected after the first two hours. Ag⁺ was only detected after 6h and 24h, both concentrations being very similar. Although, for the AgNW_s and AgNPs it looked like the amount of ionized silver was not increasing, it is possible that the ionization rate could increase with more time.

For none of the nanomaterials was 100% ionization was observed, indeed the higher value was only 17%, meaning that the duration of the experiment was not long enough to observe the complete dissolution of the nanomaterials. However, the results obtained allow an indication of the ionization behaviour of each of the materials in the first hours.

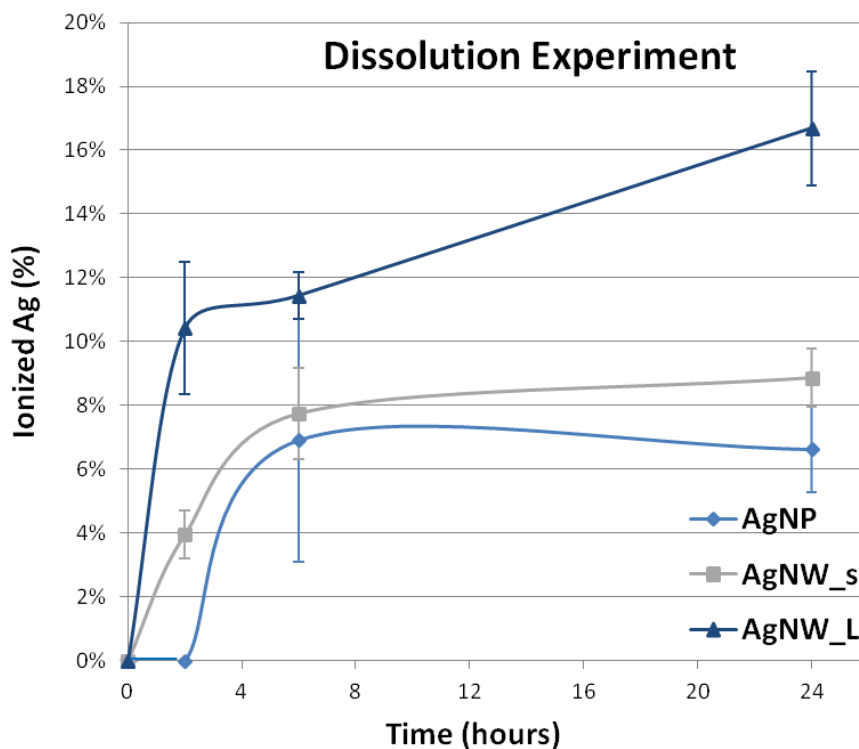


Figure 62 – Dissolution experiment: ionized silver along time.

6.4. Conclusion

Morphology and size characteristics of the starting nanomaterials dispersions have been proved to match the expected requirements by electron microscopy. Ag NPs presented a very monodisperse distribution while the nanowires were more polydisperse. The longer the nanowires, the higher the amount of broken nanowires fragments were found, what increased the polydispersity. All the nanomaterials could be observed on the textiles. Once the nanomaterials are impregnated in the textile their morphology can be modified. The most relevant change being the nanowires fragmentation in smaller sections.

From the textiles characterization along washings it was demonstrated that the NMs shape and morphology do affect in the attachment efficiency to the textile. The silver concentration after 10 washing compared with the Ag initially present in the textile for AgNP_SW, AgNW_s_SW and AgNW_L_SW was 30%, 41% and 27% respectively. Ag concentration in washing waters was also determined, which agreed with the results obtained from the textiles analysis. Electron microscopy performed on released waters was able to detect Ag nanowires (both long and short) but no Ag nanoparticles were found. Using electron microscopy together with EDX analysis, dissolution of Ag nanowires and a potential sulphurization was observed.

7. FCCCO: photocatalytic coating for roads

7.1. Introduction

Air pollution is a local, regional and international problem caused by the emission of pollutants and can lead to negative impacts on human health and ecosystems. There are many sources of air pollution, including transport. While engine pollutants have decreased significantly in the last 50 years the appreciation of their impact has increased and NO_x in urban atmospheres has been associated with lung diseases [19], [20]. In order to mitigate the problem, multiple initiatives are being developed, some of them considering the use of nanotechnology.

One of them is FCCCO's case study, a photocatalytic coating for roads containing TiO₂ nanoparticles to remove NO_x pollutants from air, using TiO₂ NPs photocatalytic properties [5]. The initiative consists of directly coating the roads in the most contaminated areas (mainly in the cities) in order to degrade some of these pollutants.

However, since the coating is exposed to outdoor conditions, concerns due to potential release of TiO₂ NPs from the coating have been raised. Due to multiple stresses such as weathering and wheel abrasions the coating/asphalt could be damaged leading to nanoparticles being released into surface water drainage systems and from there to the environment, either discharged directly to rivers or via waste water treatment plants. Since the potential application of the coating is very big (there is a very large area of roads that could be coated), it is important to study and analyze if release could occur and in what forms and amounts.

7.2. Materials and methods

Hot Bituminous Mix (HBM) is the most used material in the most city streets and highways. HBMs are manufactured in agglomerate plants at temperatures between 160 °C and 180 °C and are made of the combination of hydrocarbonated binders and aggregates. Combinations of different aggregates granulometrics and different percentages of bitumen, provides different kinds of mixes with different intrinsic properties, and consequently their fields of application are also different. One of the most used mixes in cities is AC16 Surf S.

The AC16 surf S corresponds to a semidense mix which is commonly used in the surface layer of roads. The aggregates used are of porphyry nature for the coarse fraction and a combination of porphyry and limestone for the fine fraction together with calcium carbonate as filler. A close view of AC16 Surf S asphalt is shown in Figure 54.

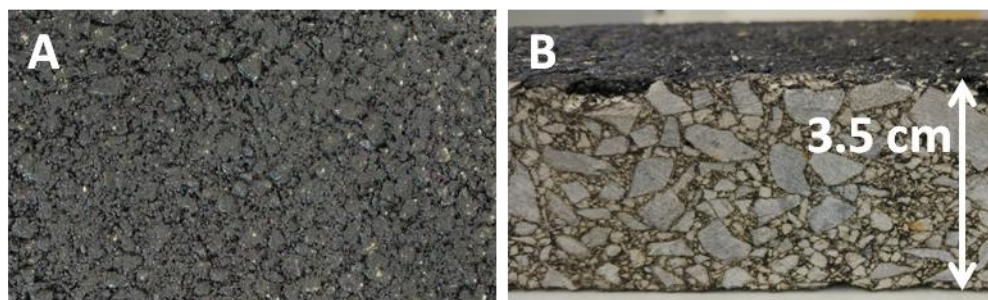


Figure 63 – Close view of the uncoated AC16 Surf S asphalt sample. A) top view, B) lateral view.

The asphalt materials with and without the photocatalytic coating were provided by FCCCO to LEITAT (WP4) for release experiments as well as the TiO₂ dispersion for characterization. 100% anatase TiO₂ nanoparticles (PC 500, Crystal Global) were bought and modified by FCCCO with an organic resin made of a copolymer dispersion based on vinyl acetate and ethylene, in order to obtain the final product. The TiO₂ dispersion was analysed by X-ray Diffraction (XRD) (D5000, Bruker) to confirm the crystalline phase and High Resolution-Transmission Electron Microscopy (JEOL JEM-2100) to show particle size and shape.

7.2.1. Coating application

The coating was applied in FCCCO's facilities by means of a paint spray gun, as shown in Figure 64B. Next to the coated samples different sheets of paper were placed, which were digested in an analytical microwave digestion system (MARS, CEM, 1600W) and further analysed by ICPMS (Agilent 7500, Agilent Technologies) to determine the TiO₂ amount sprayed per area.

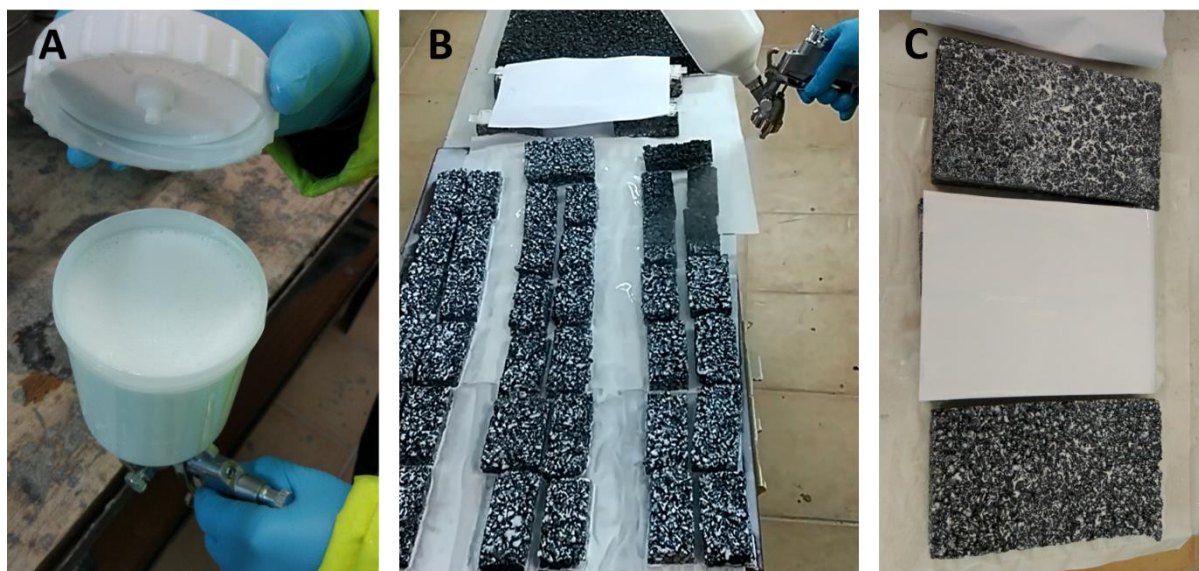


Figure 64 – TiO₂ coating application on asphalt samples. Nano-TiO₂ dispersion A) in the air spray gun container; B) being sprayed on the asphalt samples; C) drying on the asphalt samples and blank papers (which have been used to determine the amount of TiO₂ deposited).

After the coating was applied the samples were dried at ambient temperature.

7.2.2. TiO₂ release monitoring due to weathering and wheel abrasion

In the release experiments two samples were studied:

- AC16_TiO₂: AC16 surf S asphalt with the coating on it.
- AC16_blank: AC16 surf S asphalt without any coating.

The release rates and release forms of TiO₂ nanoparticles coming from the photocatalytic coating on the different asphalts were evaluated. The four samples were introduced into a climatic chamber (Suntest XXL, Atlas) where dry and rain cycles were alternated (29 minutes dry and 1 minute rain). The weathering parameters are shown in Table 15. LEITAT's climatic chamber has been adapted to include individual sample holders and being able to collect the water from the rain cycles after being in contact with the samples, an image of the climatic chamber modification is shown in Figure 65.

Table 15 – Climatic chamber weathering parameters.

Irradiance at 320 nm (W/(m ² · nm))	Black Standard Temperature (°C)	Chamber Temperature (°C)	Relative Humidity (%)	Dry cycle duration (min)	Wet cycle duration (min)
0.51 ± 0.02	65 ± 3	38 ± 3	50 ± 10	29	1

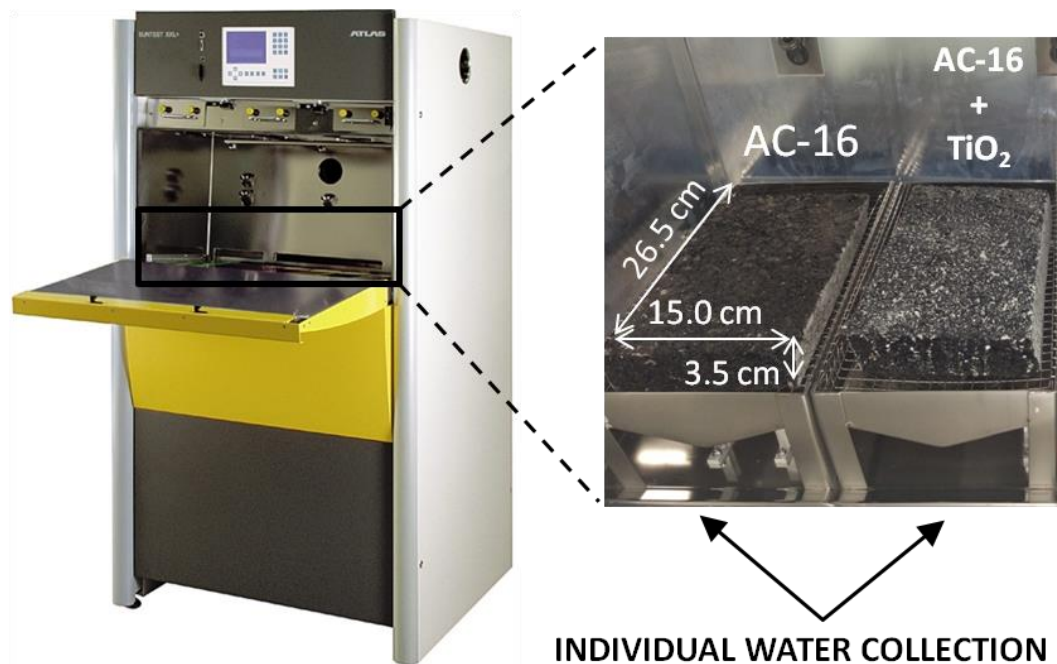


Figure 65 – Asphalt samples distribution inside the climatic chamber

After 14 and 28 days of weathering simulation the samples were taken out from the climatic chamber and were submitted to wheel tracking assays following an adaptation of EN 12697-22:2003 +A1:2007 [21]. In Figure 66 an image of the standardized equipment to perform the assay is shown. The assays were performed at 25°C with a load of 5000 ± 50 N. The wheel width was 80 ± 5 mm and a total of 2000 cycles were applied in each assay, considering one cycle as the wheel going back and forward at a frequency of 1.0 ± 0.1 Hz. After the wheel abrasion simulation the samples were introduced in the climatic chamber to continue with the weathering simulation.



Figure 66 – Standardized equipment used to perform the wheel abrasion simulation.

During some of the rain cycles the water from each sample was individually collected, freeze-dried (CoolSafe 100-9 PRO Freeze Dryer, water sublimation at -95 °C and ~0.3 mbar), digested with acid and further analysed through ICP-OES (Inductively coupled plasma optical emission spectroscopy, Optima 8000, Perkin Elmer) to determine the Ti concentration and the resulting release rate in each case. Characterization with HR-TEM (JEOL JEM-2100) and FE-SEM (field emission scanning electron microscopy, Merlin, Zeiss) with Energy Dispersive X-ray analysis (Oxford Instruments INCA X-Max) was also performed to obtain information regarding the release forms. To provide a more realistic scenario, weathering cycles were alternated with wheel abrasion. The samples collection and wheel abrasion times are shown in Figure 58. It shall be emphasized that waters were collected just before and after abrasion to determine its impact on release. The total simulation time was 42 days (1008h), which is equivalent to approximately 1 year exposure in outdoor conditions in a low altitude, Mediterranean climate with an average annual temperature of 15 °C: temperate winters, rainy springs and autumns, hot and dry summers.

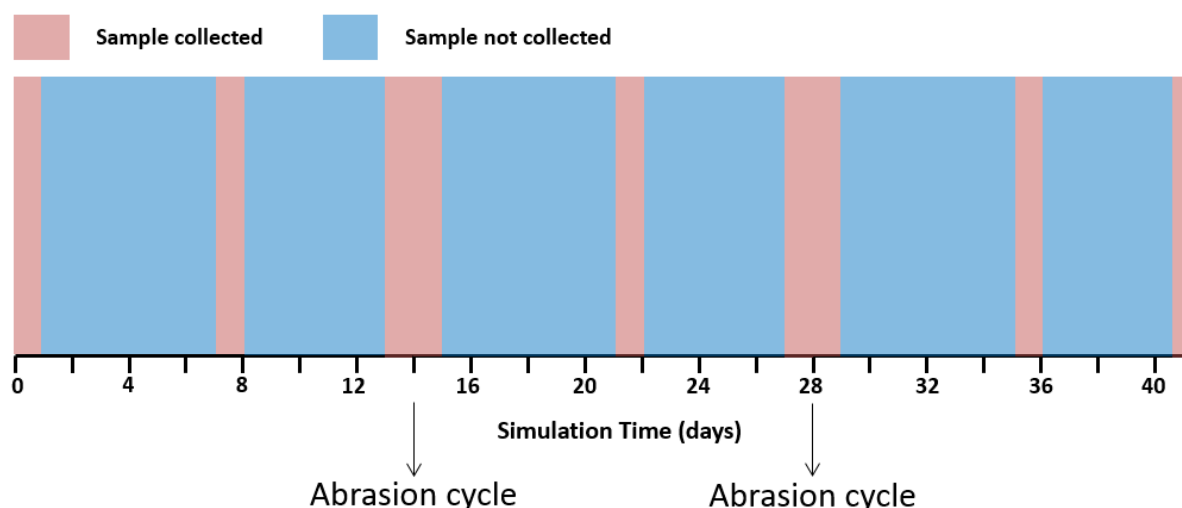


Figure 67 – Water collection and abrasion cycles planned for the climatic chamber simulation.

7.3. Results

7.3.1. ENMs characterization

Electron microscopy

The initial concentration of the TiO₂ dispersion was 30g of TiO₂ per litre. This was diluted to 100 ppm for HR-TEM. The images are shown in Figure 59. The nanoparticles were highly agglomerated but some individual nanoparticles were also observed. Due to the high agglomeration state a size distribution analysis could not be performed, but as seen in Figure 59B some of the individual particles were around 10 – 20nm. Agglomerates sizes ranged from few nanometers to some micrometers.

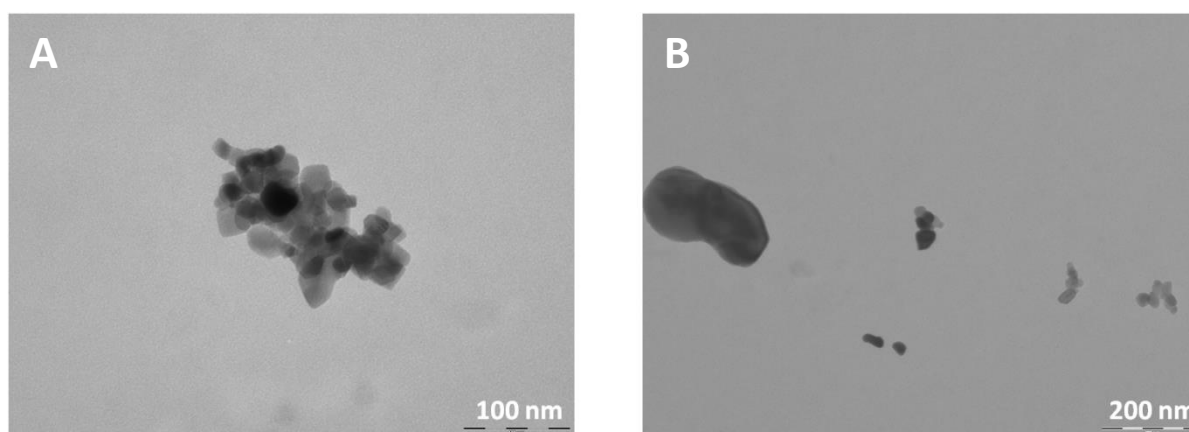


Figure 68 – HR-TEM images of TiO₂ dispersion used in FCCCO's case study.

X-Ray diffraction

XRD measurements of dried TiO₂ matched with the anatase TiO₂ entry in the International Centre for Diffraction Data (ICDD) powder diffraction database (www.ICDD.com) confirming this as the crystalline phase in the coating material, as expected since anatase is the crystallographic phase providing a higher photocatalytic activity [5].

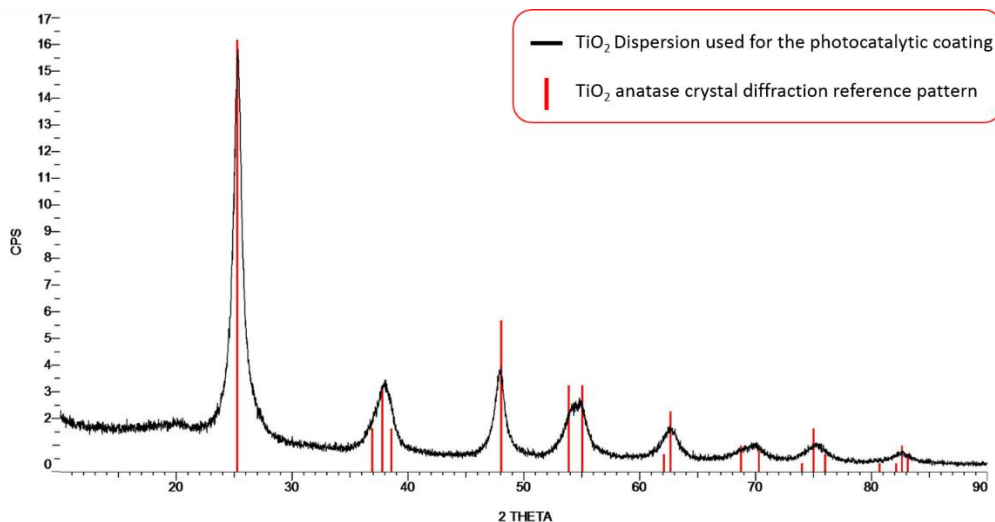


Figure 69 – XRD measurement of FCCCO TiO₂ dispersion

7.3.2. Coating application

From all the sheet papers coated together with the samples, 6 representative areas of 65 cm² were cut, digested and analysed through ICPMS, the results are shown in Table 13. Apart from the coated paper, uncoated paper was also analysed as a control. A small amount of Ti was detected in the uncoated paper as expected since paper whitening is a major use of TiO₂ however this background Ti amount can be neglected since it is 4 orders of magnitude below the concentrations detected in the coated paper. As the ICPMS results show the TiO₂ concentration sprayed on the surface was around 2.5 TiO₂ g/m², a concentration very close to the one used in real applications.

Table 16 – ICPMS results of Ti and calculated TiO₂ concentration in coated papers.

Samples	Ti concentration (g/m ²)	TiO ₂ concentration (g/m ²)
Coated Paper_A	1.6	2.6
Coated Paper_B	1.3	2.2
Coated Paper_C	1.8	3.1
Coated Paper_D	1.4	2.3
Coated Paper_E	1.6	2.6
Coated Paper_F	1.2	1.9
Average ± St. dev.	1.47 ± 0.23	2.45 ± 0.39

7.3.3. TiO₂ release due to weathering and wheel abrasion

Inductively Coupled Plasma Optical Emission Spectrometry

The concentrations of TiO₂ detected in the collected waters with time and normalized per m² are represented in Figure 61. The blank sample (without TiO₂ coating used as control) presented much smaller concentrations than the one with the TiO₂ coating, confirming that contamination during the experiment did not occur.

The release behaviour can be divided in three main different types, in the figure represented by A, B and C. High release occurs at the beginning (A). This may be due to weakly attached coating or weakly attached asphalt containing coating that is easily released with the first raining cycles in the climatic chamber. Then release diminishes and starts to increase again (B). This increase is probably related to matrix/coating degradation, which produce TiO₂ release. The longer time the sample is in the climatic chamber, the higher the degradation and as a consequence the higher the TiO₂ release is. A maximum is achieved, and the release diminishes again reaching a constant level (C). Probably, most of the TiO₂ available due to the sample surface damage has already been released, ending up in a release rate decrease.

When looking at the abrasion effect (around 350h and 700h), two different tendencies are observed. In the first abrasion, an effect on the TiO₂ release is not so significant. However, in the second abrasion a clear release increase was measured. The reason could be that in the beginning the asphalt/coating were not very damaged, so the sample could resist the abrasion and TiO₂ release did not increase (B tendency). When the second abrasion was performed, the asphalt/coating were more damaged, as can be seen by the previous TiO₂ release increase. In this occasion the stress produced by the abrasion was more critical resulting in a release increase. These results suggest that it is very important to consider the state of the asphalt/coating when the abrasion is performed. Since the capacity of the sample to resist the mechanical stress will depend on its state.

Since the TiO₂ concentration with time is known and the total amount of water produced during the experiment is also known. The total amount of TiO₂ released in the experiment simulating one year was calculated as 0.93 g TiO₂/m². Since the initial amount of TiO₂ in the sample is also known (see section 7.3.2 (2.45 g TiO₂/m²)) the release amount can be calculated with the following equation:

$$\frac{0.93 \frac{\text{g TiO}_2 \text{ released}}{\text{m}^2}}{2.45 \frac{\text{g TiO}_2 \text{ before aging}}{\text{m}^2}} \cdot 100 = \mathbf{38\%}$$

This means that 38% of the TiO₂ initially present in the sample was released in the experiment which simulated one year weathering and wheel abrasion post application.

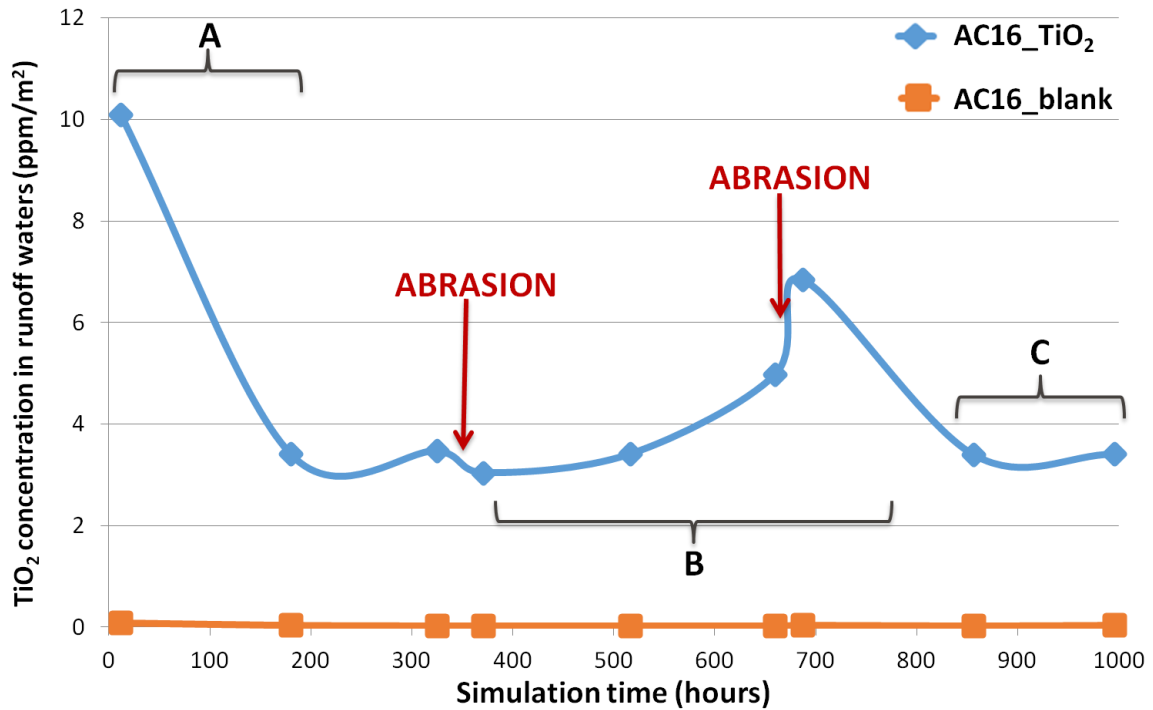


Figure 70 – TiO₂ release along time due to weathering and wheel abrasion.

It could seem that 38% is a lot, but indeed, if the samples before and after aging are observed (Figure 71A) it can be clearly appreciated that most of the coating (whitish substance) have disappeared. Indeed, both blank and sample containing the coating look almost the same after the aging (as shown in Figure 71B).

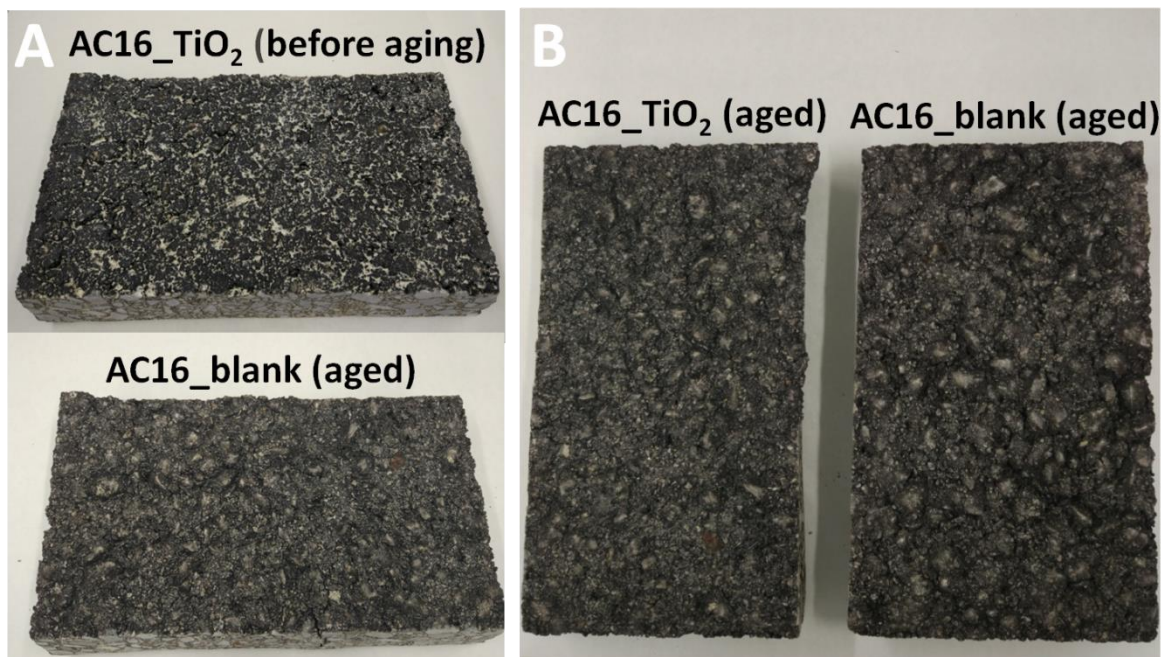


Figure 71 – Asphalt samples with and without coating, before and after aging.

Electron microscopy

The release waters presented a high amount of inorganic and organic content, which made difficult to distinguish one component from the other. EDX provided an essential tool to determine what was being observed. Ti signal was detected in multiple aggregates always together with inorganic and organic content, presumably from the substrate. The aggregates found presented sizes of few micrometers.

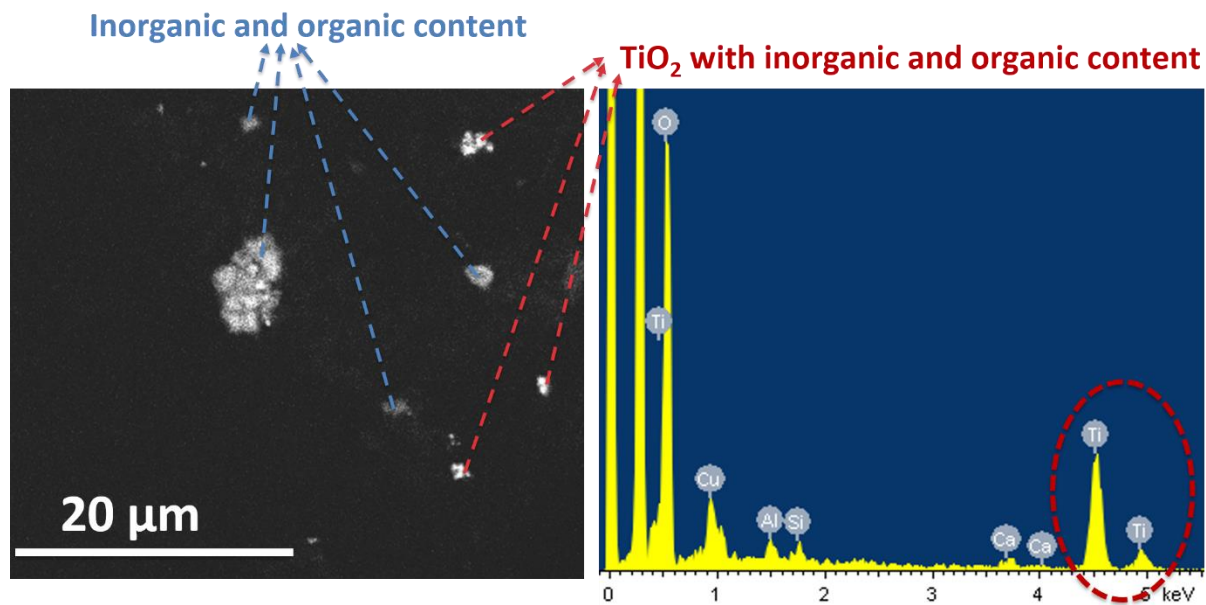


Figure 72 – Field emission SEM image with EDX analysis of the release waters from AC16_TiO₂.

7.4. Conclusion

It was confirmed that the crystallographic form of the TiO₂ present in the coating is anatase, which is the most photocatalytically active phase. The amount of TiO₂ sprayed on the lab produced sample was also determined, which was in the range of the concentrations used in the real road coating applications.

A realistic and controlled use phase simulating weathering and wheel abrasion was performed and the corresponding released materials collected and characterized. From the experiments it was determined that the amount of TiO₂ released varies with time and initially a higher release occurs. Wheel abrasion effect on release depended on the asphalt/coating condition. The release increased due to wheel abrasion when the sample was aged, while a release increase was not observed in the first abrasion when the weathering had not affected the sample for long. Through the whole duration of the experiment, which approximately relates to 1 year of weathering in outdoors conditions, 38% of the TiO₂ was released in the form of few micrometer sized aggregates together with other inorganic compounds and organic material presumably from the substrate.

8. AMEPOX: conductive inks for printed circuits

8.1. Introduction

AMEPOX Enterprise Ltd. (AXME) is a Small-to-Medium Enterprise (SME) that synthesises conductive formulations. As previously mentioned in D1.2, AMEPOX provided as a case study in NANOFASE conductive inks containing Ag NPs. Although AMEPOX only synthesizes the ink they were able to provide printed circuits such as the ones shown below, which were used to test the silver release.

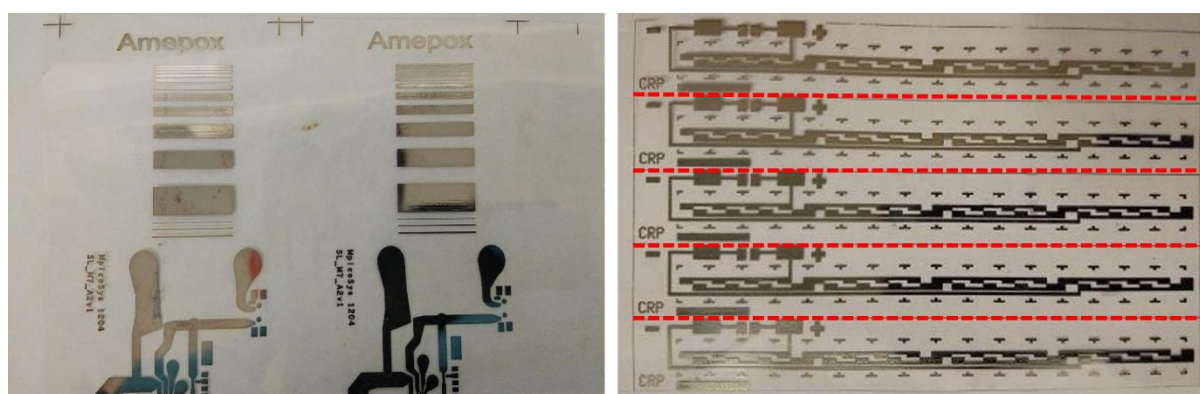


Figure 73 – Electric circuits printed with Ag Ink provided by AMEPOX.

8.2. Materials and methods

The ink printed in the circuits provided by AMEPOX is the Nano Ink JP, which contains 60 nm Ag particles. The substrate used was polyethylene terephthalate (PET), a material on which conductive inks are commonly printed. As stated in D1.2, after the printing process the nanoparticles are sintered. This is a process by which the individual nanoparticles fuse together removing nanoscale characteristics. However, it was decided to perform a leaching experiment simulating an end-of-life process in landfill to determine the release rate and form of Ag released from the printed circuit. The experiments were performed following the standardized protocol EN – 12457-4: Test for leaching of granular waste materials and sludges [13], the same protocol as described in INOTEX's second case study (camping tents). Experiments were carried out in LEITAT (WP4).

From the two circuits provided the one on the right side (Figure 73) was selected because it presented a higher number of repeated patterns, which were used to perform replicates experiments. The circuit was cut through the red dashed lines shown in Figure 73, providing 5 pieces with the same structure. Three of them were used to perform the experiments and one of them was digested with an acid solution in an analytical microwave digestion system (MARS, CEM, 1600W) and later analysed by ICPMS (Agilent 7500, Agilent Technologies) to determine the initial Ag content. The piece left (the one from the top) was discarded because part of the printed pattern was a bit damaged. The printed area in each of the three replicates was the same. Weight differences were expected to be only due to differences in the amount of substrate present as a result of manually cutting the starting circuit into pieces.

The weight of the cut circuits was around 0.4 g each, as a consequence, in order to maintain the 10L/g ratio proposed by the standardized protocol, the leaching experiment was performed with 4 ml of water. Each of the cut pieces were cut in fragments smaller than 10 mm diameter (Figure 74A). Then, they were introduced in 15 ml falcon tubes where 4 ml of ultrapure water was added. Then, the samples were shaken with an end-over-end shaker (OVAN, NR50 E) at 10 ± 3 rpm during 24h at ambient temperature (25°C). From each replicate 1 mL was directly collected for Ag determination through ICPMS; 1.5 ml were collected, diluted up to 15 ml (with 13.5 ml of ultrapure water) and filtered through a filter paper of approximately 20 μm pore size (Filter-Lab quantitative filter paper, ANOIA); from the filtered water 5 ml were digested and analyzed through ICPMS and the 10ml left were filtered through a Nylon 0.45 μm syringe filter (Phenex). 5 ml were digested and analyzed through ICPMS and the rest (around 4ml) was centrifugated with 3kDa centricons (Amicon Ultra-4 Centrifugal Filter Units, Millipore). The filtrate from the centricons was analyzed through ICPMS to determine the ionic content.

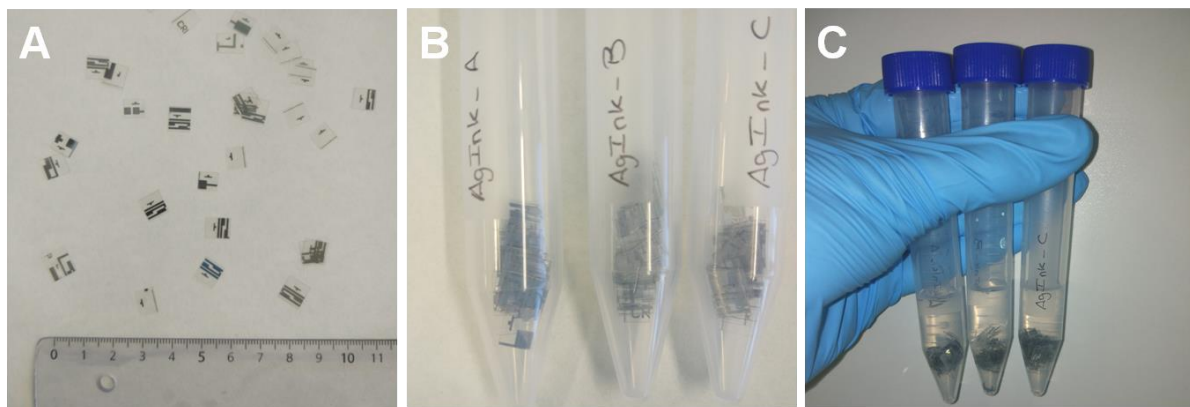


Figure 74 – Printed circuit: A) Cut in pieces; B) replicates inside the vial; C) replicates inside the vial with 4 ml of water.

8.3. Results

Inductively Coupled Plasma Mass Spectrometry

From the ICPMS results of the Ag concentration total amount, the one collected directly from the vial (without passing through any filter) and the concentration of the digested circuit, the release rate was calculated. The Ag amount in each circuit was estimated in 2.05 Ag mg. In this case, since there was only one printed circuit to analyze, there were no replicates and thus no standard deviation. The measured Ag concentration in the leaching waters was 57.2 ± 11.9 ppm (Ag mg/leaching water L). Since all the experiments were conducted with 4ml of ultrapure water, the amount of Ag leached from the printed circuits is 0.229 ± 0.047 mg which gives a calculated release rate of Ag from the printed circuit due to leaching of **$11.1 \pm 2.3\%$** .

As is seen in Figure 75A, the release of the ink from the substrate occurs very fast, detached fragments of ink were already observed at the start of the experiment. After 24h, at the end of the experiment (Figure 75B) some Ag small fragments were also observed, but not as many or as big as in the beginning. In the 24h that the experiment lasts most of the Ag fragments released were partially dissolved reducing their size.

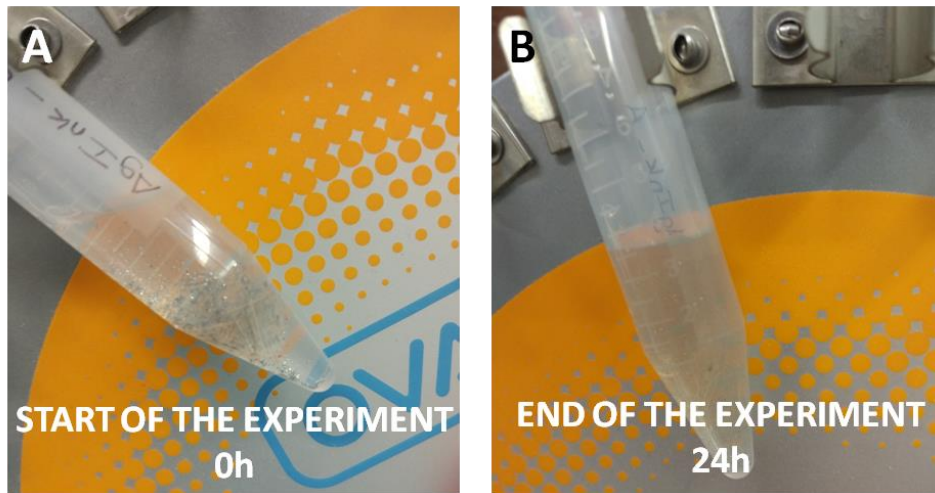


Figure 75 – Leaching waters at the start and at the end of the experiment.

From the ICPMS results from the leaching waters filtered through different pore sizes, a quantitative value of the amount of Ag in different range sizes was determined. The main result was that $81.1 \pm 3.9\%$ of the silver was bigger than $20\mu\text{m}$. i.e. around 81% of silver was lost when the leaching waters were filtered with paper filter (pore size $\sim 20\mu\text{m}$). For the rest of the sized ranges the concentration found was: $<20\mu\text{m} \rightarrow 12.1 \pm 3.0\%$; $<0.45\mu\text{m} \rightarrow 6.4 \pm 0.7\%$; ionic $\text{Ag}^+ \rightarrow 0.3 \pm 0.1\%$. It makes sense that the concentration increases, since in the $<20\mu\text{m}$ range for example, both $<0.45 \mu\text{m}$ and ionic are considered. If the release in a specific size range has to be determined, the percentage of smaller size ranges has to be deducted. For example, the amount of silver in a range smaller than 450 nm but not ionic would be $6.4\% - 0.3\% = 6.1\%$.

Table 17 – AMEPOX ink release rates

RELEASE FORM
Ionic (Ag^+): $0.3 \pm 0.1\%$
$<0.45 \mu\text{m}$: $6.4 \pm 0.7\%$
$<20 \mu\text{m}$: $12.1 \pm 3.0\%$
$>20 \mu\text{m}$: $81.1 \pm 3.9\%$

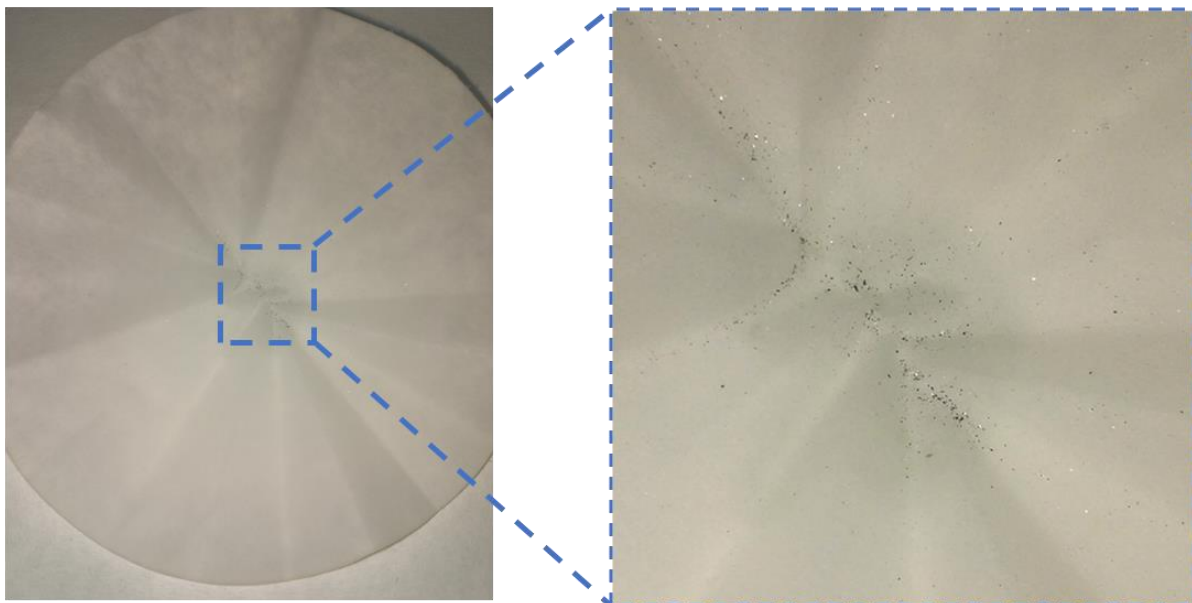


Figure 76 – Paper filter presenting Ag fragments after filtering the leaching waters in contact with the printed circuit.

8.4. Conclusion

The main outcome of these experiments is that most of Ag is released in fragments bigger than 20 μm . This is understandable since the ink is sintered the nanoparticles form a continuous film, necessary to improve the conductivity. When Ag is released due to leaching most of it remains as intact fragments. During the experiment the size of some of the fragments can be reduced, but it still presents a large ($>20\mu\text{m}$) size. Indeed, in Figure 76, in the paper filter magnification it is clearly appreciated how a high amount of Ag was remaining in the filter during the filtration process.

Some of the Ag released could be in a nanometre size range or ionic form, but the amount would be very small. If a worst case scenario with a 6.4% (Ag passing through 0.45 μm filter) of the Ag released is considered to be nanoscale and ionic. From the total Ag in the circuit, the amount released in nano/ionic form would be 6.4% of the 11.1%, which is 0.7%.

9. Sunscreens (SC)

9.1. Introduction

TiO₂ nanomaterials (NM) are currently present in a large variety of consumer products, including cosmetics. According to the current European regulation (EC Regulation No. 1223/2009) on cosmetic products, all ingredients in NM form must be indicated in the list of ingredients followed by the word (nano). Therefore, knowing the units of sunscreen (SC) products sold in a country, the percentage of products containing nano-ingredients and the average amount of NM per unit of product, it is possible to hypothesize the amount of NM that could be potentially released to the environment. Market research performed in Spain revealed that 25.000.000 units of SC were sold in Spain (2014) and almost the 30% of these products contained TiO₂ NM. Assuming an average TiO₂ concentration of the 4 wt.%, a potential release of 71,28 Tonne of TiO₂ could occur in the costal water of Spain during the summer.

In recent years, it has been proved that NMs from sunscreens (i.e., inorganic UV filters such as TiO₂ and ZnO nanoparticles) are released and accumulate in the sea waters and recreational water with potential toxic effects on aquatic organisms. (i.e.: Sunscreens in seawater [22], in lake [23], in river [24] and in swimming pool [25]).

In this study, five commercial sunscreens were characterized to determine the presence, amount, crystalline phase, size and shape of TiO₂ or ZnO NM. A release experiment was set up to investigate the release of NM contained in the sunscreens to water media. The objectives of this study are: i) characterize the amount and form of NM contained in commercial SC and check the conformity of the labelling of the nano ingredients: ii) use release data to refine the mass flow model to predict the potential impact of sunscreens on environmental exposure levels, iii) compare the environmental concentrations of TiO₂ with the ones predicted by the mass flow models.

9.2. Materials and methods

9.2.1. Sunscreens

Five commercial sunscreens with high sun protection factor (SPF 50+) were selected for the study and were encoded as SC1, SC2, SC3, SC4 and SC5. SC1 is a popular sunscreen (white brand), SC2 and SC4 are very popular sunscreens (known brand), SC3 is a sunscreen for sensitive skin (white brand) and SC5 is an anti-age and make-up sunscreen (white brand). According to the list of ingredients, SC1, SC2 and SC4 contained nanoparticles of TiO₂, SC3 contained both TiO₂ nano and TiO₂, and sample SC5 contained nanoparticles of ZnO and TiO₂. The SC were characterized by ICP-MS to confirm the presence of the Ti and Zn, and quantify their amount. The SC were subjected to XRD to determine the crystalline phase of the NM contained and were analyzed by TGA to determine the organic compounds content.

9.2.2. ICP-MS of sunscreens for total Ti content, Ti content of extracted materials and Ti content of NMs released in ultrapure water

SC samples and extracted material from the SC were digested with an acid solution mixture of HNO₃ 70% and HF 49% 9:1 in an analytical microwave digestion system (MARS, CEM). Before the digestion, samples were directly weighed (0.01 to 0.2 g depending on the kind of sample and the amount available) into 55 ml perfluoroalkoxy alkanes (PFA) microwave vessels (MARSXPress, CEM). Then, 10 ml of acid mixture was placed into the vessel to perform the microwave acid digestion program. After digestion, all samples were filled with ultrapure water until 50 ml. Then, further dilutions were made with 2% HNO₃ aqueous solution to obtain the desired concentrations for ICP-MS characterization. Al, Si, Ti, Fe and Zn analysis was performed by ICP-MS (Agilent 7500, Agilent Technologies). The quantification was done by interpolation in a standard curve obtained from commercial 1000 ppm standards of the elements of interest (Sigma Aldrich).

9.2.3. XRD analysis on sunscreens for crystalline phase determination

Aliquots of the SC were sandwiched between films of polyester of 3.6 μm of thickness and subjected to XRD analysis. PANalytical X'Pert PRO MPD $\theta/2\theta$ powder diffractometer of 240 millimeters of radius, in a configuration of convergent beam with a focalizing mirror and a transmission geometry with flat samples sandwiched between low absorbing films were used with the following conditions: Cu K α radiation ($\lambda = 1.5418 \text{ \AA}$); work power: 45 kV - 40 mA; incident beam slits defining a beam height of 0.8 millimetres; incident and diffracted beam 0.04 radians Soller slits; PIXcel detector: active length = 3.347 ° θ scans from 2 to 88 ° 2θ with a step size of 0.026 ° 2θ and a measuring time of 150 seconds per step.

9.2.4. TGA of sunscreens

To determine the presence and amount of organic compounds and to confirm the presence of TiO₂ and/or ZnO, a TGA analysis was performed directly on the SC samples. The analyses were performed using a TGA Q500 (TA Instruments) thermo gravimetric analyser. Measurements were made under nitrogen atmosphere at a flow rate of 10 mL·min⁻¹. Samples were placed in a platinum pan for the analysis. The mass of the sample loaded to the thermal-balance varied in the range of 3-5 mg. The measurements were performed at a temperature range of 25-900 °C with heating rates of 10 °C·min⁻¹.

9.2.5. NM extraction from Sunscreens

To remove the organic matrix of the sunscreens and isolate the NM, SC were extracted one time with methanol and two times with ethanol, as depicted in Figure 77, reported below. Following the extraction protocol, one gram of SC was weighted into a vial and then 15 mL of methanol were added. The dispersion of cream with the solvent was homogenized during 5 minutes in a sonication bath. The dispersion was subjected to centrifugation at 5000 rpm for 5 minutes to separate the solid residue from the supernatant, which was discarded. The above mentioned procedure was applied to the following extractions with ethanol. After the extractions, a white pellet was obtained (SC1, SC2, SC3 and SC4 whilst for SC5 a brownish colored pellet was obtained) and dried at room temperature. The powder material obtained

was characterized by ICP-MS to determine the amount and purity of the TiO₂ or ZnO NM extracted and by SEM-EDX to observe NM size, shape and to confirm their composition.

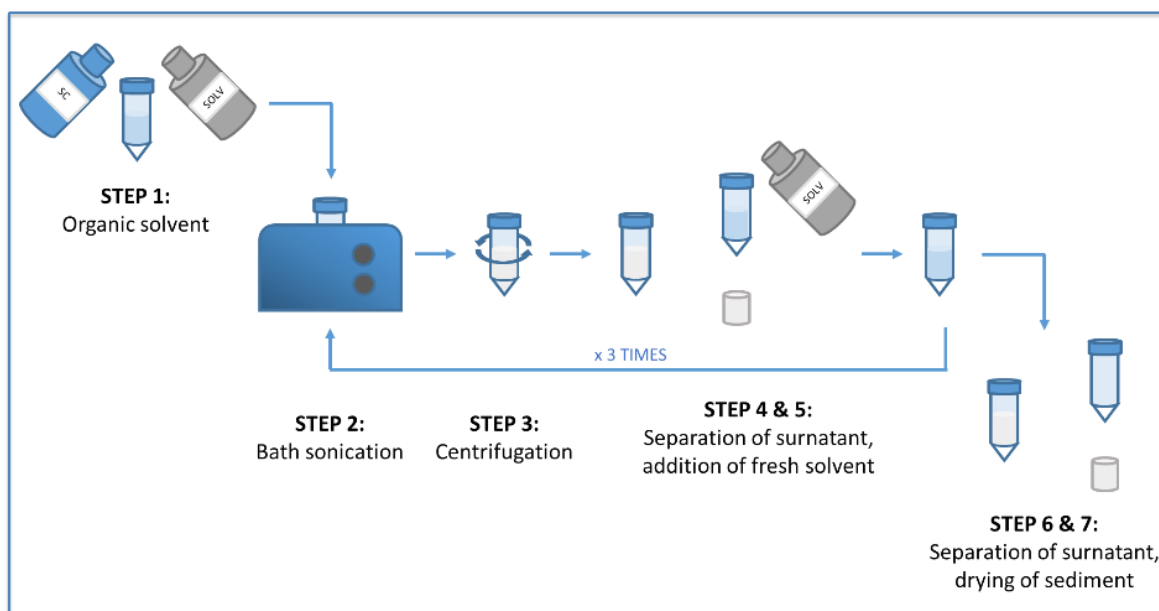


Figure 77 - Schematic of the extractions protocols applied to the sunscreen to extract NM.

9.2.6. SEM-EDX of extracted materials and of NMs released in ultrapure water

For FE-SEM observation, a small amount of the extracted material was dispersed in water and a drop of the dispersion was deposited on a silicon wafer, placed on FE-SEM stub previously covered by double-sided conductive tape, and left to dry overnight for the following FE-SEM observation. The samples of water from the release experiment were prepared directly by placing a drop of the dispersion on the silicon wafer. The observation was performed with the condition reported at the bottom of the images using a Merlin FE-SEM (ZEISS, Germany) equipped with a EDS Detector Oxford INCA X-Max (High Wycombe, UK).

9.2.7. Release experiment: sunscreens released from the finger to ultrapure water

To investigate the release of NM from sunscreens once applied on the skin, the following experiment was performed using SC3, SC4 and SC5. For each release experiment, three volunteer applied the SC at 2 mg/cm² (according to the recommendation by the US Food and Drug Administration) in a skin area of around 3 × 5 cm (dorsal part of a finger), applying a total amount of 30 mg of SC (Jeon et al. 2016). The SC applied was left to dry for 30 minutes and then the finger was immersed in a beaker containing 150 ml of ultrapure water under mild stirring. Every 5, 10, 15, 20, and 30 minutes an aliquot of "release water" was sampled for following ICP-MS analysis and FE-SEM observation and EDX analysis. A schematic of the release experiment is depicted in Figure 78.

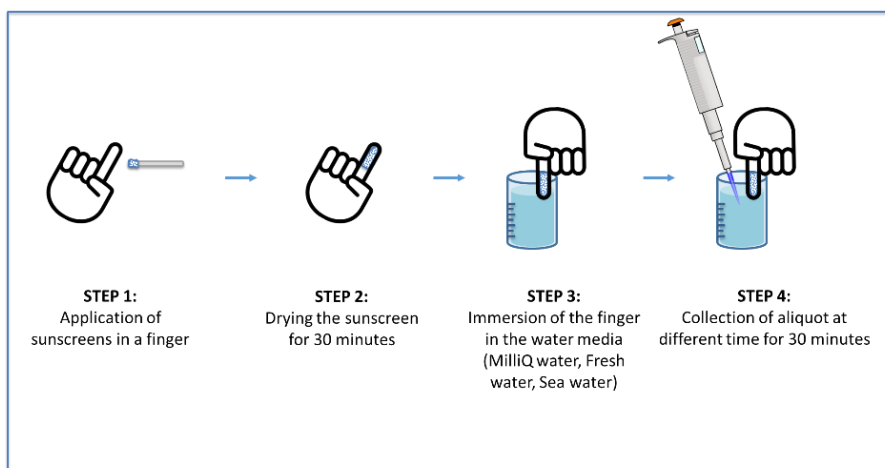


Figure 78 - Schematic of the release experiment performed with the sunscreen applied on the skin.

9.3. Results

9.3.1. ICP-MS of sunscreens for total Ti content, Ti content of extracted materials and Ti content of NMs released in ultrapure water

SC samples were analyzed by ICP-MS to confirm the presence of the TiO_2 as declared in the product label and to quantify the amount of Ti and Zn, in case of SC5. Figure 79 and Table 18 show the results obtained:

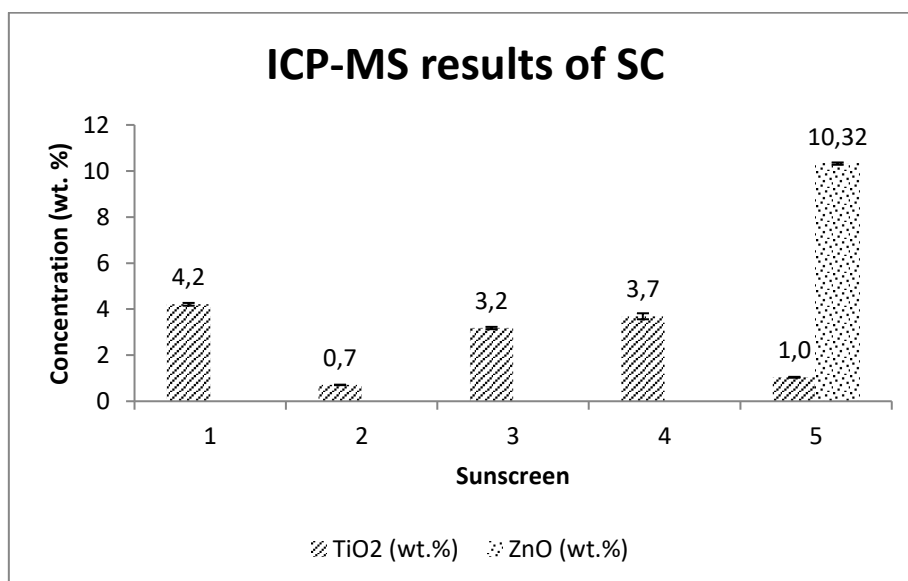


Figure 79 - Concentration of TiO_2 and ZnO in sunscreens determined by ICP-MS.

Table 18 - Concentration of TiO_2 and ZnO in sunscreens determined by ICP-MS.

	Al_2O_3 (wt.%)	SiO_2 (wt.%)	TiO_2 (wt.%)	ZnO (wt.%)
SC1	-	-	$4,21 \pm 0,06$	-
SC2	-	-	$0,71 \pm 0,01$	-
SC3	-	-	$3,18 \pm 0,05$	-
SC4	$0,49 \pm 0,02$	-	$3,69 \pm 0,13$	-
SC5	$0,21 \pm 0,01$	$2,28 \pm 0,09$	$1,04 \pm 0,02$	$10,32 \pm 0,05$

The ICP-MS provided the elemental concentration of Ti and Zn which were considered to be present in the sample as TiO₂ and ZnO, as declared in the label. The data reported was calculated following this hypothesis. All the sunscreens contained TiO₂ in a percentage ranging from 0,7 to 4,4 wt.% and only the SC5 contained ZnO, which was present at a concentration of 10.3 wt%.

The material extracted from the SC was subjected to ICP-MS to determine the purity and calculate the yield of extraction. The results obtained are reported in the following Figure 80 and Table 19.

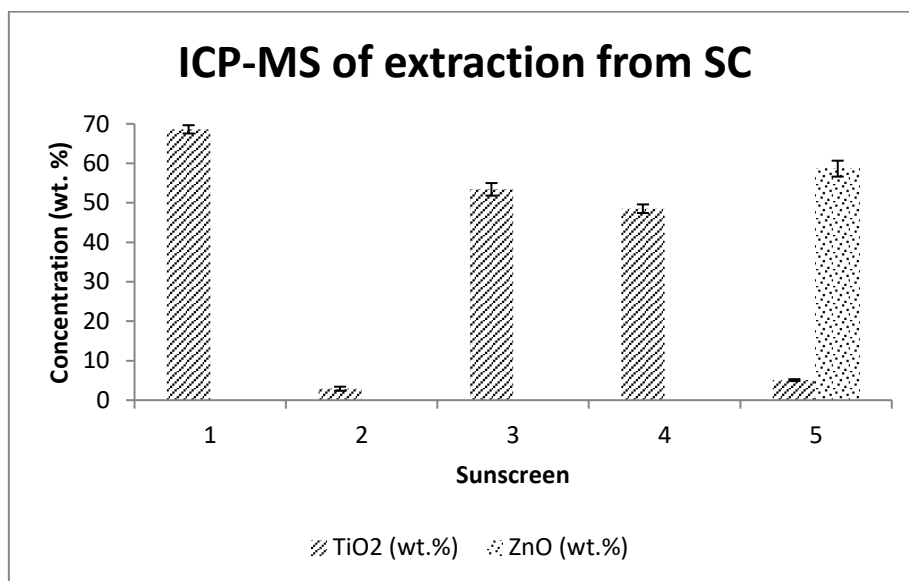


Figure 80 - Concentration of TiO₂ and ZnO in the extracted material from sunscreens by ICP-MS.

Table 19 - Concentration of TiO₂ and ZnO in the material extracted from sunscreens.

Extraction from SC	TiO ₂ (wt.%)	ZnO (wt.%)	Ratio TiO ₂ in extracted material and TiO ₂ in SC	Ratio ZnO in extracted material and ZnO in SC
SC1	68,6 ± 1,1	-	16	-
SC2	2,9 ± 0,5	-	4	-
SC3	53,4 ± 1,6	-	17	-
SC4	48,5 ± 1,1	-	13	-
SC5	5,1 ± 0,2	58,7 ± 2,0	5	6

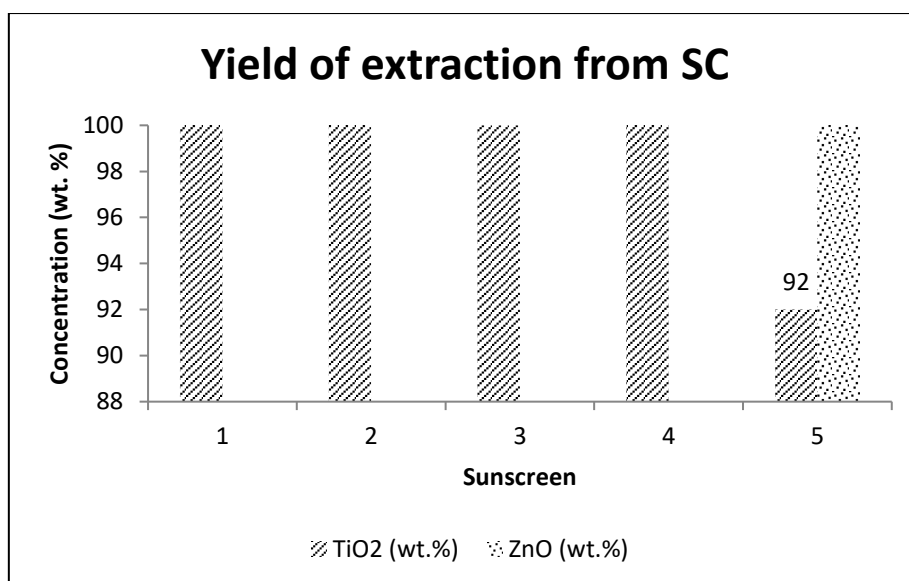


Figure 81 - Yield of extraction of TiO₂ and ZnO.

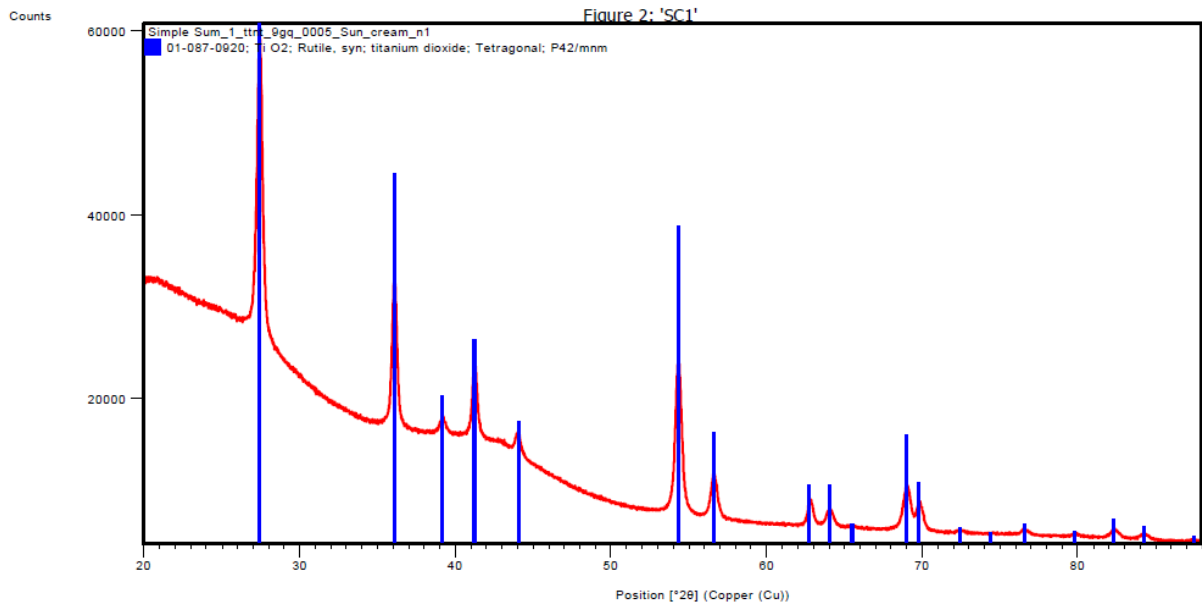
The purity of the TiO₂ in the extracted materials ranged from 3 to 68 wt.% while for the SC5, the purity of ZnO in the extracted materials was around the 60 wt.%.

From the amount of extracted material and the TiO₂ and ZnO content obtained from the ICP-MS analysis, the yield of extraction of the two NM was calculated. For example, for SC3, from 1g of sunscreen 0.060g of extracted material were obtained. In the extracted material 53,4 wt% corresponded to TiO₂, what was 3.2 wt% of the sunscreen ($53.4 \text{ wt}\% \cdot 0.06 = 3.2 \text{ wt}\%$). The value obtained matched with the ICP-MS analysis of the SC (Table 18), suggesting that the recovery of TiO₂ with the extraction methodology was 100%. For the other samples, according to the results, the extraction procedure allowed to extract almost all the TiO₂ material from SC1-4. For SC5, all the ZnO was extracted and the yield of extraction for TiO₂ was around 90 wt.%.

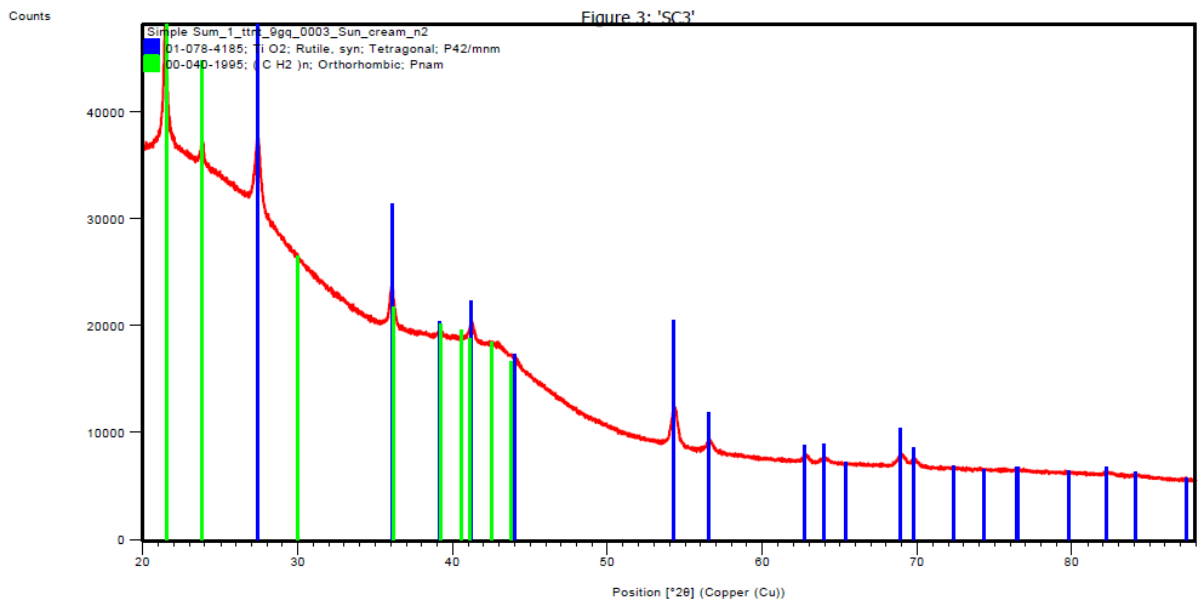
9.3.2. XRD analysis on sunscreens for crystalline phase determination

The XRD of the SC showed that SC1-4 contained TiO₂ in form of rutile, while SC5 contained TiO₂, in the form of both rutile and anatase, zincite and goethite, from a colouring pigment. The presence of broad peaks in all the diffraction diagram, suggested the presence of nano sized crystallites. The X-ray diffraction diagram with the patterns of the identified phases superimposed are shown in Figure 82.

A)



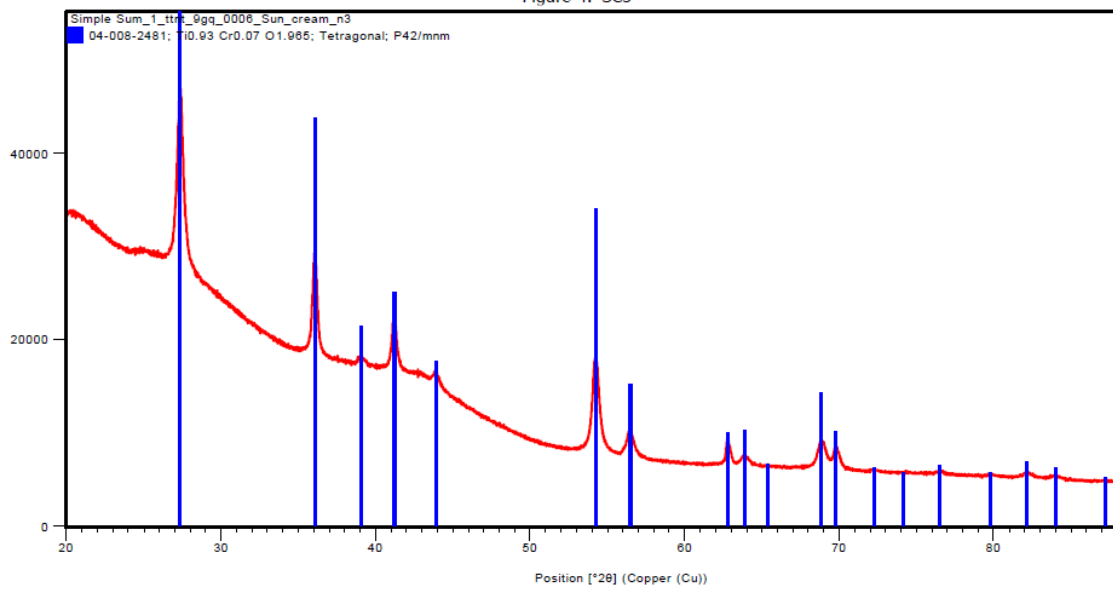
B)



C)

Counts

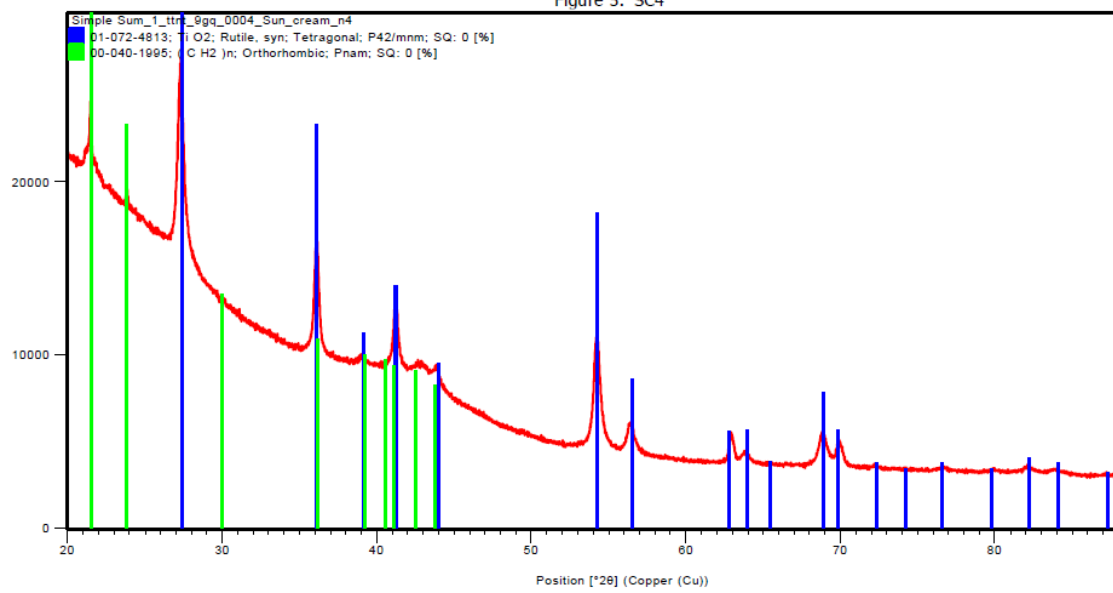
Figure 4: 'SC3'



D)

Counts

Figure 5: 'SC4'



E)

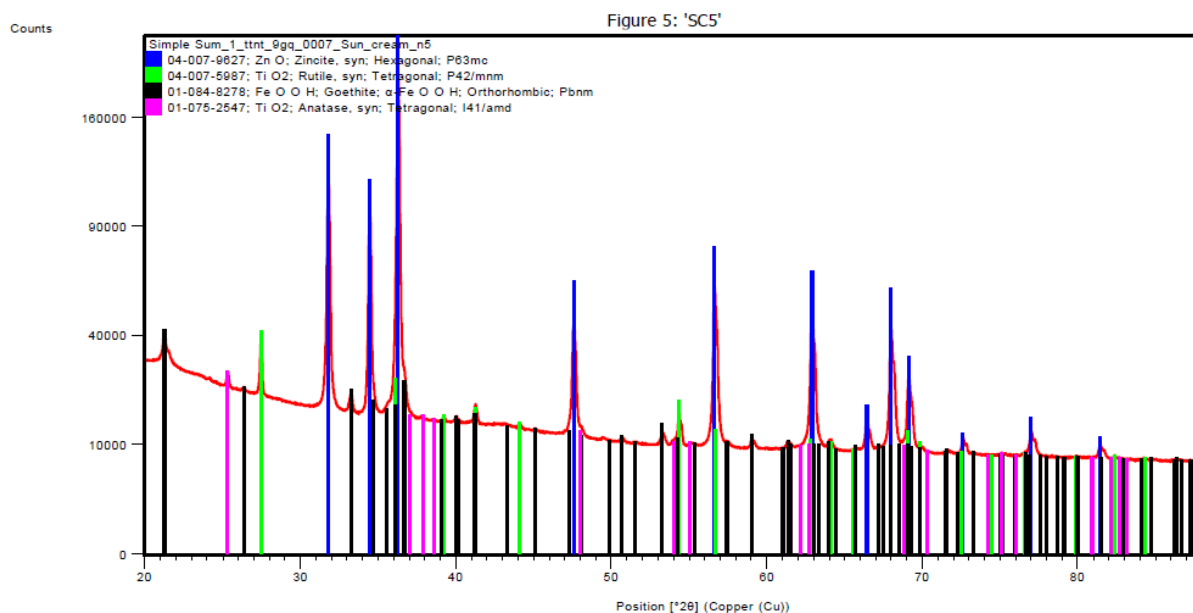


Figure 82 - X-ray diffraction diagram with the patterns of the identified phases superimposed, from the top to the bottom: a) SC1, b) SC2, c) SC3, d) SC4 and e) SC5.

Table 20 - Crystalline phase of TiO₂ and ZnO in sunscreens by XRD.

Sample	Ingredients labelled as nano	Ingredients NOT labelled as nano	Crystalline phase of SC by XRD
SC1	TiO ₂ (nano)		Rutile, broad peaks
SC2	TiO ₂ (nano)		Rutile, broad peaks
SC3	TiO ₂ (nano)	TiO ₂	Rutile, broad peaks
SC4	TiO ₂ (nano)		Rutile, broad peaks
SC5	ZnO (nano)	TiO ₂	Zincite, Rutile, Goethite, Anatase, broad peaks

9.3.3. TGA of sunscreens

A summary of the results obtained is reported in Figure 83.

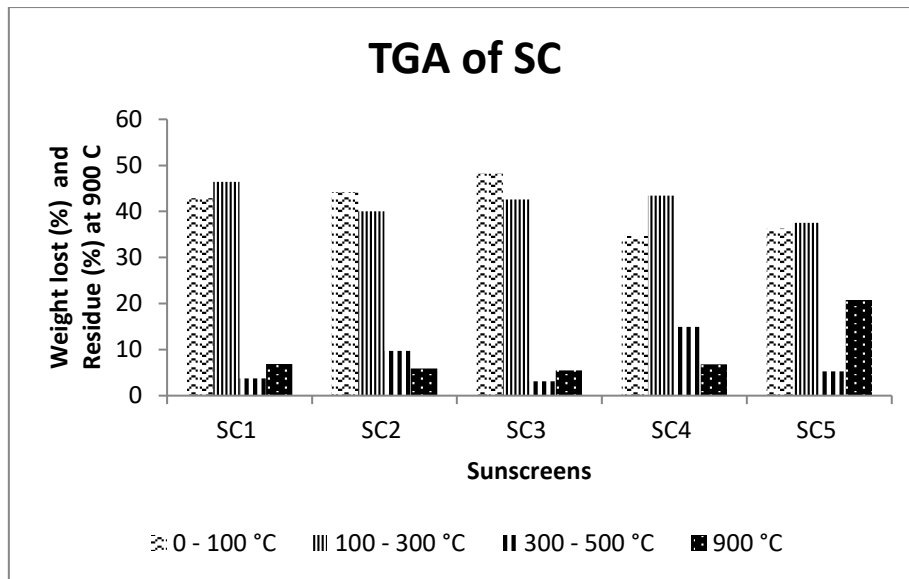
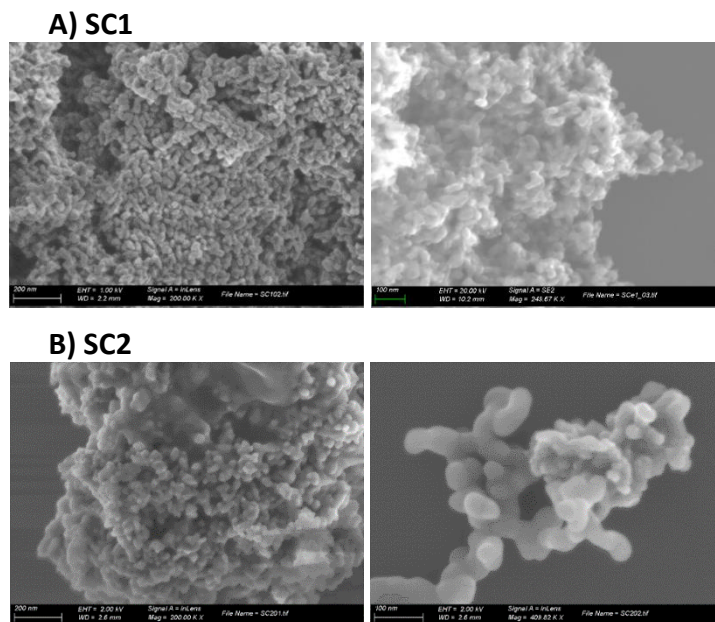


Figure 83 - Weight loss of sunscreens at different ranges of temperatures according to the TGA.

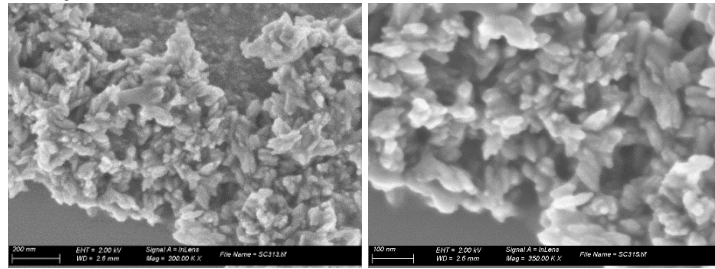
The TGA analysis confirmed the presence of organic components, the weight lost from 0-300°C ranged from 73 to 91 wt.%. The solid residue at 900°C ranged from 5,5 wt.% to 6.9 wt.% for SC1-4, while for SC5 the residue was 21 wt.% confirming the higher presence of inorganic compounds, such as ZnO, TiO₂ and iron based pigments.

9.3.4. FE-SEM-EDX of extracted materials and of NMs released in ultrapure water

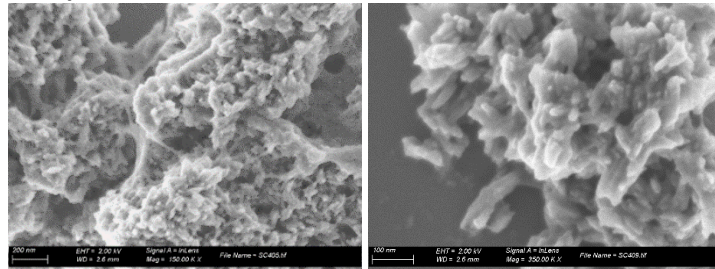
The materials extracted from SC were dispersed in ultrapure water to further characterize them by FE-SEM. In Figure 84 images of the NM contained in the SC are shown.



C) SC3



D) SC4



E) SC5

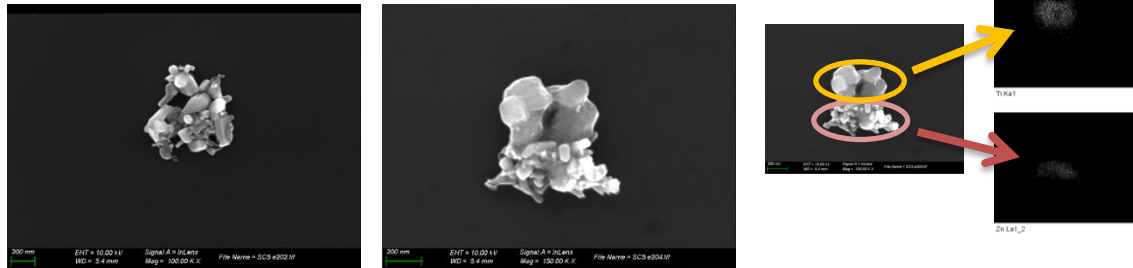
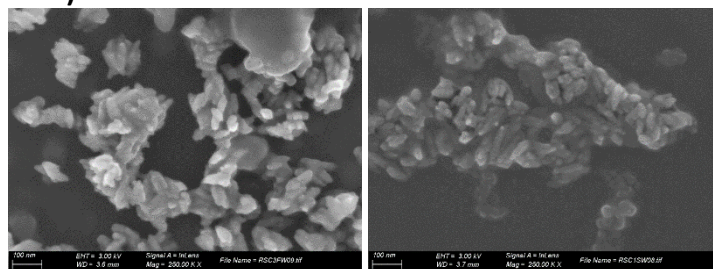


Figure 84 - TiO₂ NM extracted from sunscreens: a) SC1, b) SC2, c) SC3, d) SC4; left-hand images scalebar length is 200nm while right-hand scalebars are 100nm. e) SC5, here both TiO₂ and ZnO are shown; scalebars size is 200 nm for both images.

The FE-SEM observation revealed the presence of TiO₂ aggregates with primary particles in the nano range in all the SC. The particles shape was similar and nearly spherical for SC1-2, also NM in SC3-4 were similar in shape, with elongated particles. The TiO₂ size was ranging from 10 to 50 nm in SC1, 10 to 60 nm in SC2, 10 to 40 nm in SC3 and 15 to 50 nm in SC4. In SC5 two different kind of particles were present, the EDX analysis showed that the bigger particles were made of TiO₂ and their size ranged from 80 to 150 nm and the ZnO particles were smaller and with a more elongated shape with size ranging from 20 to 70 nm. Release water samples collected during the release experiment with SC3, SC4 and SC5 confirmed the presence of TiO₂ and ZnO particles, which are shown in Figure 85.

A)



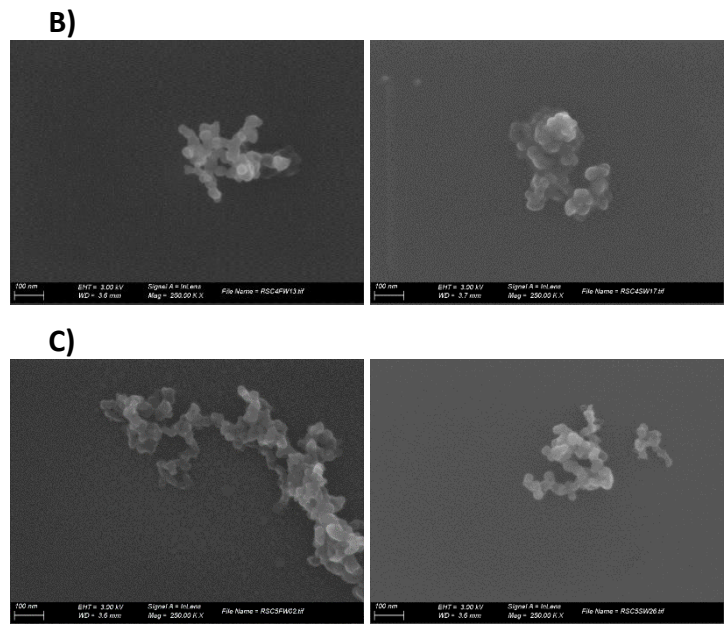


Figure 85 - TiO₂ and ZnO (SC5) NM released from sunscreens: a) SC3, b) SC4 and c) SC5, here only ZnO NM are shown. The scalebars size of all the images are 100nm.

The FE-SEM observation showed the presence of small aggregates of TiO₂ or ZnO, for SC5, with primary particles with the same shape and size of those observed in the material extracted from the SC. The TiO₂ NM released from SC3 showed an elongated shape with particles ranging from 20 to 50 nm. In SC4, the TiO₂ NM size ranged from 15 to 50 nm. In SC5, only ZnO particles were observed in a size range from 20 to 50 nm.

9.3.5. Release experiment: sunscreens released from the finger to ultrapure water

The TiO₂ released from SC3, SC4 and SC5 in ultrapure water was analysed by ICP-MS and the results obtained are shown in Figure 86.

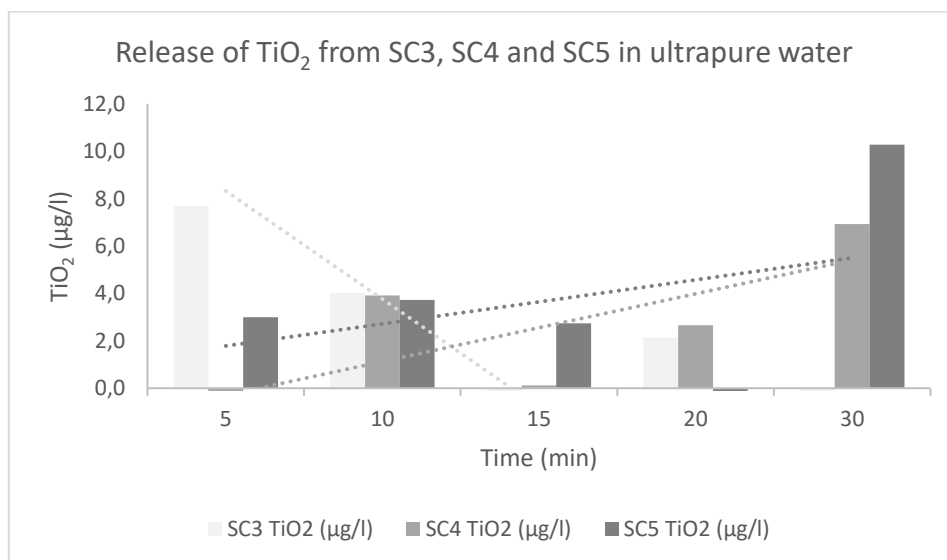


Figure 86 - Release of TiO₂ and ZnO (SC5) from sunscreens to ultrapure water.

The determination of the Ti in the release water was challenging due to the low Ti concentration and the presence of the cream matrix. SC3 was the one showing the higher

release of TiO₂ in the first 10 minute of the experiment, but after 15 minutes, the TiO₂ was not detected in the release waters. The decrease of TiO₂ present in the dispersion was correlated with the formation of a surface layer of released SC and probably TiO₂ NM, which was progressively getting attached to the beaker wall, lowering the concentration of NM present in the dispersion. In SC4 and SC5, the release of TiO₂ NM increased mildly along the 30 minutes, reaching a final concentration of respectively 7 and 10 mg/l. Considering the amount of TiO₂ present in the SC applied on the finger for the release experiment, it was calculated that the 1,2%, 0,9% and 5,0% of the TiO₂ was released during the experiment respectively from SC3, SC4 and SC5.

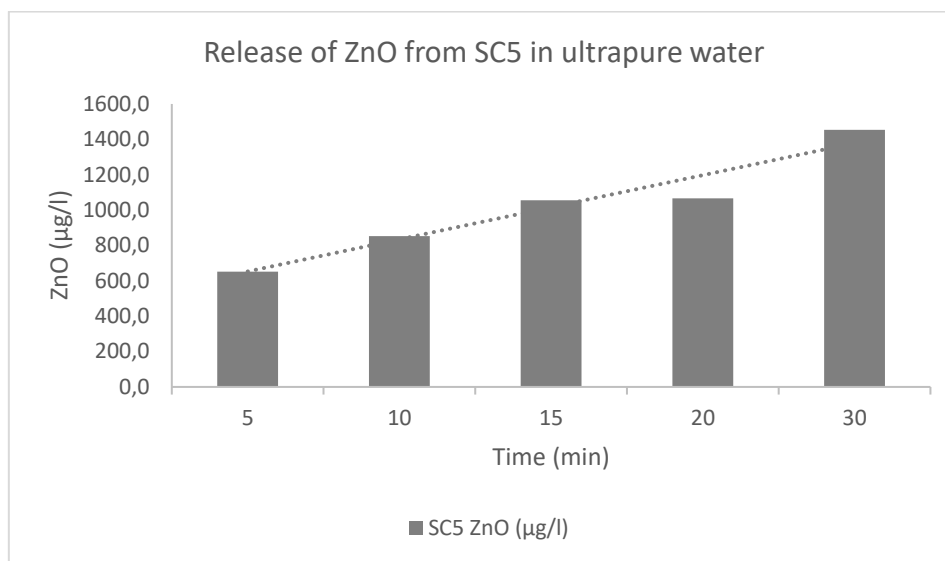


Figure 87 - Release of ZnO from SC5 to ultrapure water.

The ICP-analysis of ZnO were easier to perform in respect to the analysis of TiO₂ because of the higher concentration of ZnO in the SC5. The result obtained showed that ZnO NM was released in relatively high quantities, ranging from 650 to 1450 µg/l, along the time of the experiment which correspond to a release of of 70,5% of the ZnO present in the SC5.

9.4. Conclusions

Five commercial sunscreens were characterized to determine the amount, size and shape of NM contained and check the conformity of the labelling of the nano ingredients.

The ICP-MS performed on the SC confirmed the presence of TiO₂ and ZnO. The average amount of TiO₂ in SC1, 3 and 4 were around the 4 wt.%, SC2 and SC5 contained a lower amount of TiO₂.

The extraction procedure was successful, allowing a complete recovery of TiO₂ and ZnO NM contained in the SC. The purity of TiO₂ were around the 50 wt.% for SC3 and SC4, the higher purity was obtained in SC1 (68,6 wt.%) while the lower purity was obtained in SC2 (2,9 wt.%). Regarding the extraction of SC5, the ZnO content in the extracted material was around the 59

wt.% and the content of TiO₂ was around 10 wt.%. In all the SC the yield of extraction for TiO₂, and ZnO in SC5, was around 100% (except for TiO₂ in SC5 which was 10 wt.%).

The XRD of the SC confirmed the presence of TiO₂ in form of rutile (SC1-4). In SC5, the ZnO was present as zincite and the TiO₂ was present in form of rutile and anatase, a crystalline phase belonging to goethite was also present due to the presence of inorganic colouring pigment.

TGA analysis on the SC confirmed the presence of a relevant fraction of organic compound in the SC. According to the values measured for the solid residue at 900°C, the inorganic materials fraction ranged from 5,5 to 6,9 wt.% which was in good agreement with the data obtained by ICP-MS.

According to the FE-SEM observation of the extracted material from the SC, all the TiO₂ ingredient should be labelled as nano according to the current EU regulation on cosmetic products, including the TiO₂ particle of SC5, which showed primary particle in the nano range, often with size smaller than 60 nm. The FE-SEM observation of the NM released from the SC confirmed the shape and size of those observed in the material extracted from the corresponding SC. The ICP-MS of released water collected during the release experiment were difficult to analyse due to the low concentration of NM and the presence of the organic matrix.

A low percentage of TiO₂ NM present in the SC was released under the experimental conditions investigated, in specific SC3 and SC4 release respectively the 1,2 and the 0,9% of the TiO₂ contained. SC5 was the SC showing a higher release for both the TiO₂ and for the ZnO NM, which were released respectively at 5,0% and 70,5%.

10. Polymers – Release after recycling processes

10.1. Introduction

Apart from use and end-of-life processes, which have been studied in the last sections, information on release during synthesis and ENMs manufacturing will be presented in the next section (section 11). Thus, in order to present a complete study of the different stages of a nano-enabled product, release after recycling must be covered. Any of the industrial partners in NANOFASE could provide information or materials for experimental analysis where recycling processes were involved. For this reason, LEITAT in-house materials were used in order to provide a relevant study on the topic.

The product selected was polypropylene (PP) nanocomposites (NC) containing multiwall carbon nanotubes (MWCNT). Carbon nanotubes are used to strengthen and stiffen different kinds of polymers as polymethyl methacrylate (PMMA) [26], polypropylene (PP) [27]–[29], polycarbonate (PC) [30] or polyamide (PA) [31]. Moreover, they can act as inner filters and antioxidants, reducing photo-oxidation of the polymers [32]–[35]. Furthermore, CNT may provide electrical conductivity [36] and magnetic behaviour [37], among other properties that are of interest for both existing and novel polymer applications [38]. In addition, polymer recycling is a common practice in many places around the world which is relevant to this study.

10.2. Materials and methods

MWCNT (97.8% pure, average diameter of 25-27 nm) were obtained by Glonatech, where were synthesized by a fluidised bed chemical vapour deposition system. Published work shows adequate dispersion of MWCNT (without any coating) in polypropylene [27], [39], so any surface modification of the nanotubes was required to improve its compatibility with the matrix. PP (Moplen HP500N) pellets with 3% nanofiller (MWCNT) content (w/w) were prepared by melt mixing the PP with MWCNT on a co-rotating twin screw extruder (45 mm extruder TSE20, Brabender).

Weathering effects were simulated on the nanocomposites during 200h in a climatic chamber (Suntest XXL+, Atlas) according to ISO 4892:2013 Plastics – Methods of exposure to laboratory light sources – Part 2: Xenon-arc lamps [40]. Weathering conditions are shown in Table 21.

Table 21 - Accelerated aging parameters used to simulate weathering conditions on the sample

Irradiation (340nm)	Filters	Black Standard Temperature	Relative humidity	Wet and dry cycle duration
0.5 W/m ² (continuous)	Borosilicate	65 ± 3 °C	50 ± 5%	1 min (wet); 29 min (dry)

Once the PP+MWCNT polymer was aged it was milled to obtain the starting material needed for a new polymer injection, simulating the nanocomposites recycling process. The specimen after the aging process and after milling is shown in Figure 88.



Figure 88 - A) Specimen before milling. B) Pellets of PP+MWCNT obtained after milling.

The recycled specimen was introduced again in the climatic chamber for weathering simulation. The weathering conditions were the same but in this occasion the total simulation time was 1000h instead of 200h. Moreover, runoff waters from the wet cycles were collected for further characterisation. Waters collected from the climatic chamber were freeze-dried (CoolSafe 100-9 PRO Freeze Dryer, LaboGene APS, Denmark; water sublimation at $-95\text{ }^{\circ}\text{C}$ and $\sim 0.3\text{ mbar}$) to isolate the release materials. At least 2.5 L ($\geq 4\%$ v/v) of the total collected water was lyophilised as representative sample, obtaining a dry residue of $\geq 3\text{ mg}$.

The solid residues were weighed to determine the release rate and were characterized by:

Attenuated Total Reflection-Fourier Transform Infrared Spectroscopy (ATR-FTIR). using a Shimadzu IR Affinity-1 8400. FTIR is used to identify the chemical composition of the material in the residue, in particular the organic/polymeric part.

Differential Scanning Calorimetry (DSC) using a mDSC, Q20, TA Instruments, USA. DSC is used to measure polymer characteristics such as melting point.

Thermogravimetric Analysis (TGA). Hi-Res TGA was performed on a Q500, TA instruments, USA). TGA monitors mass against a continually increasing temperature. Changes in mass can occur with events such as combustion and is used here to measure the MWCNT component of the NC by combusting off the polymer leaving the MWCNT remainder. TGA analysis were performed in air atmosphere.

The nanocomposites were also observed through scanning electron microscopy (SEM) using a JSM-6010 LV, JEOL Ltd. with an InTouchScope™ operation system (V1.06, JEOL Ltd.).

The results were compared with previous experiments performed in LEITAT where 1000h weathering simulations were performed on new (non-recycled) nanocomposites.

10.3. Results

As can be seen in Figure 89, after aging, some areas of the recycled PP+MWCNT NC were a bit worn away, especially in the centre, but the specimen did not present a very damaged aspect.



Figure 89 – Specimen recycled and aged during 1000h.

The FT-IR spectra of the solid residues obtained after freeze drying the runoff waters, are shown in Figure 90. The spectra matched with the PP and PP+MWCNT-aged spectrums, confirming that the recovered material corresponded to the NC.

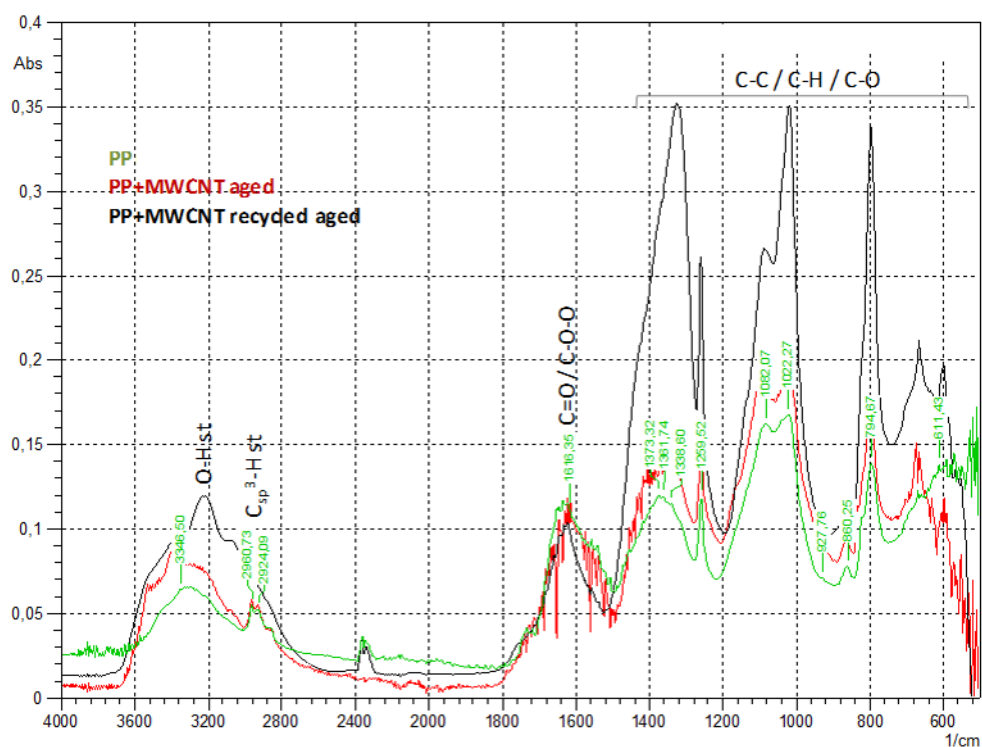


Figure 90 - FT-IR of the freeze-dried material released during aging of PP+MWCNT before and after its recycling, and the PP (without MWCNT and without aging).

The released amounts obtained from weighing the solid residues after freeze-drying are shown in Figure 91. The results have been normalized by the polymer area in square meters (m²) for easier determination of the release rate. The values corresponding to the polymer without nanomaterials (PP) and the non-recycled polymer containing CNT (PP+MWCNT) were obtained from previous studies performed in LEITAT. The graph clearly shows that more material is released from the recycled NC. The aged non-recycled sample produced 151 mg released per m² of NC compared with 1399 mg released/NC·m², from the recycled polymer, almost one order of magnitude higher. Comparing the NC (recycled and non-recycled) with the PP material the non-recycled NC presented a lower release, probably due to the protection provided by the MWCNT. However, the recycled NC presents a much higher

release. In addition, while in the non-recycled polymers no NM presence was detected, in the recycled polymer a high amount of NMs were found. This shows that not only the release rate changes but also the release form. The results obtained prove that the recycled material has a different release behaviour compared with the non-recycled.

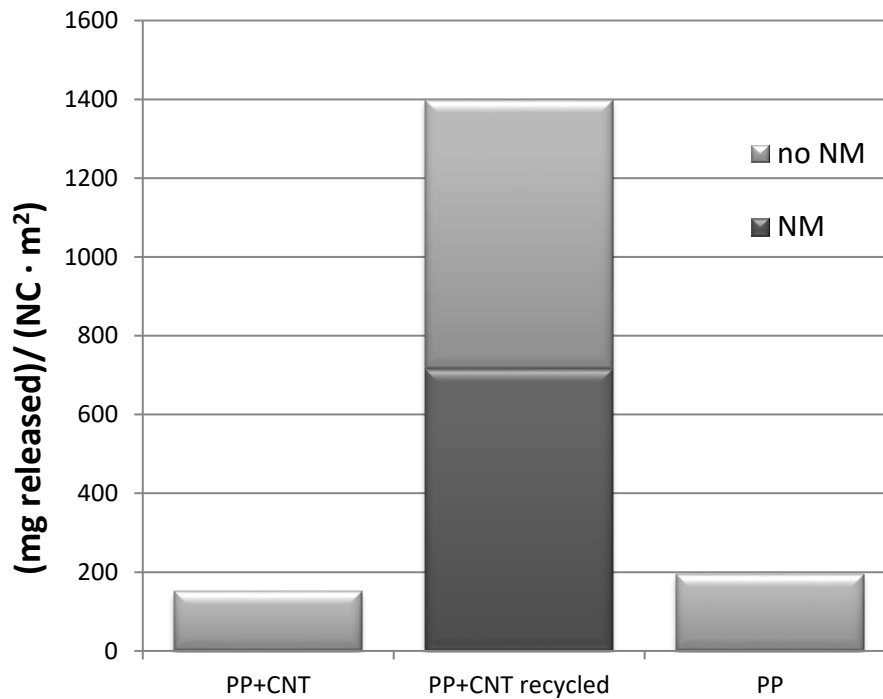


Figure 91 – Weight (mg) released per nanocomposites area (m²) due to weathering for the three polymers tested. Both fractions containing and non-containing nanomaterials (NM) are represented.

In the calorimetric analysis a small degradation of the polymer was evident in the DSC (Differential Scanning Calorimetry) curves (Figure 92), where the melting temperature was slightly lower after the recycling process. For the DSC only the polymers (with and without NMs) were analyzed, any measurements were performed with the solid residues recovered from the climatic chamber because all the material was used in the TGA (thermogravimetric analysis).

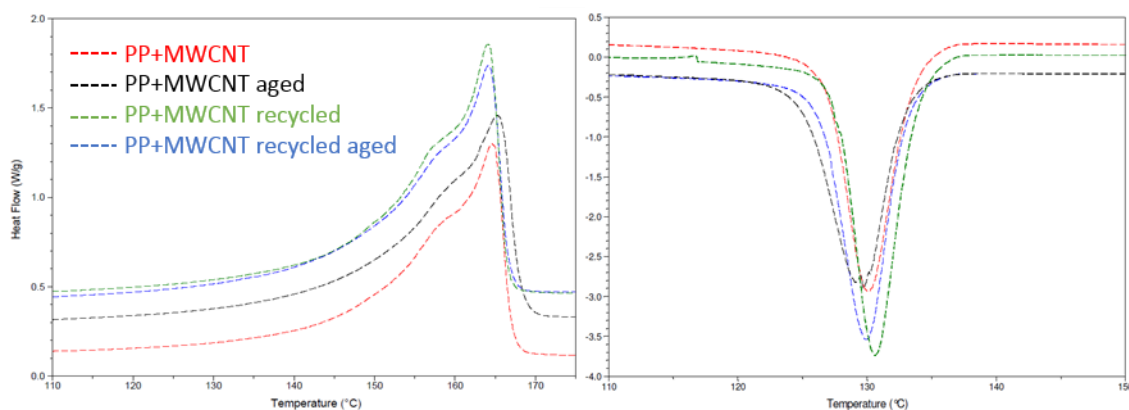


Figure 92 – DSC analysis of PP+MWCNT composites in the different stages.

In Figure 93 the TGA results obtained for the MWCNT, the PP and the recycled NC residues in air atmosphere are shown. The solid lines refer to the weight (%), which is the left y-axis and the dashed line corresponds to the derived weight (%/°C), right y-axis. The temperature selected to determine the amount of NM content in the residue was 500°C. This particular temperature was selected for the following reasons. The PP specimen degradation (green line) occurred around 400°C, with almost no material left at 500°C. In the raw MWCNT (black line) at 500°C 100% of the material was still present, the degradation occurred at higher temperatures (around 600°C). For this reason, 500°C was an optimum temperature since the entire polymer was degraded and the MWCNTs were not. As the values shown in the arrows, from the TGA results it was confirmed that 51% of the material released was CNT.

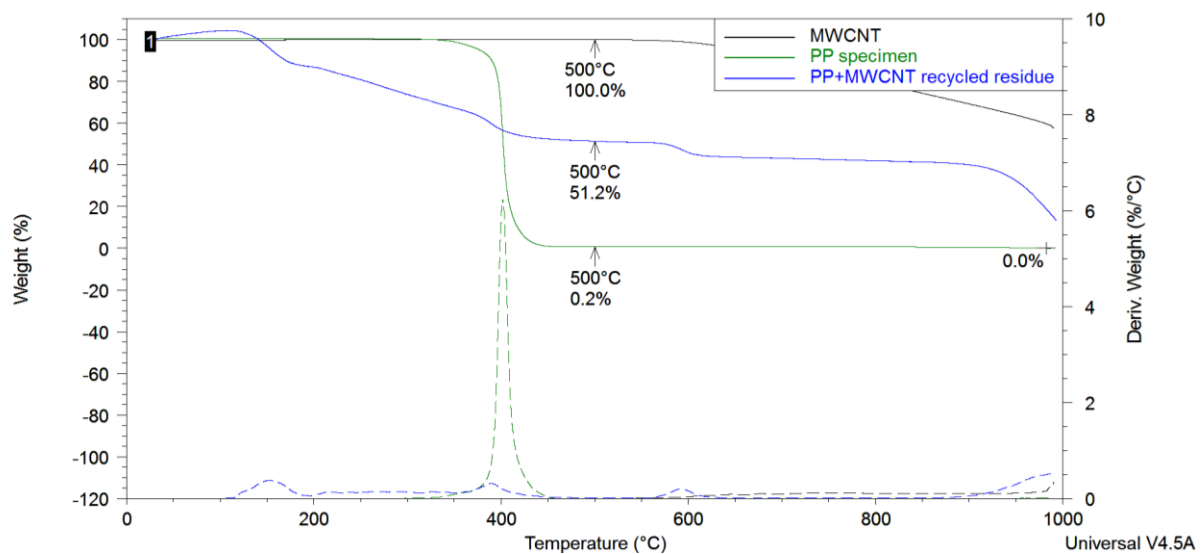


Figure 93 – TGA graph of the MWCNT, PP specimen (without MWCNT) and recycled PP+MWCNT residue obtained from freeze-drying the runoff waters from the climatic chamber.

For the non-recycled nanocomposite in the first aging process the polymer was cracked at microscopic scale (comparing Figure 94A,B with Figure 94C,D), and nanotubes were not only visible in some regions of the surface, but also in between the fragmented areas of the polymer. After the mechanical recycling, the surface appeared at low magnification to be similar to the non-aged and non-recycled NC, however some distributed nanotubes were observed at higher magnification. After the second accelerated aging, changes in the polymer morphology were more evident, and the surface was visibly inhomogeneous (see Figure 89). The SEM images showed the darkest areas contained more MWCNT. The results indicated the nanotubes had coalesced and were not as evenly distributed after losing the protective coating of PP.

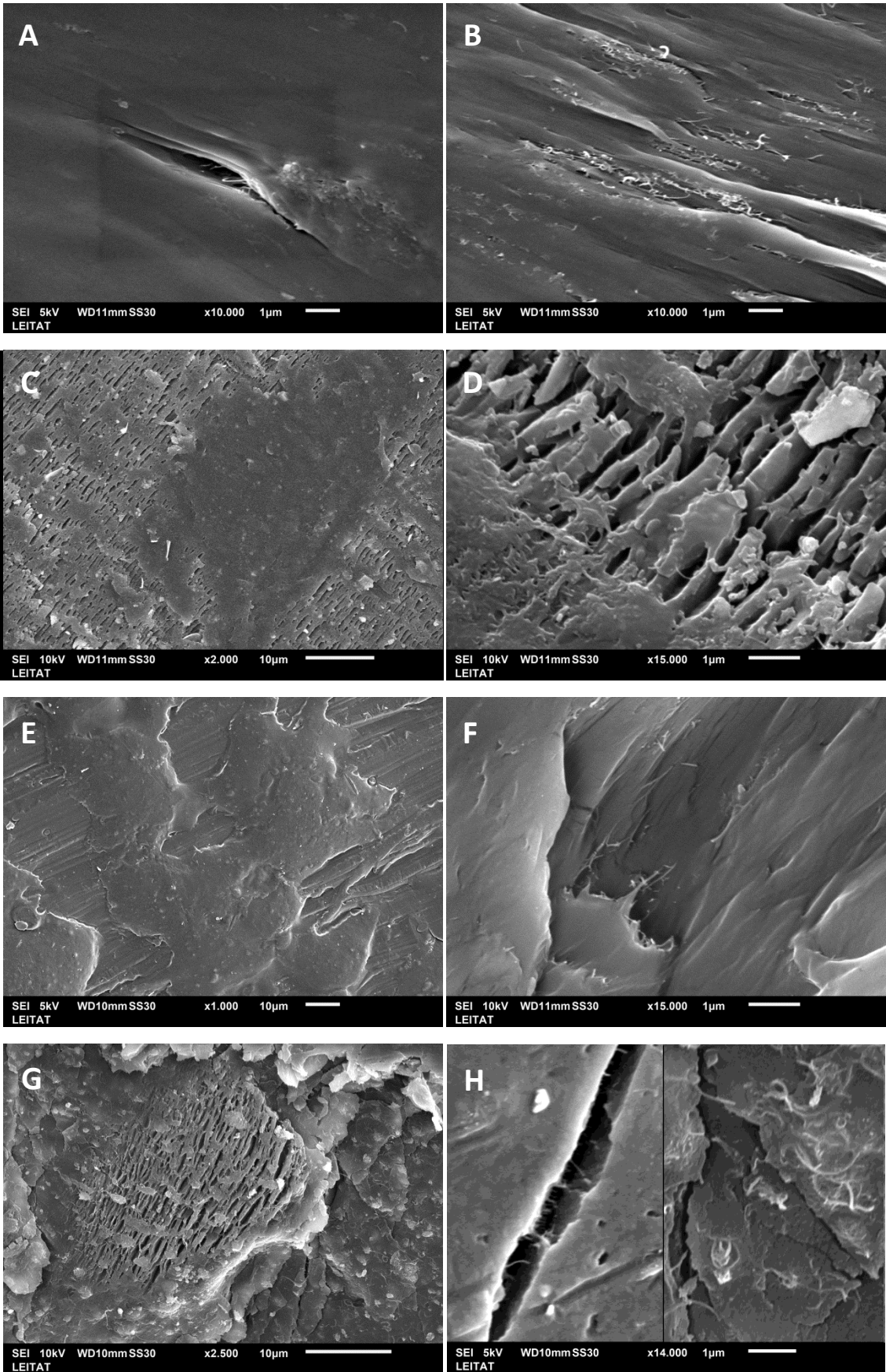


Figure 94 - SEM images showing the surface of PP+MWCNT specimen tests in different stages of their life cycle: PP+MWCNT (A-B), PP+MWCNT aged (C-D), PP+MWCNT recycled (E-F) and PP+MWCNT recycled aged (G-H).

10.4. Conclusions

A large difference was observed between the amount of material released when PP+MWCNT nanocomposites were made with new materials and from when the NCs were performed simulating a recycling process and aged. The difference was of almost one order of magnitude higher for the recycled polymer. According to this calculation using recycled material in a NC leads to 9.3 times more released material released than using non-recycled material.

$$\frac{\text{Recycled NC release}}{\text{Non recycled NC release}} = \frac{1399 \text{ mg released/ NC} \cdot \text{m}^2}{151 \text{ mg released/NC} \cdot \text{m}^2} = \mathbf{9.3}$$

In addition, what must also be highlighted is that in the recycled material 51% of the solid residue was NM, while in the non-recycled nanocomposites presence of NMs were not found. Thus, the present study suggests that the recycling process in this particular kind of NC modifies not only the release rate but also the release form of the materials released due to weathering effects.

11. FIELD CAMPAIGNS

11.1. Introduction

The transformations of ENM were experimentally investigated under real ambient conditions by field campaigns carried out in two industrial sites. The aim was to quantify and characterize the emissions at stack and measure also the concentration in the environment and ground deposition (for use in WP6) near the sites. Characterization of stack emissions during production process or use process (fluxes, chemical nature of substances, particle sizes, morphologies) are described hereafter. The materials and methods section is valid for both field campaigns performed.

11.2. Materials and methods

The parameters of stack emissions and the corresponding experimental set up to measure them are presented below:

- Flow rate measurement: volumetric flow rate.
- Morphology, size and elemental composition: sampling on TEM grid by means of MPS with a by-pass (illustrated in Figure 95) and diluted flow.
- Sampling of M-O particles was performed based on a standard protocol for sampling heavy metal particles in flue gases (NF EN 14385). A filter was used to collect the total suspended particles (TSP), it was combined for collection in absorption solutions and coupled with chemical analysis to investigate total particulate mass concentration and total M-O particles concentration (see Figure 96).
- Number concentration: ELPI impactor (7 nm - 2.5 μm) directly on the emission flow and after dilution.
- Mass concentration: sampling using manual impaction on filter (weighted before and after sampling) combined with chemical analysis, DGI Impactor (Dekati Gravimetric Impactor, 200 nm - 2.5 μm) after dilution.

An illustration of dilution system, connected to sampling used at stack 1, is given in the figure below.

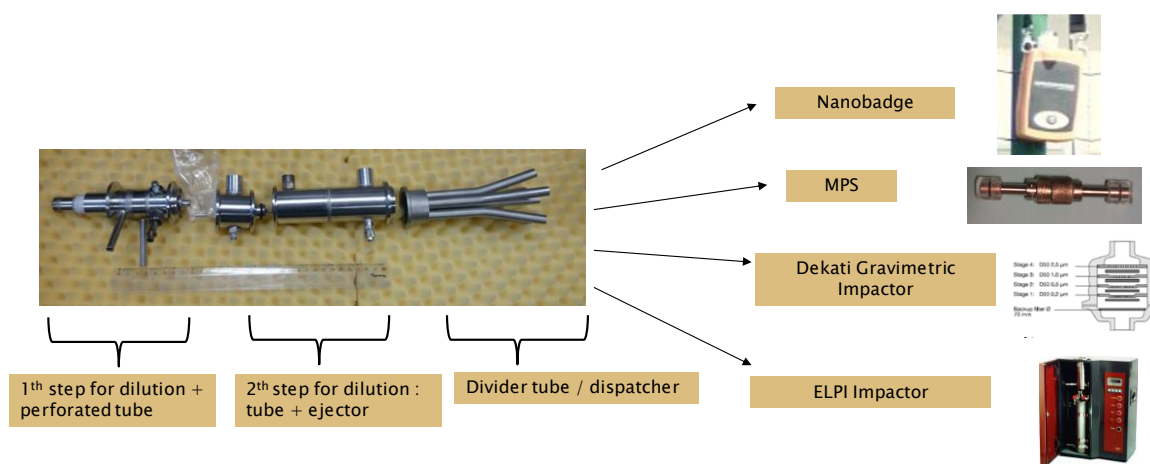


Figure 95 – Dilution equipment set up at French producer site.

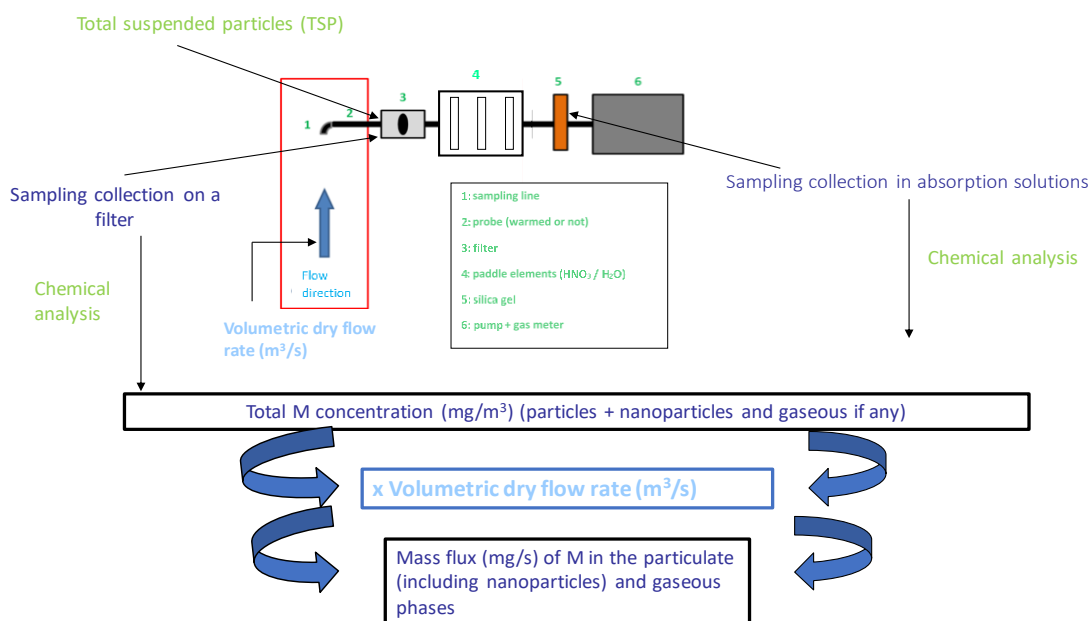


Figure 96 - Schematic of total suspended particulate coupled with chemical analysis.

11.3. Results

11.3.1. French TiO₂ producer

INERIS carried out a field campaign at a French industrial site between 19th of September and 19th of October 2017.

The industrial producer site was composed of:

- Metal oxide (M-O) ENM production line that uses a filtration system before exhausting effluents by stack.
- Metal oxide (M-O) non ENM milling line that uses a filtration system before exhausting effluents by stack.

The emissions parameters measured at stack of metal oxide (M-O) ENM production line and post processed data during the campaign are presented in the table below.

Table 22 - Emissions flux parameters measured.

MEASUREMENT SET UP	PARAMETERS	COMMENTS
	Volumetric dry flow rate: 27 800 (m ³ /h ⁴)	/
	Volumetric humid flow rate: 36 800 (m ³ /h) (~ 25% of v/v humidity)	/
	Temperature: 65 °C	/
	PM2.5 PM1 PM0.5 PM0.2	/

⁴ m³/h : normal cubic meters per hour

DGI Impactor (after dilution)	(mg/m ³)	(mg/m ³)	(mg/m ³)	(mg/m ³)	
	37.5	34.6	31.6	24.9	
NF EN 14385 (note: 1 h of time sampling is recommended but only 38 min was done)	TSP				/
	(mg/m ³)				
	24.8				
ELPI					Technical issue, results not reliable
NF EN 14385 and ICP/OES analysis to detect M	Total M particle concentration in the flow = 139 µg/m ³ . Under hypothesis of total conversion in M-O the total M particle concentration in the flow is equal to 234 µg/m ³ .				M-O particle concentration is less than 1% of total particles concentration total collected on the filter
Sampling with DGI Impactor combined with chemical analysis	/				Sampling time too short (due to power electric supply problems), concentration of M-O could not be assessed
Nanobadge	Mass concentration of M-O = 82 µg/m ³				This equipment is deemed as a semi- quantitative measurement apparatus.
	POST PROCESSED PARAMETERS				
	Total M-O mass flow rate = Total M-O particle concentration (234 µg/m ³) x volumetric dry flow rate (27 800 m ³ /h) = <u>6.5 g/h</u>				

Particles matter concentrations obtained by DGI Impactor shown higher value than the ones obtained by TSP. It could be explained by some condensation phenomena happening when diluting the flue gas. These condensate phenomena are particularly likely to happen here, since the raw flue gas is very wet.

It is worth noting that the total M-O (M) particle mass flow rate collected on the filter (see Figure 96) is less than 1% of total mass flow rate of total particles.

Some representative photographs of M-O aggregate are presented in Figure 97 and Figure 98. Within sample carried out at the stack on 19th of September, a large number of quasi-spherical droplets (100 to 300 nm) were observed. Micron-sized nanostructured M-O aggregates were also found.

Another sample was analysed on 21th in which nanostructured M-O aggregates were still present, but this time numerous crystals (platelet shape) were also seen. This demonstrates a great variability of nature for compounds emitted with M-O.

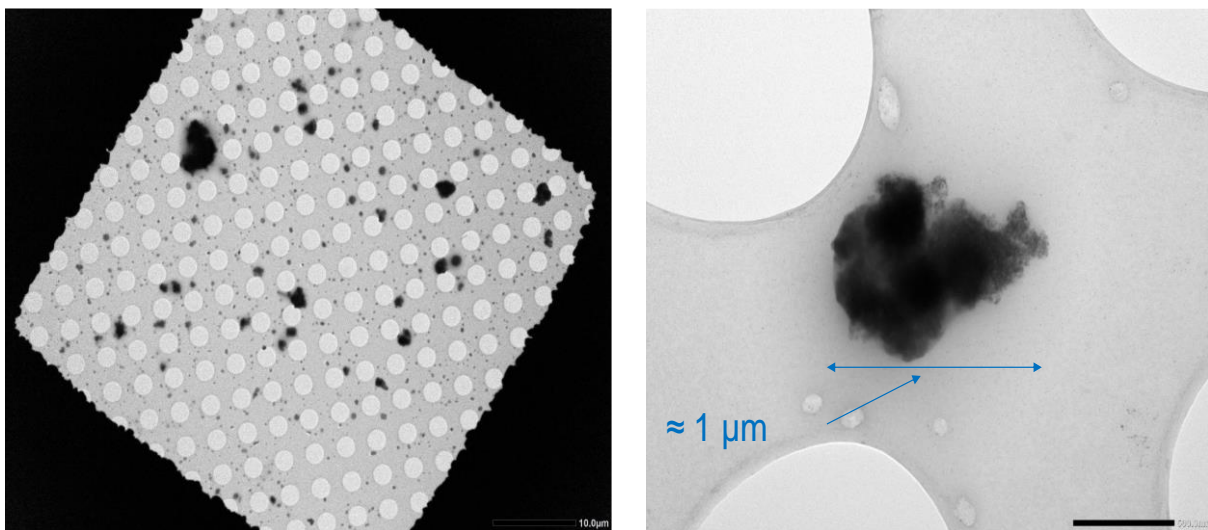


Figure 97 - General view of a TEM grid (left photograph, 10 μm bar), view of M-O aggregate (right photograph, 0.5 μm bar)

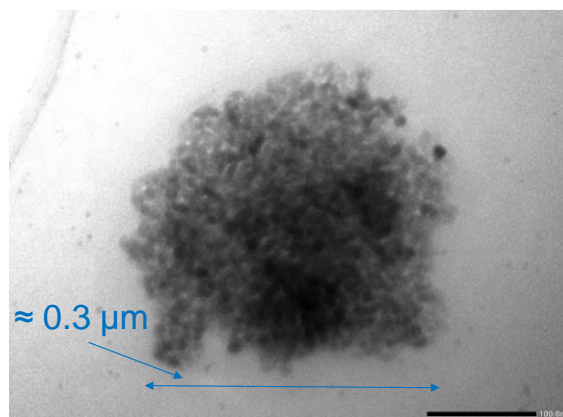


Figure 98 - view of M-O aggregate by microscopic analysis of TEM grid (0.1 μm bar)

11.3.2. Danish paint manufacturing site

Field measurements were conducted between 29th of January and 2nd February, 2018 at Beck and Jorgensen (BJ) (Söborg) during production of paint batches. The mineral powders used at

BJ were: clay, silica, talc, kaolin, titanium oxide and calcium carbonate. The relevant elements were Al, Ca, Si, Mg, Ti; due to ubiquity of these elements the background was controlled carefully. Ambient measurements were performed very close to the buildings present inside the site. During the experimental campaign, in the pouring station (ground floor), all raw materials in powder form were poured either from bags through a quadratic opening and conducted into a mixing tank. Pouring station had local exhaust ventilation (LEV) at the rim along three sides of the pouring inlet. The exhaust duct of the LEV was connected to the “small chimney”. In the mixing station (first floor), coating grade TiO₂ from small bags were opened with a knife and manually poured directly to the closed mixing tank that had a LEV located under the pouring point attached to the funnel leading to the mixer. The LEV was connected to the “big chimney”.

Emission parameters measured at mixing chimney

Mass emission flux parameters and mass concentration measured by DGI Impactor and TSP are listed in Table 23. Focus was put on TiO₂, which is in the nanometric range, other products were rather in the micron range (see later with TEM images).

Table 23 - Mass emissions flux parameters and mass concentration measured at mixing chimney.

MEASUREMENT SET UP	PARAMETERS					COMMENTS
Hot-wire anemometer	5 m·s ⁻¹ ; Volumetric dry flow rate: 10 700 (m ₀ ³ /h)					Pitot tube flow meter was not reliable because of low velocity
DGI Impactor (after dilution)	Total	PM2.5	PM1	PM0.5	PM0.2	
	(mg/m ₀ ³)	(mg/m ₀ ³)	(mg/m ₀ ³)	(mg/m ₀ ³)	(mg/m ₀ ³)	
	0,38	0,34	0,28	0,18	0,16	
NF EN 14385	TSP					Total particle concentrations are not directly comparable between DGI and TSP due to the known effect of particle losses on walls for DGI.
	(mg/m ₀ ³)					
	0.55					

ELPI	Measured particle sizes by using ELPI ranged from 50 nm to 3 μm Total Number = 2.69E+03 $\#/\text{cm}^3$	
	POST PROCESSED PARAMETERS FOR TiO₂	
TiO₂ mass flow rate	Total TiO ₂ mass flow rate = Total TiO ₂ particle concentration (46.7 $\mu\text{g}/\text{m}^3$) x volumetric dry flow rate (10,700 m^3/h) = 0.51 g/h	
Total number of TiO₂ particles	Total Number of TiO ₂ can be approximated by: (Total TiO ₂ particle concentration) / (TiO ₂ agglomerate Mass) TiO ₂ agglomerate diameter can be roughly estimated by microscopic observation (see Figure 101), a value of 300 nm is representative. By assuming a TiO ₂ density value of 4,000 kg/m^3 , (upper range), the value of total number of TiO ₂ is estimated equal to $\sim 800 \#/\text{cm}^3$.	

The relevant chemical elements found were Si at a concentration of 62 $\mu\text{g}\cdot\text{m}^{-3}$, Ti at 28.7 $\mu\text{g}\cdot\text{m}^{-3}$ (TiO₂ at 46.7 $\mu\text{g}\cdot\text{m}^{-3}$), Mg at 28 $\mu\text{g}\cdot\text{m}^{-3}$, Ca at 24 $\mu\text{g}\cdot\text{m}^{-3}$ and Al at 26 $\mu\text{g}\cdot\text{m}^{-3}$. On Wednesday 31st January 2018, results from the stack emission (“big chimney”) corresponded to TiO₂ pouring activity (1,475 kg from SBs). Therefore, it can be estimated a value of 1.7 mg TiO₂ released per kg of TiO₂ poured. Knowing that in 2018, B&J paint manufacturer registered a consumption of 500 ton TiO₂/year, it could be estimated that a total amount of 0.9 kg TiO₂ is released to outdoors per year. Measured particle sizes using ELPI ranged from 50 nm to 3 μm (Figure 99). The size distribution given by DGI results (Table 23) shows the same trend: DGI results show a majority of particles (by mass) under 2.5 μm and a significant proportion below 0.2 μm .

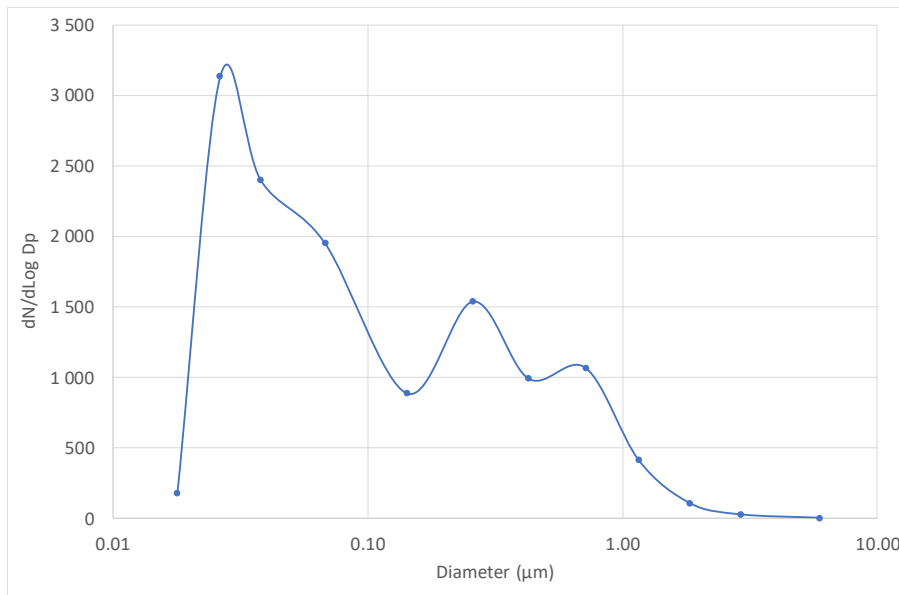


Figure 99 - Particle size distribution measured by ELPI at the big chimney (mixing station).

Mass concentrations were assessed by Nanobadge measurement, that is deemed as a semi-quantitative method. It was found that Si, Al, Ca, Ti concentrations were 3 times lower than those measured in the quantitative method. This factor of 3 was also found in other similar measurements performed by INERIS at industrial sites.

Emission parameters measured at pouring chimney

The emissions parameters measured at the pouring chimney and post processed data from the campaign are presented in Table 23 in terms of the mass emission flux parameters and mass concentration (average over 3 measurements) measured for total particles by DGI Impactor and TSP with a focus on TiO₂. The average flux measured in the stack emission during 3 days (Tuesday 30 January, Wednesday 31 January and Thursday 01 February 2018) was 8.6 g h⁻¹ in total suspended particles at a concentration of 4 to 9 mg·m⁻³. Measured particle sizes by using ELPI varied from 200 nm to 3 µm (see Figure 100). The relevant chemical elements found (average of 2 measurements where TSP filters were collected) were Si at 352 µg·m⁻³ (flow 0.44 g/h), Ti at 92 µg·m⁻³ (flow 0.12 g/h), Mg at 804 µg·m⁻³ (flow 1 g/h), Ca at 150 µg·m⁻³ (flow 0.19 g/h), and Al at 202 µg·m⁻³ (flow 0.26 g/h).

Table 24 - Mass emission flux parameters and mass concentration measured at pouring chimney.

MEASUREMENT SET UP	PARAMETERS	COMMENTS
Hot-wire anemometer	5 m/s; Volumetric dry flow rate: 1258 (m ³ /h)	Pitot tube flow meter was not reliable because of low velocity

DGI Impactor on 30 th of January (7:30 to 12:32)						Spectrum distribution not estimated due to saturated sampling
	Total	PM2.5	PM1	PM0.5	PM0.2	
DGI Impactor	(mg/m ⁰ ³)	(mg/m ⁰ ³)	(mg/m ⁰ ³)	(mg/m ⁰ ³)	(mg/m ⁰ ³)	
on 31 st of January (13:00 to 14:40)	56.59	47.88	27.46	11.43	3.9	
on 1 st of February (12:13 to 14:57)	99.75	87.66	51.87	21.58	8.49	
NF EN 14385	TSP (average over 3 measurements)					
	(mg/m ⁰ ³)					
	6.93					
ELPI	Measured particle sizes by using ELPI varied from 200 nm to 3 μm N total = 6.35 10 ³ #/cm ³ (average over 3 measurements)					
	POST PROCESSED PARAMETERS FOR TiO ₂					
Average over 2 measurements	Total TiO ₂ mass flow rate = 0.19 g/h					
	The total number of TiO ₂ value (see approach presented in Table 23) is estimated to be equal to ~2,700 #/cm ³					

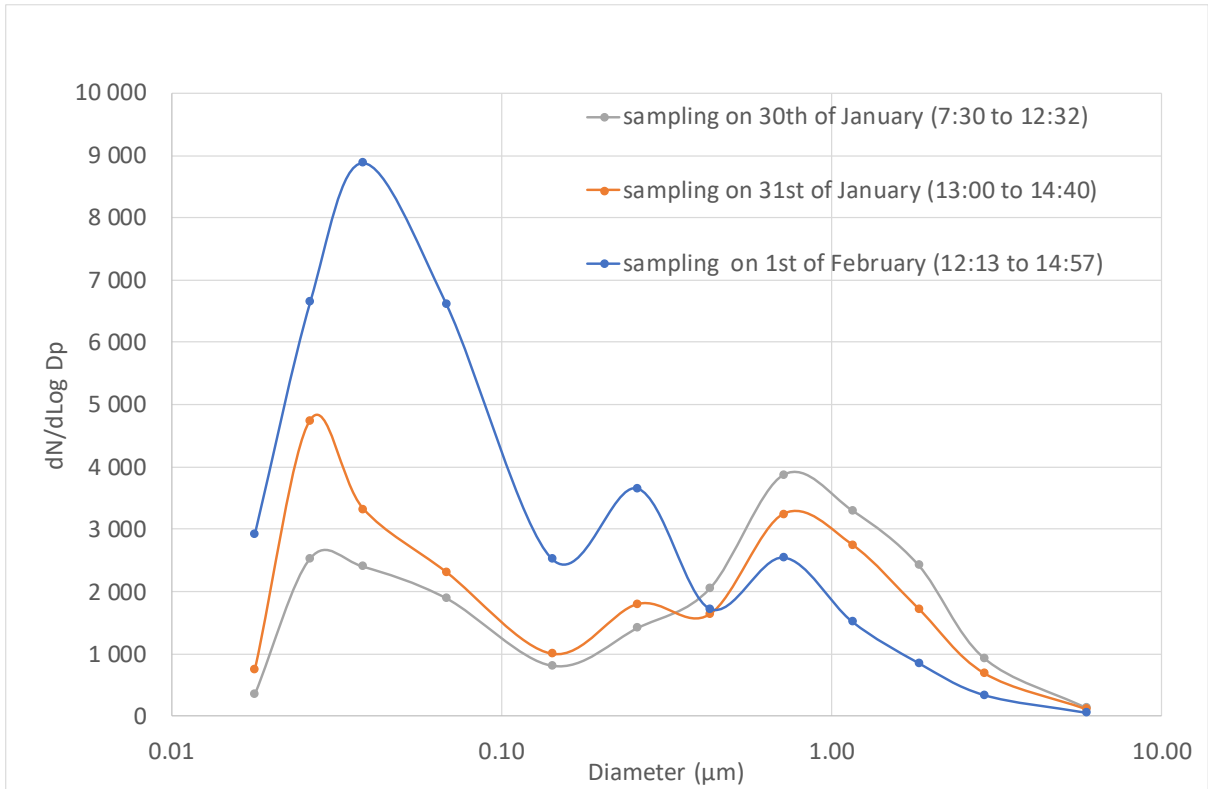


Figure 100 : Particle size distribution measured by ELPI at the small chimney (pouring station).

Sampling on TEM grid allowed to obtain microscope images of particles collected in the stack emissions during TiO₂ and clay pouring. Example of images are shown in Figure 101.

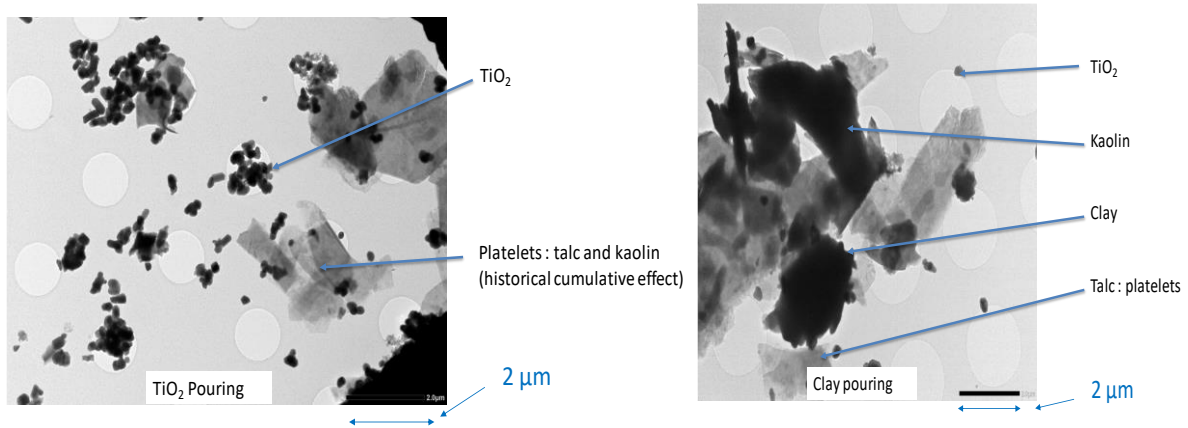


Figure 101 - General view of a TEM grid (2 µm bar), left : TiO₂ aggregate during TiO₂ and clay pouring, right : TiO₂ aggregate during clay pouring.

As illustrated by images in Figure 101, part of TiO₂ was in the nanometric range and other products are in the micrometric size range.

Overall, the used pigments or mineral fillers were always visible by TEM analysis of the samples collected in the stack emissions. The pigment/filler poured or mixed at the time of sampling was the main component visible, but other products can also be detected due to historical cumulative effects by previous pouring process.

11.4. Conclusions

11.4.1. French TiO₂ producer

The site emissions were well characterized in terms of nature, morphology and quantities of M-O particles emitted. There was a wide range in the nature and morphology of the particles (containing or not M-O) emitted by the stack 1 which was the main site emitter. Stack 2 emitted non-nanostructured M-O aggregates.

It was clearly observed that there were ENM emitted as nanostructured M-O agglomerates. These agglomerates were above the nanometric size range. These nanostructured M-O did not further agglomerate or transform after their release because very similar morphologies were consistently observed downwind (up to 300 m) by TEM analysis for a significant number of samples. A structure modification was never observed in any of the samples taken downwind the stacks.

11.4.2. Danish paint manufacturing site

The main outcomes of emission measurements are the following:

- The used pigments or mineral fillers were always easily visible by TEM in the stack emissions.
- The filler poured or mixed at the time of sampling is the main component visible, but other products are also visible (historical cumulative effects).
- Part of TiO₂ is in the nanometric range, other products are rather in the micron range (TEM images).
- The number concentration of particles measured in the stacks is within the same order of magnitude of ambient air.
- The measured mass flow rate of TiO₂ is below 0.5 g/h.
- Knowing that in 2018, B&J paint manufacturer registered a consumption of TiO₂ of 500 tons/year, it could be estimated that a total amount of 0.9 kg TiO₂ is released outdoors per year.

12. DISCUSSION AND FINAL CONCLUSIONS

The main outcomes from the release studies presented in this deliverable are release rates and forms, which can be use as inputs of nanospecific modeling tools as the one being developed in NANOFASE.

Table 25 – Deliverable summary table with the release rates, release forms and compartments where release from the different case studies is more likely to go to.

CASE STUDY	ENMs	LCS STUDIED	RELEASE RATE	RELEASE FORM	COMPART -MENT
Camping tents (1 coating)	Ag-PEI NPs	End of life (leaching)	183 ± 3 (Ag µg / textile m ²) 1.07 ± 0.02%	Ionic (Ag ⁺): 41 ± 0% <20 µm: 37 ± 6% >20 µm: 22 ± 2%	Soil
Camping tents (2 coatings)	Ag-PEI NPs	End of life (leaching)	161 ± 7 (Ag µg / textile m ²) 0.53 ± 0.02%	Ionic (Ag ⁺): 45 ± 4% <20 µm: 36 ± 2% >20 µm: 19 ± 4%	Soil
Curtains	TiO ₂	Use (washing)	9 ± 2 % (in 10 washings)	Aggregate	WWTP
Antibacterial textile	Ag-PVP NPs	Use (washing)	70 ± 2 % (in 10 washings)	Ag ⁺	WWTP
Antibacterial textile	Ag-PVP NWs (~3 µm)	Use (washing)	59 ± 9 % (in 10 washings)	Ag ⁺ and free NWs	WWTP
Antibacterial textile	Ag-PVP NWs (~30 µm)	Use (washing)	73 ± 2 % (in 10 washings)	Ag ⁺ and free NWs	WWTP
Antifouling paints	Nano-Cu ⁰	Use (immersion in marine water)	Cu: 0.00026 ± 0.00004% Zn: 0.00235 ± 0.00101%	Cu ²⁺ and malachite Zn ²⁺	Water
Antifouling paints	Nano-Cu ₂ O	Use (immersion in marine water)	Cu: 0.00050 ± 0.00029% Zn: 0.00681 ± 0.00915%	Cu ²⁺ and malachite Zn ²⁺	Water

Antifouling paints	Micro-Cu ⁰	Use (immersion in marine water)	Cu: 0.00203 ± 0.00016% Zn: 0.00208 ± 0.00084%	Cu ²⁺ and malachite Zn ²⁺	Water
Antifouling paints	Micro-Cu ₂ O	Use (immersion in marine water)	Cu: 0.00043 ± 0.00010% Zn: 0.00195 ± 0.00058%	Cu ²⁺ and malachite Zn ²⁺	Water
Antifouling paints	Nano-Cu ⁰	Use (immersion in ultrapure water)	Cu: 0.00050 ± 0.00004% Zn: 0.02103 ± 0.00094%	Cu ²⁺ Zn ²⁺	Water
Antifouling paints	Nano-Cu ₂ O	Use (immersion in ultrapure water)	Cu: 0.00034 ± 0.00029% Zn: 0.01041 ± 0.00903%	Cu ²⁺ Zn ²⁺	Water
Antifouling paints	Micro-Cu ⁰	Use (immersion in ultrapure water)	Cu: 0.00028 ± 0.00013% Zn: 0.01509 ± 0.00070%	Cu ²⁺ Zn ²⁺	Water
Antifouling paints	Micro-Cu ₂ O	Use (immersion in ultrapure water)	Cu: 0.00024 ± 0.00005% Zn: 0.02135 ± 0.00124%	Cu ²⁺ Zn ²⁺	Water
Asphalt coating	TiO ₂	Use (weathering and wheel abrasion)	38% (per year)	0.5 – 5 µm aggregates	WWTP or directly to rivers and soil
Printed circuit	Ag	End of life (leaching)	11.1 ± 2.3 %	Ionic (Ag ⁺): 0.3 ± 0.1% <0.45 µm: 6.4 ± 0.7% <20 µm: 12.1 ± 3.0%	Soil

				>20 μm : 81.1 \pm 3.9%	
Sunscreens	TiO ₂ and Zn	Use (immersion in ultrapure water)	Sample 1: 1.2% of TiO ₂ Sample 2: 0.9% of TiO ₂ Sample 3: 5.0% of TiO ₂ 70.5% of ZnO	/	Water
Polymer	MWCN T	Recycling	9.3 times higher than in non-recycled NC	Embedded in the matrix	It will change depending on the polymer application
Field campaign	M-O NM producer	Synthesis	6.5 g M-O/h	Aggregates of \sim 0.5 μm	Air
Field campaign	TiO ₂	Manufacturing	Mixing chimney: 0.51 g/h Pouring chimney: 0.19 g/h	Mixing chimney: <2.5 μm and a significant proportion <0.2 μm Pouring chimney: from 0.2 to 3.0 μm	Air

13. BIBLIOGRAPHY

- [1] International Organization for Standardization, "ISO 15181:2007 -- Paints and varnishes -- Determination of release rate of biocides from antifouling paints," 2007.
- [2] American National Standard (ASTM), "D 1141- 98 (2003) -- Standard practice for the preparation of substitute ocean water."
- [3] E. Goldstein, G. I.; Newbury, D. E.; Echlin, P.; Joy, D. C.; Fiori, C.; Lifshin, *Scanning Electron Microscopy and X-Ray Microanalysis*. New York: Plenum Press, 1981.
- [4] I. O. for Standardization, "ISO 105-C06:2010 Textiles -- Tests for colour fastness -- Part C06: Colour fastness to domestic and commercial laundering."
- [5] J. Schneider *et al.*, "Understanding TiO₂ Photocatalysis: Mechanisms and Materials," *Chemical Reviews*, vol. 114. pp. 9919–9986, 2014.
- [6] A. J. Koivisto *et al.*, "Quantitative material releases from products and articles containing manufactured nanomaterials: Towards a release library," *NanoImpact*, vol. 5, pp. 119–132, 2017.
- [7] M. J. Hajipour *et al.*, "Antibacterial properties of nanoparticles," *Trends Biotechnol.*, vol. 30, no. 10, pp. 499–511, Oct. 2012.
- [8] A. Besinis, T. De Peralta, and R. D. Handy, "The antibacterial effects of silver, titanium dioxide and silica dioxide nanoparticles compared to the dental disinfectant chlorhexidine on *Streptococcus mutans* using a suite of bioassays," *Nanotoxicology*, vol. 8, no. 1, pp. 1–16, Feb. 2014.
- [9] S. Ferraris *et al.*, "Chemical, mechanical and antibacterial properties of silver nanocluster/silica composite coated textiles for safety systems and aerospace applications," *Appl. Surf. Sci.*, vol. 317, pp. 131–139, 2014.
- [10] P. Dallas, V. K. Sharma, and R. Zboril, "Silver polymeric nanocomposites as advanced antimicrobial agents: Classification, synthetic paths, applications, and perspectives," *Adv. Colloid Interface Sci.*, vol. 166, no. 1, pp. 119–135, 2011.
- [11] L. Kvitek *et al.*, "Antibacterial activity and toxicity of silver – nanosilver versus ionic silver," *J. Phys. Conf. Ser.*, vol. 304, p. 012029, Jul. 2011.
- [12] L. Wang, C. Hu, and L. Shao, "The antimicrobial activity of nanoparticles: present situation and prospects for the future.," *Int. J. Nanomedicine*, vol. 12, pp. 1227–1249, 2017.
- [13] EN 12457-4, "Characterisation of waste. Leaching. Compliance test for leaching of granular waste materials and sludges. Part 4: One stage batch test at a liquid to solid ratio of 10 l/kg for materials with particle size below 10 mm (without or with size reduction)."
- [14] J. Schindelin *et al.*, "Fiji: an open-source platform for biological-image analysis," *Nat. Methods*, vol. 9, no. 7, pp. 676–682, Jul. 2012.
- [15] "GUIDEnano - Home." [Online]. Available: <http://www.guidenano.eu/>. [Accessed: 31-Oct-2017].
- [16] C. Steger, "An unbiased detector of curvilinear structures," *IEEE Trans. Pattern Anal.*

- Mach. Intell.*, vol. 20, no. 2, pp. 113–125, 1998.
- [17] T. Wagner, M. Hiner, and xraynaud, “thorstenwagner/ij-ridgedetection: Ridge Detection 1.4.0,” Aug. 2017.
- [18] International Organization for Standardization, “ISO/TS 80004-2:2015 -- Nanotechnologies -- Vocabulary -- Part 2: Nano-objects,” 2015.
- [19] D. for E. F. and R. Affairs, “National Statistics Release: Emissions of air pollutants in the UK.”
- [20] European Environment Agency, “Air quality in Europe — 2018 report,” 2018.
- [21] ISO, “EN 12697-22:2003 +A1:2007 Bituminous mixtures. Test methods for hot mix asphalt - Part 22: wheel tracking.”
- [22] D. Sánchez-Quiles and A. Tovar-Sánchez, “Sunscreens as a Source of Hydrogen Peroxide Production in Coastal Waters,” *Environ. Sci. Technol.*, vol. 48, pp. 9037–9042, 2014.
- [23] A. P. Gondikas, F. Von Der Kammer, R. B. Reed, S. Wagner, J. F. Ranville, and T. Hofmann, “Release of TiO₂ Nanoparticles from Sunscreens into Surface Waters: A One-Year Survey at the Old Danube Recreational Lake,” *Environ. Sci. Technol.*, vol. 48, p. 47, 2014.
- [24] R. B. Reed, D. P. Martin, A. J. Bednar, M. D. Montañó, P. Westerhoff, and J. F. Ranville, “Multi-day diurnal measurements of Ti-containing nanoparticle and organic sunscreen chemical release during recreational use of a natural surface water,” *Environ. Sci. Nano*, vol. 4, no. 1, pp. 69–77, Jan. 2017.
- [25] S.-K. Jeon, E.-J. Kim, J. Lee, and S. Lee, “Potential risks of TiO₂ and ZnO nanoparticles released from sunscreens into outdoor swimming pools,” *J. Hazard. Mater.*, vol. 317, pp. 312–318, 2016.
- [26] J. Zeng, B. Saltysiak, W. S. Johnson, D. A. Schiraldi, and S. Kumar, “Processing and properties of poly(methyl methacrylate)/carbon nano fiber composites,” *Compos. Part B Eng.*, vol. 35, no. 2, pp. 173–178, 2004.
- [27] S. P. Bao and S. C. Tjong, “Mechanical behaviors of polypropylene/carbon nanotube nanocomposites: The effects of loading rate and temperature,” *Mater. Sci. Eng. A*, vol. 485, no. 1, pp. 508–516, 2008.
- [28] J. C. Kearns and R. L. Shambaugh, “Polypropylene fibers reinforced with carbon nanotubes,” *J. Appl. Polym. Sci.*, vol. 86, no. 8, pp. 2079–2084, Nov. 2002.
- [29] E. M. Moore, D. L. Ortiz, V. T. Marla, R. L. Shambaugh, and B. P. Grady, “Enhancing the strength of polypropylene fibers with carbon nanotubes,” *J. Appl. Polym. Sci.*, vol. 93, no. 6, pp. 2926–2933, Sep. 2004.
- [30] A. Sharma, B. Tripathi, and Y. K. Vijay, “Dramatic Improvement in properties of magnetically aligned CNT/polymer nanocomposites,” *J. Memb. Sci.*, vol. 361, no. 1, pp. 89–95, 2010.
- [31] I. Y. P. Tianxi Liu, Lu Shen, A. Shue Yin Chow, and W.-D. Zhang, “Morphology and Mechanical Properties of Multiwalled Carbon Nanotubes Reinforced Nylon-6 Composites,” 2004.

- [32] S. Morlat-Therias, E. Fanton, J.-L. Gardette, S. Peeterbroeck, M. Alexandre, and P. Dubois, "Polymer/carbon nanotube nanocomposites: Influence of carbon nanotubes on EVA photodegradation," *Polym. Degrad. Stab.*, vol. 92, no. 10, pp. 1873–1882, 2007.
- [33] L. Guadagno, C. Naddeo, M. Raimondo, G. Gorrasi, and V. Vittoria, "Effect of carbon nanotubes on the photo-oxidative durability of syndiotactic polypropylene," *Polym. Degrad. Stab.*, vol. 95, no. 9, pp. 1614–1626, 2010.
- [34] S. P. Lonkar *et al.*, "Self photostabilizing UV-durable MWCNT/polymer nanocomposites," *RSC Adv.*, vol. 2, no. 32, p. 12255, 2012.
- [35] S. Bocchini, A. Di Blasio, and A. Frache, "Influence of MWNT on Polypropylene and Polyethylene Photooxidation," *Macromol. Symp.*, vol. 301, no. 1, pp. 16–22, Mar. 2011.
- [36] H. Yazdani, B. E. Smith, and K. Hatami, "Electrical conductivity and mechanical performance of multiwalled CNT-filled polyvinyl chloride composites subjected to tensile load," *J. Appl. Polym. Sci.*, vol. 133, no. 29, Aug. 2016.
- [37] S. Glenis *et al.*, "Magnetic properties of carbon nanotube poly(ether-ester) nanocomposites," *J. Appl. Phys.*, vol. 108, no. 5, p. 054314, Sep. 2010.
- [38] D. R. Paul and L. M. Robeson, "Polymer nanotechnology: Nanocomposites," *Polymer (Guildf.)*, vol. 49, no. 15, pp. 3187–3204, 2008.
- [39] E. Assouline *et al.*, "Nucleation ability of multiwall carbon nanotubes in polypropylene composites," *J. Polym. Sci. Part B Polym. Phys.*, vol. 41, no. 5, pp. 520–527, Mar. 2003.
- [40] ISO, "ISO 4892-2:2013 Plastics – Methods of exposure to laboratory light sources – Part 2: Xenon-arc lamps," International Standards Organization, 2013.